

Universidad Autónoma de Madrid



Programa de Doctorado en Biociencias Moleculares

Tesis doctoral

**Cytoskeletal remodeling and enhanced autophagy drive an adaptive response to loss of Calsequestrin in a model of inherited arrhythmias**

**Andrea Cancemi**

Madrid 2021

Departamento de Bioquímica  
Facultad de Medicina  
Universidad Autónoma de Madrid

**Cytoskeletal remodeling and enhanced autophagy drive an adaptive response to  
loss of Calsequestrin in a model of inherited arrhythmias**

Doctorando:

**Andrea Cancemi**

Licenciado en biología molecular y genética

Director de tesis:

Silvia Giuliana Priori, MD, PhD

Co-director de tesis:

Demetrio Julián Santiago Castilllo, PhD

Tutor de tesis:

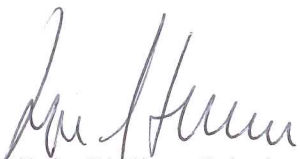
Carmen Delgado Canencia, PhD

La Doctora Silvia Giuliana Priori, líder del grupo de investigación "Cardiología molecular" del Centro Nacional de Investigaciones Cardiovasculares (CNIC) y el Doctor Demetrio Julián Santiago Castillo, senior post-doc del grupo de investigación de investigación "Cardiología molecular" del Centro Nacional de Investigaciones Cardiovasculares (CNIC)

CERTIFICAN

Que la Tesis Doctoral "*Cytoskeletal remodeling and enhanced autophagy drive an adaptive response to loss of Calsequestrin in a model of inherited arrhythmias*" ha sido realizada en la Fundación Centro Nacional de Investigaciones Cardiovasculares Carlos III, bajo su tutela, y que reúne las condiciones para optar al grado de Doctor.

Madrid, 2021



Fdo. Silvia Giuliana Priori



Fdo. Demetrio Julián Santiago Castillo

# Abstract

Calcium transients between the Sarcoplasmic Reticulum (SR) and the cytoplasm are essential for coordinated contraction in cardiomyocytes. Loss of the SR protein Calsequestrin 2 (CASQ2) causes the recessive form of Catecholaminergic Polymorphic Ventricular Tachycardia (CPVT2) by increasing the diastolic opening probability of the main SR calcium channel Ryanodine receptor 2 (RyR2), and by causing an unexplained decrease of its regulatory protein Triadin (TRDN). Here we studied the mechanisms of TRDN reduction in CASQ2-KO mice and show that ablation of CASQ2 activates histone-deacetylase HDAC6, which regulates several cellular processes. In CASQ2 deficient cardiomyocytes, HDAC6 reduces alpha-Tubulin acetylation, thus impairing microtubule stability and altering TRDN trafficking and co-localization with RyR2. Misplaced TRDN binds HSP70, forming Aggresomes that are degraded by autophagy. The study identifies a novel cascade of post-transcriptional events initiated by the loss of CASQ2 that leads to a major rearrangement of SR protein trafficking and stability in cardiomyocytes

## Resumen

El flujo de calcio que tiene lugar entre el Retículo Sarcoplasmático (SR) y el citoplasma es esencial para la contracción coordinada de los cardiomiocitos. La ausencia de la proteína del SR Calsecuestрина 2 (CASQ2) ocasiona la forma recesiva de la Taquicardia Ventricular Polimórfica Catecolaminérgica 2 (CPVT2), causando un incremento en la probabilidad de apertura “open probability” diastólica del principal canal de calcio del SR, el Receptor de Rianodina 2 (RyR2), y causando un descenso inexplicado de la proteína reguladora Triadina (TRDN). En este proyecto, se estudiaron los mecanismos responsables de la reducción de TRDN presentes en el modelo murino CASQ2-KO y se muestra como la ablación de CASQ2 activa la histona deacetilasa HDAC6, encargada de regular diversos procesos celulares. En los cardiomiocitos deficientes en CASQ2, HDAC6 reduce la acetilación de la  $\alpha$ -tubulina, perjudicando la estabilidad de los microtúbulos y alterando tanto la movilización de la TRDN como su colocalización con RyR2. La TRDN mal posicionada se une a la HSP70 formando Agresomas que terminan siendo degradados mediante autofagia. Este estudio identifica una novedosa cascada de sucesos post-transcripcionales iniciados a causa de la pérdida de CASQ2, lo que desemboca en una reorganización importante tanto del tráfico proteico desde el SR como de la estabilidad proteica en los cardiomiocitos.



# Abbreviation

3MA: 3-Methyladenine  
AAV9: Adeno-associated viral vector serotype 9  
AbH: Aspartyl beta-hydroxylase  
ALP: Autophagy-lysosome pathway  
CAM1: Calmodulin 1  
CASQ2: Calsequestrin 2  
CICR: Calcium Induced Calcium Release  
CLIMP63 : cytoskeleton-linking membrane protein 63  
CMA: chaperone-mediated autophagy  
CP: core particle  
CPVT: Catecholaminergic polymorphic ventricular tachycardia  
CQ: Chloroquine  
CRUs: Calcium release units  
DAD: delayed afterdepolarization  
DADs: Delayed afterdepolarization  
DHPRs: Dihydropyridine receptors  
DTT: Dithiothreitol  
EC: Excitation-contraction  
ECC: Excitation-contraction coupling  
ER: endoplasmic reticulum  
FDR: false discovery rate  
FRET: Förster resonance energy transfer  
FWHM: full width at half magnitude  
GO: Gene Ontology  
HCQ: Hydroxychloroquine  
HDAC6: Histone Deacetylase 6  
HSP70: Heat Shock Protein 70  
IF: Immunofluorescence  
IP: intraperitoneal injection  
IP3: inositol 1,4,5-trisphosphate  
JNT: Junctin  
JSR: junctional Sarcoplasmic Reticulum  
KO: Knockout  
LAMP1: Lysosomal-Associated Membrane Protein 1

LC3: microtubule-associated protein 1A/1B-light chain 3

LQTS: long QT syndrome

MAP: microtubule associated protein

MCS: Multi Cloning Site

MiNA: Mitochondrial Network Analysis

MS: Mass spectrometry

NBR1: next to BRCA1 gene 1 protein

NCX: Na<sup>+</sup>/Ca<sup>2+</sup> exchanger

NEM: *N*-Ethylmaleimide

NS: not statistically significant

OP: Open Probability

PBS: Phosphate-Buffered Saline

PE: phosphatidylethanolamine

PKA: Protein kinase A

PLA: Proximity Ligation Assay

PLA: proximity ligation assay

PTM: post-translational modification

REEP: Receptor expression enhancing proteins

ROI: Region of Interest

RP: regulatory particle

RyR2: Ryanodine receptor 2

SD: standard deviation

SR: Sarcoplasmic Reticulum

STED: Stimulated Emission Depletion Microscopy

TECRL: Trans-2,3-enol-CoA reductase-like

TEM: Transmitted Electron Microscopy

TMT: tandem mass tag

TRDN: Triadin

UBD: ubiquitin-binding domain

UPS: ubiquitin-proteasome system

WB: Western Blot

WT: Wild Type



# Acknowledgements

I would like to thank my PhD thesis director, Professor S.Priori for the opportunity given to me to develop the project and for the scientific guide during the last 6 years.

I would also like to thank my PhD thesis co-director Dr. D.J. Santiago for the crucial help for my formation during my PhD.

Ringrazio di cuore Valeria Caiolfa e Moreno Zamaì, che in questi anni mi hanno appoggiato non solo scientificamente, ma anche personalmente, diventando per me la mia famiglia al CNIC.

Me gustaría agradecer todos los miembros presentes y pasados del laboratorio de Cardiología Molecular (CNIC): Carmen, Kevin, Cristina, Francesca, Andreu, Riccardo, Demetrio, Elena, Gian Piero, Isa, Francesca A., Jarek. ¡Gracias por vuestra ayuda, compañía y apoyo!

Ringrazio a te, per grande appoggio e l'amore che mi hai regalato. Mi hai dato forza e accompagnato in questo viaggio. Grazie Amore mio!

Ringrazio la mia famiglia, Martina, Nadia e Salvo, senza i vostri sacrifici e aiuto non avrei mai potuto raggiungere i miei obiettivi.

Me gustaría agradecer todas las trabajadoras del CNIC, todas las unidades, el personal de limpieza, de mantenimiento y administrativo; si nuestra investigación funciona es gracias a vuestro trabajo, ¡gracias!

# Table of Contents

1.	Introduction .....	14
1.1	T-Tubule.....	15
1.2	Excitation-Contraction Coupling (ECC) .....	16
1.3	The cardiac $\text{Ca}^{2+}$ release unit .....	17
1.4	Ryanodine receptor 2 (RyR2).....	17
1.5	Calsequestin 2 (CASQ2) .....	19
1.6	Triadin (TRDN) .....	19
1.7	Junctin (JNT) .....	21
1.8	Junctophilin 2 (JPH2) .....	21
1.1	Catecholaminergic polymorphic ventricular tachycardia (CPVT) .....	22
1.2	Different forms of CPVT.....	23
1.2.1	CPVT 1.....	23
1.2.2	CPVT 2.....	23
1.2.3	CPVT 3.....	24
1.2.4	CPVT 4.....	24
1.2.5	CPVT 5.....	24
1.3	Microtubular network .....	25
1.4	Histone deacetylase 6 (HDAC6).....	27
1.5	Protein degradation pathways .....	27
1.6	The ubiquitin-proteasome system (UPS).....	29
1.7	Aggresomes .....	31
1.8	The autophagy-lysosome pathway (ALP) .....	32
1.9	Sarcoplasmic reticulum architecture.....	34

2.	Objectives of the work.....	36
3.	Results.....	37
3.1	Whole CASQ2-KO hearts Proteomic Analysis.....	37
3.2	Microtubule structural and molecular alterations in CASQ2-KO cardiomyocytes.....	38
3.3	Tau alteration in CASQ2-KO cardiomyocytes .....	39
3.4	Alpha-Tubulin deacetylation in CASQ2-KO cardiomyocytes .....	41
3.5	HDAC6 involvement in microtubule alterations in CASQ2-KO cardiomyocytes .....	41
3.6	TRDN interacts with the microtubule network .....	43
3.7	Defective TRDN trafficking in CASQ2-KO cardiomyocytes .....	44
3.8	Microtubule polymerization modulation affects TRDN position in CASQ2-KO cardiomyocytes ....	44
3.8.1	Colchicine treatment .....	45
3.8.2	Taxol treatment .....	46
3.9	HADAC6 inhibition improves TRDN localization in CASQ2-KO cardiomyocytes.....	47
3.10	Microtubule-associated proteins could be involved in the expansion of CASQ2-KO jSR.....	48
3.11	Microtubule derangement explains the expansion of the jSR in CASQ2-KO .....	49
3.12	TRDN degradation in CASQ2-KO.....	51
3.13	TRDN mRNA content in CASQ2-KO heart.....	51
3.14	Proteasome inhibition .....	51
3.15	Autophagy flux in CASQ2-KO heart .....	52
3.16	Inhibition of early autophagosome formation in CASQ2-KO cardiomyocytes.....	53
3.17	TRDN is degraded by autophagy in CASQ2-KO.....	55
3.18	Aggrephagy drives TRDN degradation in CASQ2-KO cardiac myocytes.....	56

3.19	Protein proximity by FRET microscopy in CASQ2-KO cardiomyocytes.....	57
3.20	AAV9-CASQ2 infection in CASQ2-KO mice .....	59
4.	METHODS.....	61
4.1	Proteomic study.....	61
4.1.1	Preparation of mouse tissue protein extracts.....	61
4.1.2	Protein digestion of protein extracts.....	61
4.1.3	Stable isotope labelling of peptides .....	61
4.1.4	LC-MS/MS analysis .....	62
4.1.5	Database searching.....	62
4.1.6	Quantification at the peptide, protein and category levels .....	62
4.1.7	Protein functional annotation .....	63
4.2	Animal procedures .....	63
4.2.1	Ethical aspects .....	63
4.2.2	Choice of mouse model.....	63
4.2.3	Drug treatments .....	63
4.2.4	Isolation of ventricular myocytes .....	64
4.2.5	AAV9-CASQ2 viral construct and infection procedure in CASQ2-KO mice.....	64
4.3	Two-Color confocal and stimulated emission depletion (STED) microscopy in immunostained ventricular myocytes.....	64
4.3.1	Immunostaining protocol .....	64
4.3.2	Colocalization (STED) and microtubule extension (confocal) experiments .....	65
4.3.3	Colocalization analysis.....	66
4.3.4	Analysis of delocalized Triadin.....	67
4.3.5	Microtubule extension analysis.....	67
4.3.6	Autophagy inhibition experiments in living cardiomyocytes .....	67
4.3.7	Sample preparation for FLIM-FRET microscopy .....	68
4.4	Quantitative Real Time PCR.....	68
4.5	Western Blot Analysis.....	68
4.6	Proteasome inhibition .....	69

4.7	HDAC6 activity assay .....	69
4.8	Co-Immunoprecipitation assay.....	69
4.9	Protein aggregation assay .....	70
4.10	Proximity ligation assay (PLA).....	70
4.11	Generation of the viral construct .....	70
4.12	Antibodies.....	71
4.13	Statistics.....	71
5.	Discussion .....	72
5.1	Disruption of microtubules drives the delocalization of TRDN .....	72
5.2	CASQ2 gene transfer in CASQ2-KO mice .....	74
5.3	Autophagy is the pathway for TRDN degradation.....	74
5.4	Microtubule derangement explains expansion of the jSR .....	75
6.	Conclusions .....	77
7.	Conclusiones .....	78
8.	Bibliography .....	79

# 1. Introduction

## 1.1 Cardiac muscle cell

Thirty per cent of the cells in the heart are contractile, specialized non-dividing striated muscle cells called cardiomyocytes. Cardiomyocytes are polynucleated cells, having in average a dimension of 20  $\mu\text{m}$  in diameter and 50-100  $\mu\text{m}$  in length (Franke et al., 2007) and given their substantial size cardiomyocytes represent 70% of the volume of the heart. They are interconnected through multimeric protein complexes called desmosomes and gap junctions (Figure 1.1). These structures not only ensure a physical connection but also allow the electrical coupling among cells (Perriard et al., 2003). Light microscopy allows to visualize the striated architecture of cardiomyocytes provided by the sarcomeres, which are composed by parallel thick and thin filaments of myosin and actin, respectively. The sarcomere is the contractile unit that allows the contraction of cardiac cells. The organization of the thin filaments forms an electron-dense structure called the I band; the A band includes both thin and thick filaments; the H zone, where there are only myosin fibers; and the Z line, formed by alpha Actinin is a structure perpendicular to the I band and A band that acts as the backbone for the binding of the actin filaments and well as the binding of the giant proteins Titin and Nebuline. The Z lines provide the boundaries for the sarcomere. Contraction of cardiac cells is mediated by the sliding of the actin filaments on the myosin filaments allowing the shortening of the sarcomere (*Ganong. Fisiologia Medica, 2021*).

Particularly interesting is the organization of the cell membrane (the sarcolemma) that is characterized by a series of invaginations along the Z-lines called T-tubules. These invaginations are coupled to extensions of the endoplasmic reticulum, called sarcoplasmic reticulum (SR).

Moreover the proximal area of the SR is called Junctional sarcoplasmic reticulum (jSR) and the adjacency of this area with the sarcolemmal membrane (T-tubule) is called *Dyad* (Clara Franzini-Armstrong et al., 2005). The term *Dyad* refers to the structural element of the assembly while a *Couplon* is the functional element, within the *Dyad*, formed by the juxtaposition of Ryanodine receptors type 2 (RYR2) in the jSR with cardiac L-type voltage-gated  $\text{Ca}^{2+}$  channels (Cav1.2) in the adjacent plasmalemma (T-Tubule) (Figure 1.2) (Scriven et al., 2013).

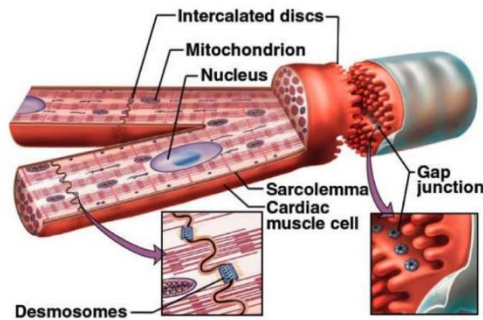


**Figure 1.1– Cardiomyocyte’s structure**

(<http://www.cardio-research.com/cardiomyocytes?tmpl=/system/app/templates/print/,showPrintDialog=1>)

## 1.1 T-Tubule

T-tubules in cardiac muscle have a mean diameter of  $\approx 200$  to  $300$  nm and they are formed mainly by invaginations along the Z-line that protrude from the sarcolemma (Sommer, 1982) (Figure 1.2). The T-tubule network is not a simple transverse system of tubules, but is a complex system of branching tubules with both transverse and longitudinal elements (Bers, 2002).

The study of cells lacking of T-tubules (atrial, neonatal and Purkinje cells) has revealed the function of these structures in ventricular myocytes. After electrical stimulation of de-tubulated cells,  $\text{Ca}^{2+}$ -release events are produced ( $\text{Ca}^{2+}$  sparks) and occur predominantly close to the sarcolemma’s surface (Lipp et al., 1996). In contrast, in adult ventricular myocytes,  $\text{Ca}^{2+}$  release events occur synchronously across the entire width of the cell and  $\text{Ca}^{2+}$  sparks arise predominantly in the vicinity of the t-tubule (Shacklock et al., 1995). These data are consistent with the notion that T-tubules play an important role in causing synchronous  $\text{Ca}^{2+}$  release in the adult ventricular myocyte, due to the presence of L-type  $\text{Ca}^{2+}$  channels in this region ( $\text{Ca}^{2+}$  Handling Proteins), therefore making this structure fundamental for Excitation-Contraction Coupling (Kohl et al., 2013).

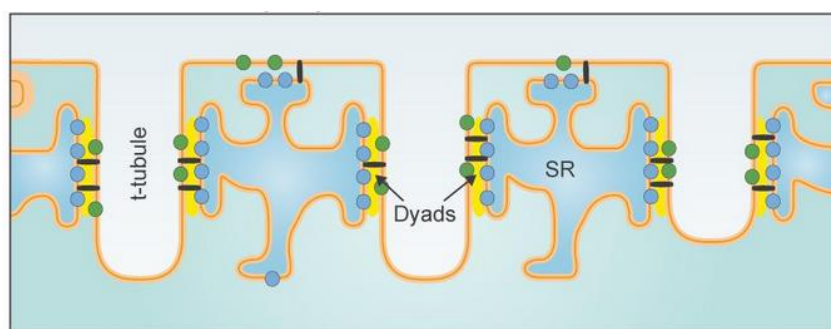


**Figure 1.2– Organization of the Dyads**

Representative image of sarcolemmal invaginations forming T-tubules facing the SR area. Green dots represent the L-type  $\text{Ca}^{2+}$  channels; Blue dots represent the  $\text{RyR2}$  complexes (P. P. Jones et al., 2018).

## 1.2 Excitation-Contraction Coupling (ECC)

The term Excitation-contraction (EC) coupling was coined in 1952 to describe the mechanism of conversion of an electrical stimulus into a mechanical contractile response (A. Fabiato, Fabiato, 1975). The process is mainly conveyed by  $\text{Ca}^{2+}$  movements in and out of SR, the main  $\text{Ca}^{2+}$  storage site in cardiomyocytes..

The activation of the process is the propagation of the membrane depolarization generated by pacemaker cells that propagates along all the cell membranes in the tissue. Thanks to the peculiar sarcolemmal organization in T-tubules, this electrical stimulus propagates in those invaginations where the L-  $\text{Ca}^{2+}$  type channels (Cav1.2) are mainly expressed. L-  $\text{Ca}^{2+}$  type channels are Voltage dependent channels and they conduce the current  $I_{\text{Ca}}$  that is an important inward current that brings calcium inside the cytoplasm.  $I_{\text{Ca}}$  is responsible for the plateau of the cardiac action potential in humans. Since T-tubules directly face the jSR, the L-type  $\text{Ca}^{2+}$  channels directly face the Ryanodine receptor 2 (RyR2) channels located in the jSR (Figure 1.2).

Since the cytoplasmic portion of RyR2 channels contain high-affinity  $\text{Ca}^{2+}$  activation sites (Eisner et al., 2017), the  $\text{Ca}^{2+}$  that enters in the dyadic space via  $I_{\text{Ca}}$  acts as a signal to promote the opening of the RyR2s therein. Once some RyR2s activate, they release more  $\text{Ca}^{2+}$ , which in turn activates more RyR2s. This positive-feedback mechanism is called  $\text{Ca}^{2+}$  induced  $\text{Ca}^{2+}$  release (CICR) (Alexandre Fabiato, Fabiato, 1979), and it continues to occur until the SR empties of sufficient  $\text{Ca}^{2+}$  so that release termination mechanisms become activated. Such mechanisms are mediated by the negative RyR2 regulator Calsequestrin 2 (see below for further details on Calsequestrin 2).

The  $\text{Ca}^{2+}$  thus released, with the small contribution of  $I_{\text{Ca}}$ , diffuses from the dyadic space towards the bulk cytosol, where its increased levels initiate a coordinated whole-cell contraction.

$\text{Ca}^{2+}$  handling homeostasis is restored by further  $\text{Ca}^{2+}$  fluxes: the  $\text{Ca}^{2+}$  released from the SR is uptaken by the Sarco-Endoplasmic Reticulum  $\text{Ca}^{2+}$  ATPase (SERCA), while the  $\text{Ca}^{2+}$  entered through the L-  $\text{Ca}^{2+}$  type channels is extruded out of the cell by the  $\text{Na}^{+}$ - $\text{Ca}^{2+}$  exchanger (NCX).

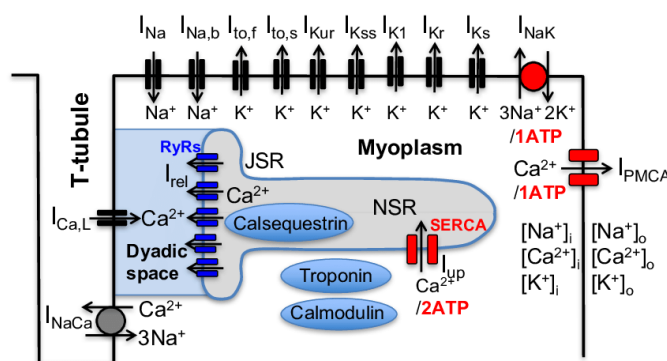


**Figure 1.3 – Excitation-Contraction coupling**

Protein complexes, cardiomyocytes architecture and intracellular organelles involved in excitation–contraction coupling. Entry of  $\text{Ca}^{2+}$  into the cell triggers the release of  $\text{Ca}^{2+}$  from the sarcoplasmic reticulum through the RyR2 channel.  $\text{Ca}^{2+}$  then binds to the troponin complex and activates the contractile apparatus (the sarcomere). Relaxation occurs upon removal of  $\text{Ca}^{2+}$  from the cytosol via  $\text{Ca}^{2+}$  uptake into the sarcoplasmic reticulum where  $\text{Ca}^{2+}$  binds to Calsequestrin and via  $\text{Ca}^{2+}$  transport out the cell by the  $\text{Na}^{+}/\text{Ca}^{2+}$  exchanger (Rees et al., 2018).



### 1.3 The cardiac $\text{Ca}^{2+}$ release unit

The Couplon region is a specialized type of Calcium release unit (CRU) in mouse ventricular myocytes, where T-tubules are very abundant and connect periodically with the jSR, most of the CRUs are couplons. However, in ventricular myocytes from large mammals such as swine or humans, which present less developed T-tubules (Dries et al., 2016), about 70% of the jSR forms couplons, whereas the remaining 30% of the CRUs do not contain T-tubules but contain all the other protein complexes needed to release calcium (the so-called corbular SR). From now on, since this Ph.D. Thesis focuses on the use of murine models (in which 99% of the CRUs are couplons), we will interchangeably use both terms.

Couplons consist of several protein complexes able to modulate the  $\text{Ca}^{2+}$  sorting from the SR. From the T-tubular side the L-type channel is complexed with its signalosome (e.g. Calmodulin, kinases). On the SR side the Ryanodine receptor 2 (RyR2) calcium release channel is complexed with Calsequestrin 2 (CASQ2), a negative regulator, and Triadin (TRDN) and Junctin (JNT), which are positive regulators (Leenhardt et al., 1995b), kinases, phosphatases and other calcium release regulators. Most authors would locate SERCA outside of the jSR, in non-junctional SR (our FLIM-FRET experiments, see Results, agree with this interpretation). The junctions between jSR and plasmalemma/T-tubules function as discrete calcium release units and are the sites where Calcium sparks are detected. The cardiac action potential, by promoting the simultaneous cell-wide opening of the L-type channels, coordinates all these independent CRUs into a whole-cell  $\text{Ca}^{2+}$  release. In pathologic cases, such as CPVT2 (see below) and heart failure, calcium release may “jump” uncoordinately from CRU to CRU to form the so-called  $\text{Ca}^{2+}$  waves, which are arrhythmogenic and force ATP expenditure on the part of the cell (to restore homeostasis).

### 1.4 Ryanodine receptor 2 (RyR2)

RyR is a homotetramer composed by four monomers each and it is the largest ion channel protein yet identified (Takeshima et al., 1989). RyR is found in the jSR membrane and is the responsible for  $\text{Ca}^{2+}$  release from the SR. In smooth muscle and non-muscle cells including blood vessels, neurons and lymphocytes RyR couples with the inositol 1,4,5-trisphosphate (IP3) receptor, generating a super family of a ligand gated intracellular cation channels.

Three types of RyRs were identified in different tissues: Ryanodine receptor Type1 (RyR1) mainly expressed in skeletal muscle, Ryanodine receptor Type2 (RyR2) mainly expressed in the cardiac tissue and Ryanodine receptor Type3 (RyR3) mainly expressed in the central nervous system. There is strong sequence homology between the three isoforms: 66% between RyR1 and RyR2; 67% between RyR1 and RyR3; 70% between RyR2 and RyR3 (Hakamata et al., 1992; Otsu et al., 1990; Protasi, 2002; Zorzato et al., 1990).

The cardiac isoform (RyR2) has a very high molecular weight (565 KDa) and it is composed by 4967 amino acids (human), encoded by the gene localized on chromosome 1 (1q42-q43) (Swan et al., 1999) (Figure 1.4).

The C-terminal region of RyR2 is composed by 6 transmembrane segments (Dhindwal et al., 2017; Du et al., 2002; Silvia G. Priori, Napolitano, 2005). Although this region represents only 10% of the protein, it contains the sequences controlling RyR2 localization and oligomerization and it composes the channel's pore (Stewart et al., 2003). The rest of the protein sequence represents the cytoplasmic structural region responsible for the channel regulation. RyR2 interacts with several regulatory proteins in different regions of its structure, to form a macromolecular complex: at the SR membrane and the SR lumen, RyR2 interacts with Junctin, Triadin and Calsequestrin; in the dyadic space, with Calmodulin, Protein Phosphatases 1 and 2, Protein Kinase A, Ca/Calmodulin-dependent Protein Kinase 2, Calcineurin, and A and B isoforms of Protein Kinase C (Masumiya et al., 2003; Meissner, 2004).

RyR2 channels have low resting activity at diastolic  $\text{Ca}^{2+}$  levels, but their “open probability” can be modulated either by RyR2-associated proteins and/or covalent modification such as phosphorylation during beta-adrenergic stimulation.

RyR2, together with its macromolecular complex, is organized in clusters. This peculiar organization plays an important role in the function of the channel: (1) The sum of numerous individual channels, coordinated via  $\text{Ca}^{2+}$  induced  $\text{Ca}^{2+}$  release, generates a fast release of ions while allowing quick release termination mechanisms (Ríos et al., 2015). (2) The RyR2 proximity to other RyR2s helps the synchronization with a small number of sarcolemmal L-type Cav channels.

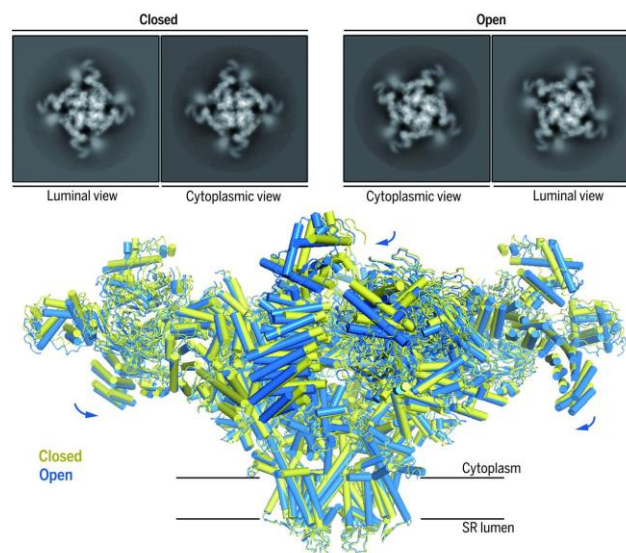


**Figure 1.4 – RyR2 structure**

(**Top**) Electron micrograph images of open/closed RyR2. (**Bottom**) overlapped RyR2 structure in open (blue) or close (green) conformation (Peng et al., 2016).

## 1.5 Calsequestrin 2 (CASQ2)

Calsequestrin (CASQ2) is a glycoprotein identified for the first time in rabbit skeletal muscle (MacLennan, Wong, 1971). The cardiac isoform was isolated later and after the study of its crystal structure, the  $\text{Ca}^{2+}$  binding ability of the protein was identified (Campbell et al., 1983). CASQ2 is composed of three domains each with negatively charged thioredoxin-like folds with four helix surrounding a sheet core. Due to high aromatic acid content, the core of each domain is hydrophobic and requires  $\text{Ca}^{2+}$  for its stabilization (Figure 1.5).

CASQ2 is a polymerized protein, whereby each addition of monomers to the polymer chain creates de-novo negatively-charged  $\text{Ca}^{2+}$ -binding pockets (S. Wang et al., 1998). Therefore, CASQ2 polymerization is dependent on  $\text{Ca}^{2+}$  concentration.  $\text{Ca}^{2+}$ -induced dimerization starts at ion concentrations in the range of 0.5–1 mM, and at 3 mM Ca there is a detectable tetramer population (H. J. Park et al., 2004). Once the polymeric state is reached 40  $\text{Ca}^{2+}$  ions are bound to the molecule (Murphy et al., 2011). By electron microscopy it has been observed that the CASQ2 network is localized under the jSR membrane (C. Franzini-Armstrong et al., 1987) and this localization, in proximity to the RyR2, is achieved thanks to the transmembrane proteins TRDN and JCT, forming a protein complex that regulates RyR2 and the  $\text{Ca}^{2+}$  release as discussed above (Scriven et al., 2000).

CASQ2  $\text{Ca}^{2+}$  binding affinity is low, so that when RyR2 releases  $\text{Ca}^{2+}$  from the SR to the cytoplasm, the local jSR  $[\text{Ca}^{2+}]$  decreases, and CASQ2 quickly releases  $\text{Ca}^{2+}$ . Therefore, CASQ2 represents a molecule responsible for local storage of  $\text{Ca}^{2+}$  and for its mobility (Murphy et al., 2011).

CASQ2 is not only important for  $\text{Ca}^{2+}$  handling but it also regulates RyR2 channel opening probability, likely through its interaction with TRDN and JNT (Györke et al., 2004; Terentyev et al., 2007).

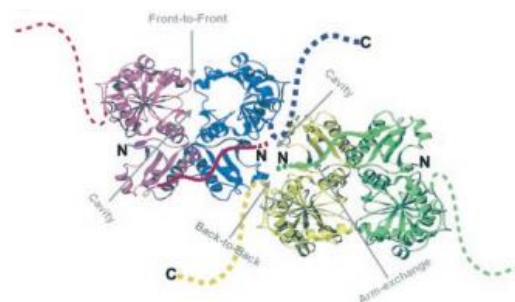


**Figure 1.5 – Crystal structure of Calsequestrin**

Illustration of the interactions between four Calsequestrin molecules each showing the crystal structure of Calsequestrin from rabbit skeletal muscle SR. Front-to-front interactions are shown between the red molecule and the blue molecule and between the yellow molecule and the green molecule. A back-to-back interaction is shown between the yellow molecule and the blue molecule (H. J. Park et al., 2003).

## 1.6 Triadin (TRDN)

Triadin (TRDN) is a transmembrane protein located in the Endoplasmic reticulum (ER) identified for the first time in the triad of the skeletal muscle (Brandt et al., 1990; K. C. Kim et al., 1990). Since its discovery, many

studies were published identifying other two isoforms (Vassilopoulos et al., 2005) and demonstrating their expression in heart (Kobayashi, Jones, 1999). The human Triadin gene TRDN is located on chromosome 6.7. It covers 420 kb and comprises at least 41 exons. The isoforms of Triadin are derived from a single gene by alternative splicing and are tissue specific (Thevenon et al., 2003): Trisk 92, Trisk 51, Trisk32 (Figure 1.6). Their name is related to the corresponding molecular weight. Trisk 95 and Trisk 51 are located in the triad of skeletal muscle where they are associated with RyR1. Therefore, these two Triadin isoforms are full members of the calcium release complex (Marty et al., 2000; Vassilopoulos et al., 2005). The situation is different for Trisk 32 (also called CT1); is found in heart and it associates with RyR2; while in skeletal muscle the protein is mainly located longitudinally across the sarcoplasmic reticulum (Vassilopoulos et al., 2005) and therefore not associated with RyR1.

The N-terminal (cytoplasmatic) and the trans-membrane region are the only domains fully shared between the isoforms; the shorter TRDN isoforms are truncated versions of Trisk92 (in the C-terminal region). Trisk 95 is able to form large polymers because of its two cysteines (Froemming et al., 1999) while Trisk 51 has only one cysteine and this causes a reduction in the size of Triadin polymers. Trisk32 is reportedly not able to form homo-polymers (Marty, 2015).

TRDN together with JNT, plays the role of a “bridge” protein between RyR2 and CASQ2. When CASQ2 is bound through the homology motif (KEKE) with TRDN, RyR2 remains closed; while if CASQ2 is free in the lumen (i.e. unbound from the RyR2), RyR2 increases its “Open Probability” (Po), increasing the  $\text{Ca}^{2+}$  leak from the SR (Györke et al., 2004). Furthermore, TRDN and JNT give structural stability to the RyR2 channel during periods of intense activity (L. Zhang et al., 1997). These results suggest that a complex of CASQ2, TRDN, and JNT confers luminal  $\text{Ca}^{2+}$  sensitivity to RyR2.

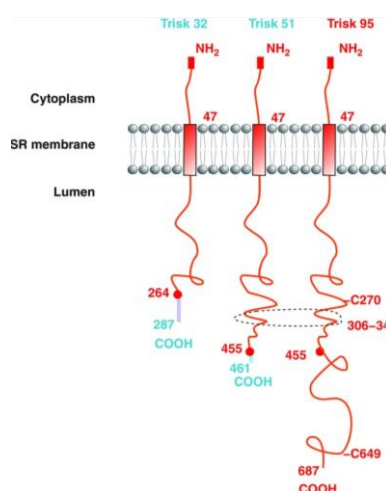


**Figure 1.6 – Representative structure of Triadin’s isoforms**

(Marty et al., 2009)

## 1.7 Junctin (JNT)

AbH-J-J genomic locus is responsible by alternative splicing of the expression of Aspartyl beta-hydroxylase (AbH), Junctin (JNT) and Junctate (Feriotto et al., 2005). AbH was first identified in bovine liver as an enzyme able to hydroxylate Asp and Asn in some epidermal growth factor (EGF)-like domains in different proteins (Jia et al., 1992; Q. Wang et al., 1991). Junctate was identified as a novel  $\text{Ca}^{2+}$  binding protein located in the endoplasmic reticulum (ER)/SR membranes (Dinchuk et al., 2000; Hong et al., 2001; Treves et al., 2000). Lastly, Junctin was first identified as a 26-kDa (210 amino acids) Calsequestrin-binding protein in the SR (L. R. Jones et al., 1995) and a further study showed that Junctin could interact with RyR, CASQ and TRDN (through the KEKE motif) at the junctional SR of striated muscle cells (L. Zhang et al., 1997). JNT and TRDN share a similar sequence, structure and interactome, confirming their similar function (L. Zhang et al., 1997). In heart as well as in skeletal muscle, Junctin and Triadin each increase the activity of RyR2 channels in the absence of CASQ2 (Györke et al., 2004).

## 1.8 Junctophilin 2 (JPH2)

A common feature of all excitable cell types are junctional membrane complexes (JCMs) which are structural contacts between the plasma membrane and the endoplasmic/sarcoplasmic reticulum. Junctophilins (JPHs) are a recently identified family of membrane spanning proteins that contribute to the formation and the maintenance of JCMs, by serving as a physical bridge between the plasma membrane and ER/SR membrane in different excitable cells. Four isoforms of JPH have been identified so far: JPH1-4. JPH1 and JPH2 are both expressed in skeletal muscle while in cardiac muscle only JPH2 is expressed (Landstrom et al., 2011). In brain both JPH3 and JPH4 are expressed in similar neuronal sites and contribute to JMCs formation (Takeshima et al., 2015). All of Junctophilin subtypes are characterized by a C-terminal hydrophobic segment spanning the endoplasmic/sarcoplasmic reticulum membrane and a remaining cytoplasmic membrane domain characterized by a conserved sequence of 14 amino acid residues (MORN motifs) which is repeated eight times in the N-terminal region (Takeshima et al., 2015).

In the heart the crosstalk between L-type  $\text{Ca}^{2+}$  channels on the sarcolemma membrane and the RYR2 on the SR membrane is a fundamental feature of excitation-contraction coupling (Minamisawa et al., 2004), in fact JPH2 dysregulation has been associated with a variety of heart diseases.

The analysis of samples from patients with hypertrophic/dilated cardiomyopathy or with myocardial ischemia revealed that JPH2 is severely downregulated compared to samples from healthy controls. Moreover, several studies have shown the marked reduction of the expression of JPH2 in response to cardiac stress. Cardiac stress can also impair trafficking of JPH2 in failing myocytes, including loss of localization at the T-tubule/Z-line region and redistribution to the peripheral plasma membrane (Takeshima et al., 2015). Previous studies demonstrated that JPH2-null mice die during the early embryonic development due to cardiac failure

(Takeshima et al., 2015). Isolated cardiomyocytes from JPH2-knockout embryos have a defective peripheral coupling, abnormal SR  $\text{Ca}^{2+}$  signaling and impaired CICR during E-C coupling, all caused by a functional uncoupling between DHPRs and RyRs. Therefore, JPH2 in the embryonic heart is an essential protein for the functional communication between DHPRs and RYRs and contributes to  $\text{Ca}^{2+}$  signalling during the heartbeat (Matsushita et al., 2007)

### **1.1 Catecholaminergic polymorphic ventricular tachycardia (CPVT)**

Catecholaminergic Polymorphic Ventricular Tachycardia (CPVT) was described for the first time in 1975 (Reid et al., 1975) and characterized by Coumel in 1978 (Coumel P FJ, Lucet V, Attuel P, 1978). CPVT is a genetic disease characterized by mutations in genes responsible for  $\text{Ca}^{2+}$  handling in cardiomyocytes. The pathological phenotype is characterized by polymorphic ventricular tachycardia, occurring in structurally intact hearts, induced by physical and/or emotional stress mediated by beta adrenergic activation. Arrhythmias occurring in CPVT patients can easily degenerate in ventricular fibrillation leading to sudden cardiac death (Lehnart et al., 2004). The onset of arrhythmias and syncopal episodes (N. Liu , Priori, 2008; Reid et al., 1975) manifest around age 12 (Hayashi et al., 2009; Silvia G. Priori et al., 2002). However sudden cardiac death can be the first manifestation of the disease (Maragna , Napolitano, 2018) therefore making difficult to establish the clinical diagnosis to the benefit of the family members, CPVT diagnosis is challenging also because patients present normal resting ECGs and unless patients are exposed to exercise stress tests (Silvia G. Priori et al., 2002) it is difficult to observe ventricular arrhythmias. Based on the clear evidence of the critical role of adrenergic stimulation as a trigger for arrhythmias in CPVT, beta-blockers were proposed as the primary pharmacological treatment for CPVT (Rosso et al., 2007; Watanabe et al., 2009). For the difficult patient (i.e. non-responsive to beta-blocker treatment), additional pharmacological treatment, sympathetic cardiac denervation and implantation of an implantable cardioverter defibrillator have been considered (Sumitomo et al., 2003).

The primary cellular cause of the disease is the alteration of  $\text{Ca}^{2+}$  handling in ventricular cardiomyocytes. Mutations on genes encoding the RyR2 channel or the proteins that regulate it, lead to untimely diastolic  $\text{Ca}^{2+}$  release from the SR into the cytoplasm, in the form of  $\text{Ca}^{2+}$  waves. The elevation in cytosolic  $\text{Ca}^{2+}$  produced by this spontaneous release, activates the sodium calcium exchanger (NCX) that produces a depolarizing current responsible for the membrane depolarization. Those spontaneous depolarizations are called delayed afterdepolarization (DADs) and, if DADs reach the membrane depolarization threshold necessary for the opening of sodium channels (-60 mV), a spontaneous action potential is generated (triggered activity). Triggered activity in turn generates extra heartbeats (Tachycardia) (Marban et al., 1986).

## **1.2 Different forms of CPVT**

Although the first characterization of the disease was made between the 1970 and 1980, it was only in 2001 that a CPVT causative mutation on RyR2 was identified and the arrhythmogenic mechanisms characterized (Silvia G Priori et al., 2001). In the following years other gain-of-function mutations in RyR2's accessory proteins were associated with the disease.

### **1.2.1 CPVT 1**

Mutations in the RyR2 channel cause the dominant form of CPVT. Until now, more than 110 RYR2 mutations have been reported (Silvia G. Priori et al., 2021). The common mechanism by which RyR2 causes CPVT relies on the reduced binding affinity of RyR2 to the regulatory protein FKBP12.6 at resting state and even more so after beta-adrenergic stimulation, which causes RyR2 phosphorylation by PKA (Wehrens et al., 2003). Another proposed mechanism is that RyR2 mutations increase endoluminal activation sensitivity for Calcium thus increasing the predisposition to spontaneous  $\text{Ca}^{2+}$  release from SR (Jiang et al., 2004; Silvia G Priori et al., 2001).

### **1.2.2 CPVT 2**

Homozygous loss-of-function mutations in CASQ2 cause the recessive form of Catecholaminergic Polymorphic Ventricular Tachycardia (CPVT) (Chopra et al., 2007; Di Barletta et al., 2006; Knollmann et al., 2006; Liu, Priori, 2008). The causative mutation impair critical functions of the protein by impairing the reversible Calsequestrin polymerization (Bal et al., 2010), reduce the binding of CASQ2 to Triadin and Junctin (Houle et al., 2004), modify the regulatory function on the Ryanodine receptor by stabilizing the closing of the channel in diastole (E. J. Kim et al., 2007; Rizzi et al., 2008; Terentyev et al., 2006; Valle et al., 2008). The presence of mutations also reduces the amount of the protein and patients with homozygous non-sense mutations can be totally deprived of CASQ2 (Postma et al., 2002). Overall, the mutations that cause recessive CPVT lead to diastolic calcium release and development of DADs as observed in CPVT1.

The first characterization of the CASQ2-KO mouse model proved that the model replicates well the CPVT2 phenotype showing that  $\text{Ca}^{2+}$  induced SR  $\text{Ca}^{2+}$  release is normal in resting condition, while under catecholaminergic challenge, spontaneous SR  $\text{Ca}^{2+}$  release occurs (Knollmann et al., 2006). CASQ2-KO mice hearts show significant reductions of protein quantities of other Couplon proteins such as TRDN and JNT (Faggioni, Knollmann, 2012). Furthermore, CASQ2-KO cardiomyocytes present ultrastructural modifications of the SR which was found to be remodeled and expanded by Electron microscopy analysis. This has been interpreted as a compensatory mechanism to maintain  $\text{Ca}^{2+}$  content in the jSR despite the absence of CASQ2. In fact the SR  $\text{Ca}^{2+}$  content is not different or very slightly decreased vs. WT myocytes.

### 1.2.3 CPVT 3

Mutations in the TECRL gene, expressing the Trans-2,3-enoyl-CoA reductase-like protein, are responsible for CPVT3. TECRL is believed to be involved in long fatty acids biosynthesis in the Endoplasmic Reticulum, which involves a redox reaction step. In adult hearts, free fatty acids represents the first energy source and alterations in long fatty acids chains oxidation has been associated with arrhythmias. Patients affected with CPVT3 show a pathological phenotype that shares features of both CPVT and long QT syndrome (LQTS) (Devalla et al., 2016).

### 1.2.4 CPVT 4

CPVT4, similarly to CPVT1, has an autosomal dominant inheritance but the affected gene is the one encoding for Calmodulin 1 (CAM1). Calmodulin 1 is a  $\text{Ca}^{2+}$ -binding protein responsible for modulating  $\text{Ca}^{2+}$  release from the SR into the sarcoplasm, establishing interactions with a large number of proteins and enzymes essential for cardiac contraction, among them the RyR2 and the L-type  $\text{Ca}^{2+}$  channel.

CAM1 has four  $\text{Ca}^{2+}$  binding sites and as calcium ions bind to its structure, the protein undergoes  $\text{Ca}^{2+}$  dependent conformational changes that increase its affinity for target proteins, therefore modulating their function. In cardiac muscle CAM1 binds to RyR2 at the cytosolic portion of the channel, and this interaction reduces the opening probability of the channel. Mutations in CAM1 reduce the affinity of the protein for RyR2, thus increasing the open probability of the channel and spontaneous release of  $\text{Ca}^{2+}$  (L. Xu , Meissner, 2004).

### 1.2.5 CPVT 5

In CPVT5, Triadin (TRDN) is mutated or absent. The work of Roux et al. revealed that a cohort of patients with CPVT had mutations in Triadin and not in RyR2 or CASQ2 (Roux-buisson et al., 2012). This investigation revealed the fifth type of CPVT, which has an Autosomal Recessive inheritance. They managed to isolate the mutations at a region within the Triadin gene that is common to the different isoforms, thereby implicating that these mutations could also affect skeletal muscle. In agreement with this interpretation, patients with CPVT5 in the Roux cohort showed muscle weakness alongise cardiac manifestations such as arrhythmias due to  $\beta$ -adrenergic stimulation, T-wave inversions, transient QT prolongation. Severe disease penetrance was found, with presentation of exercise-induced cardiac arrest in early childhood (Clemens et al., 2019).

Ablation of TRND or the presence of homozygous missense mutations have been reported to induce calcium leak from the SR. This is due to the fact that TRDN serves as an scaffolding protein for CASQ2, so with Triadin missing the RyR2s suffer from lack of binding to Triadin (Cacheux et al., 2019; Terentyev et al., 2005)



In addition, the TRDN-KO mice showed a reduction in the expression of RyR2, JNT, CASQ2, JPH2, JPH1. Moreover, the junctional SR domains of TRDN-KO myocytes were less extensive, jSR width was reduced and showed a decrease of 50% in areas occupied by RyR2 (Chopra et al., 2009). Besides, the (transient) QT prolongation has been attributed to lack of calcium dependent inactivation of the L-type  $\text{Ca}^{2+}$  channel. It is believed that the SR structural arrangements may play a role in this phenotype, since the RyR2s get separated from the L-type  $\text{Ca}^{2+}$  channel (Chopra et al., 2009).

### 1.3 Microtubular network

Microtubules have a diameter of roughly 25 nm and are formed by polymerization of dimers of alpha and beta Tubulin. Their size is variable between cells and individual microtubules can reach up to 10 microns in length (Gittes et al., 1993). The microtubular network is characterized by a dynamic equilibrium since cells undergo phases of growth (polymerization), shrinkage (catastrophe) or stability (Desai , Mitchison, 1997). This ability relies on the fact that 50% of the expressed tubulin is free in the cytoplasm, ready for the polymerization phase (Cooper , 2006; J. Fassett et al., 2019; J. T. Fassett et al., 2013). In adult cardiomyocytes, different populations of microtubules coexist and play different roles (mainly structural or involved in protein transport): mitochondrial localization dynamic, perinuclear shaping, cortical microtubules (that wrap around the cell) and inter-myofibrillar microtubules. The latter is particularly interesting for its function in organelle positioning, T-tubule-SR morphology (Meunier et al., 2009; Prosser et al., 2011; C. Zhang et al., 2014), intercalated disc maintenance (S. S. Zhang , Shaw, 2014) and in the regulation of myofilament mechanics (Caporizzo et al., 2018; Robison et al., 2016; Tsutsui et al., 1993) .

The dynamics, structure and transport management of microtubules are controlled by interactions with microtubule associated protein (MAPs) and post-translational modification (PTMs).

There are two primary classes of MAPs: molecular motors and structural MAP (Bodakuntla et al., n.d.; Monroy et al., 2018; Portran et al., 2013.; Stanhope , Ross, 2015)

The function of cargo transport is mediated by the motor protein kinesin (transport in the direction of the growing filament) and dynein (retrograde transport) (Caporizzo et al., 2019). Structural MAPs can influence the stability of microtubules by directly acting on microtubule's structure, by either blocking or recruiting structural proteins or by affecting the association of microtubules with other cytoskeletal elements (Logan , Menko, 2019; Ramkumar et al., 2018; Xiao et al., 2012). MAPs interact with each other, either cooperatively or competitively, and the affinity of MAPs for microtubules is strongly affected by PTMs.

For example, phosphorylation precludes the incorporation of tubulin dimers into microtubules thus downregulating microtubule polymerization while also affecting the MAPs' binding ability (Wandosell et al., 1987). For instance, phosphorylation regulates the microtubule-associated protein TAU. While being famous for its role in neurodegenerative diseases, TAU is also expressed in the heart (Gu et al., 1996). TAU can protect microtubules from severing (Sudo, Baas, 2010) and may provide additional stabilization of cardiac microtubules (Betrie et al., 2017)

Detyrosination of microtubules is a PTM that facilitates the interaction of intermediate filaments that form complexes with the sarcomere by altering myocyte stiffness, contractility, and mechano-signalling (Robison, Prosser, 2017). Glutamylation and glycylation, particularly studied in neurobiology, can regulate microtubule density (Song et al., 2013). Polyamination of tubulin stabilizes microtubules and prevents their depolymerization (Song et al., 2013). Acetylation of the lysine 40 (K40) of  $\alpha$ -tubulin has received particular attention since it is the only tubulin PTM to be found in the lumen of microtubules: most of tubulin's PTMs are instead found on the outer surface of the microtubule (Soppina et al., 2012). Acetylated microtubules were found to last longer and be more stable. Acetylation of  $\alpha$  tubulin at conserved lysine 40 (K40) does indeed protect microtubules from destabilization, making them softer and thus more resistant to the damage induced by mechanical bending (Janke, Montagnac, 2017). Acetylation alters the conformational landscape of the flexible loop that contains  $\alpha$  tubulin K40, restricting the range of motion of the K40 loop. In the deacetylated state, the loop extends deeper into the microtubule lumen and samples a greater number of conformations, increasing its accessibility to the acetylases, influencing lateral contacts affecting microtubule stability and function (Eshun-Wilson et al., 2019) (Figure 1.7).

The acetylation of  $\alpha$ -Tubulin is mediated by  $\alpha$ TAT1 (Janke, Montagnac, 2017) while histone deacetylase 6 (HDAC6) has been reported to be implicated in the deacetylation (Hubbert et al., 2002).

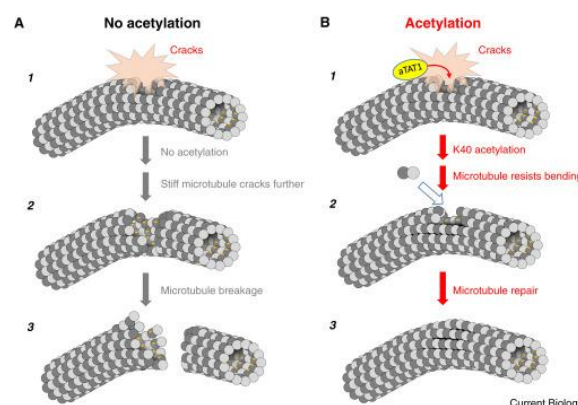


**Figure 1.7 – Effect of  $\alpha$ -Tubulin acetylation on microtubule stability**

- A- Deacetylation of  $\alpha$ -Tubulin causes microtubules breakage under physical stress
- B-  $\alpha$ -Tubulin K40 acetylation helps microtubules to resist to bending (Janke, Montagnac, 2017).

#### **1.4 Histone deacetylase 6 (HDAC6)**

Histone Deacetylases (HDACs) is a family of several enzymes firstly described as DNA packaging proteins. HDACs catalyze the removal of an acetyl group from lysine residues on histone tails. Therefore, when HDACs are more active, histone proteins are bound more tightly to DNA, making it more difficult for transcriptional proteins to make contact with DNA, thus resulting in the inhibition of gene transcription (Eberhartner, Becker, 2002). HDACs have recently been recognized as key modulators in controlling cardiac Proteostasis by changing the acetylation status of various proteins (McKinsey, 2012). In 2002 an HDAC isoform located in the cytoplasm was identified and reported to have an alpha-Tubulin de-acetylating ability (Hubbert et al., 2002). In atrial fibrillation, hyper-activation of HDAC6 has been reported to depolymerize microtubules thus causing structural remodeling (D. Zhang et al., 2014). Specifically, tachypacing increases HDAC6 expression and activity, causing the deacetylation of  $\alpha$ -tubulin in HL-1 cardiomyocytes and in dog atrial cardiomyocytes. This study further found that deacetylated  $\alpha$ -tubulin is degraded by Calpain and leads to microtubule structure alterations and consequently contractile dysfunction (D. Zhang et al., 2014, 2016).

HDAC6 has been reported to be involved also in the Aggresome formation and degradation (Kawaguchi et al., 2003). It is equipped with Ub-binding domain (UBD), it binds to ubiquitinated targets and is associated with both microtubules and the F-actin cytoskeleton (Hubbert et al., 2002; Seigneurin-Berny et al., 2001) enabling it to mediate the retrograde transport of ubiquitinated proteins along the microtubules to form Aggresomes (Kawaguchi et al., 2003).

HDAC6 is also involved in the subsequent autophagic clearance of the Aggresomes (Hao et al., 2013; Pandey et al., 2007)

The growing interest on HDAC6 activity has enhanced the development of several molecules able to inhibit the enzyme: Tubacin, ACY1215, ACY241, SKLB-23bb, Tubostatin A (F. Wang et al., 2018). Among them, noteworthy for the in vivo use is Tubostatin A that, thanks to its specificity, efficacy and delivery is a good candidate for future therapeutic approaches (Butler et al., 2010; Vishwakarma et al., 2013; F. Wang et al., 2018).

#### **1.5 Protein degradation pathways**

Proteostasis, the maintenance of a healthy proteome, is a fundamental condition for the cell's metabolism, organelle biogenesis, stress adaptation and the long-term viability of any cell type and organ. A major challenge in Proteostasis concerns its protection against the detrimental consequences of unfolded, misfolded, un-trafficked or damaged proteins that can disturb cellular functions.

Since Proteostasis is essential, cells have evolved a sophisticated protein quality control system based on interconnected processes that survey the cellular proteome throughout the protein's life cycle. During protein translation, mRNA surveillance processes recognize aberrant mRNA molecules and mediate the degradation of their nascent proteins. The folding of newly synthesized polypeptide chains on ribosomes is guided by molecular chaperones, in order to minimize misfolding. Chaperones not only assist protein folding, but also facilitate protein degradation when proper folding fails. Furthermore, as cells are permanently subjected to external and internal rearrangements as well as stressful insults a functional proteome requires constant remodeling, repair and elimination of damaged proteins. Disused, defective and misfolded proteins are removed by regulated degradation or, in case of extensive damage that exceeds the intracellular refolding and degradative capacity, are sequestered into dedicated compartments (called inclusion bodies, or Aggresomes) where they await elimination via different mechanisms.

Two major degradation systems have evolved to handle these tasks, the ubiquitin–proteasome system and the autophagy-lysosome pathway (Dikic, 2017) (Figure 1.8).

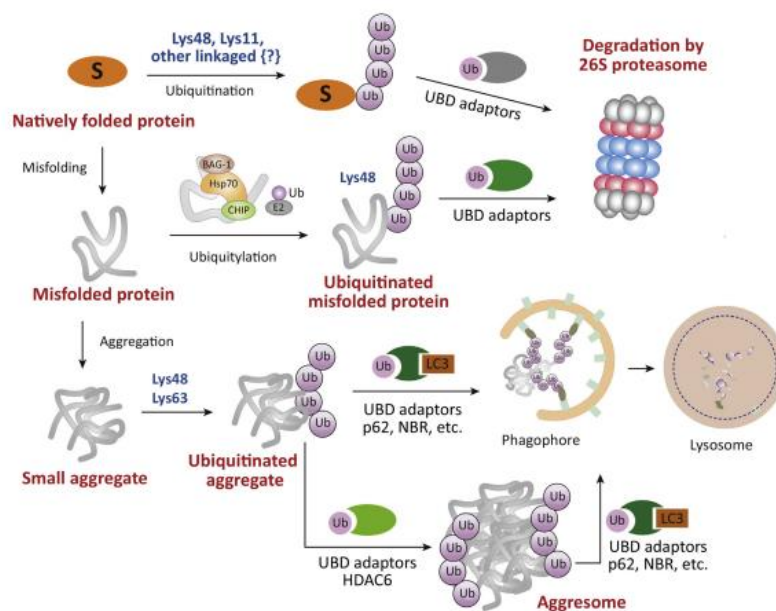


**Figure 1.8 – degradation pathways involving protein ubiquitination**

(Kwon, Ciechanover, 2017)

## 1.6 The ubiquitin-proteasome system (UPS)

The ubiquitin-proteasome system (UPS) catalyzes the great majority of proteins degradation in cells, including both the rapid degradation of misfolded and most of the slower breakdown of the bulk of cellular proteins. Consequently, proteasome function is essential for proteostasis and influences the regulation of the majority of cellular processes. One of the main players of this system, the 26S proteasome, recognizes and degrades only proteins tagged with ubiquitin (Collins , Goldberg, 2017).

Specifically, the 26S proteasome, a multicatalytic ATP-dependent protease of approximately 2.5 MDa, is made up of two subcomplexes: a barrel-shaped twofold-symmetric core particle (CP, or 20S proteasome) and a regulatory particle (RP, or 19S particle) attached to either one or both ends of the CP. Three  $\beta$ -type subunits:  $\beta 1$ ,  $\beta 2$ , and  $\beta 5$  face the interior space and possess catalytic activities (Figure 1.9). The subunits are associated with caspase-like, trypsin-like, and chymotrypsin-like activities respectively, and digest the ubiquitinated substrate into peptides of 2–24 amino acids, ensuring that no protein will remain intact upon entering the CP (Tanaka, 2009).

The RP is composed of base and lid subassemblies that recognize the ubiquitinated substrate proteins and prepare them for degradation in the CP. The central part of the RP base consists of six AAA ATPases (Rpt1–Rpt6) that form a hexameric Rpt ring and are endowed with several crucial functions: they hook the RP via their C-terminal tails to the heptameric  $\alpha$ -ring of the CP and they cause the opening of the gated substrate-entry channel in the CP. These ATPases use the energy deriving from ATP hydrolysis to unfold the substrates and translocate them through the narrow pore into the 20S chamber.

The base of the RP also contains non-ATPase proteins; in particular, Rpn13 and Rpn10 possess ubiquitin-binding domains that function as receptors for ubiquitinated substrates. In addition, shuttling factors (Rad23, Dsk2, and Ddi1) deliver ubiquitinated proteins to the proteasome for degradation. Three deubiquitinases RP subunit Rpn11 (Poh1), RP-associated Usp14 and Uch3 release the ubiquitin chain from the substrate and disassemble it. The binding of ubiquitinated substrates to Usp14 and Uch37 stimulate ATP hydrolysis by AAA ATPases as well as the opening of the 20S gate (Bar-Nun , Glickman, 2012).

Another fundamental role in the UPS is played by the ubiquitination, which is mediated by the cooperative action of three enzymes: the ubiquitin-activating enzyme (E1), the ubiquitin-transferring enzyme (E2), and the ubiquitin ligase (E3). E1 activates ubiquitin using ATP and forms a ubiquitin adenylate. The activated ubiquitin is transferred to E2 through a thioester bond. E3 subsequently promotes the transfer of ubiquitin from E2 to the Lys of substrates. This generates an isopeptide bond between the C-terminal glycine (Gly) of ubiquitin and

the Lys residue on the substrate protein. In rare cases, ubiquitin is conjugated to non-Lys residues of substrates such as serine (Ser), threonine (Thr), and cysteine (Cys) (W. Liu et al., 2020).

There are several different types of ubiquitin linkage: the simplest type of ubiquitination is mono-ubiquitination, which often occurs at multiple Lys residues of the target (multi-mono-ubiquitination). Mono-ubiquitination has been thought to be non-proteolytic and to act as a phosphorylation-like modification that regulates the interactions and activities of substrates. However, emerging evidence shows that mono-ubiquitination produces a powerful proteasomal degradation signal which is much stronger and more universal than previously thought (Sadowski et al., 2012).

Following mono-ubiquitination, ubiquitin can be conjugated by another ubiquitin through any of its seven Lys residues or, alternatively, the Met1 (poly-ubiquitination). These linkages are not only involved in the proteasomal degradation but have many different functions. Among the eight linkages, the most prominent is the Lys48 linkage, which represents up to half of all polyubiquitin linkages and drives proteins to the proteasome. Second to Lys48 linkage is the Lys63 linkage, which facilitates the autophagic degradation of protein substrates together with their associated cellular materials. Lys63 linkages can also modulate non-degradative processes such as protein transport, DNA repair, and the activation of protein kinases (Jacobson et al., 2009; Tenno et al., 2004).

When terminally misfolded proteins can escape from proteasomal degradation, those polyubiquitin-tagged substrates (mostly Lys48-linked but occasionally also Lys63-linked) tend to form aggregates. To prevent uncontrolled aggregation, HDAC6 binds to the ubiquitin of these protein aggregates and temporarily stores them in Aggresomes, whose contents are eventually degraded in the autophagosome-lysosome pathway (Li , Ye, 2008; Morimoto et al., 2015).

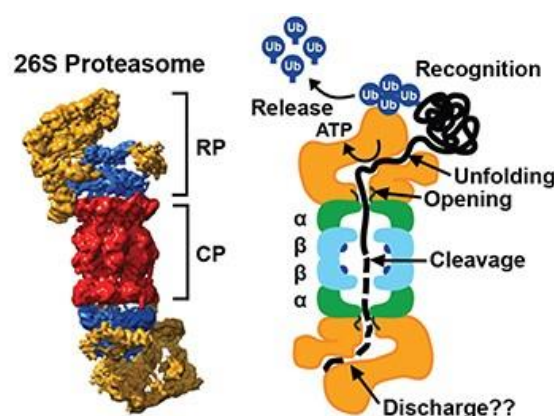


**Figure 1.9 – The assembly and structure of 26S proteasome**

(Marshall, Vierstra, 2019)

## 1.7 Aggresomes

Eukaryotic cells have evolved well-organized mechanisms to cope with misfolded polypeptides caused by aging, oxidative damage, pharmaceuticals, protein overload and defective protein targeting (Dikic, 2017). For instance, in order to minimize the accumulation of misfolded polypeptides which would otherwise be degraded by the ubiquitin-proteasome system, molecular chaperones such as heat shock proteins assist the refolding of such misfolded polypeptides.

When the ubiquitin-proteasome system is overwhelmed or damaged, the misfolded or un-trafficked ubiquitinated polypeptides, tend to form small cytoplasmic aggregates. Through dynein-mediated retrograde transport, small cytoplasmic aggregates are transported to the minus end of a microtubule, forming a larger aggregate, a so-called Aggresome (Y. Park et al., 2018) (Figure 1.10).

In more detail, Aggresomes are stress-inducible aggregates consisting of ubiquitinated proteins, chaperones, and proteasome components which share many toxic characteristics with pathogenic inclusions in several diseases, such as: the Parkinson disease, Huntington's disease, Familial amyotrophic lateral sclerosis, Amyloidosis, Alzheimer's disease, Alexander's disease, Alcoholic liver disease, Wilson's disease, Spinocerebellar ataxia, Prion diseases and dilated cardiomyopathy (Garcia-Mata et al., 2002; Su, Wang, 2011a; te Rijdt et al., 2016)

p62/SQSTM1, Histone Deacetylase 6 (HDAC6) and Dynein play critical roles in Aggresome formation. Similarly to the proteasome degradation pathway, Aggresome formation implies poly-ubiquitination of the protein that has to be degraded (Seigneurin-Berny et al., 2001). P62/SQSTM1 is a ubiquitin receptor that interacts with ubiquitinated proteins. During aging and under acute cellular stress, the P62/SQSTM1 complex binds to ubiquitinated protein aggregates and interacts with microtubule-associated deacetylase HDAC6; this complex is then transported to the cytoplasmic perinuclear region (microtubule-organizing center) to form Aggresomes (Su, Wang, 2011a) also interacts with dynein, promoting the mobilization of the protein aggregates to a specific cell region where they will be finally degraded. Those findings identified HDAC6 as a crucial player in cellular management of protein degradation (Kawaguchi et al., 2003)

Another mechanism for Aggresomes formation has recently been discovered; it is mediated by the multifunctional Heat Shock Protein 70 (HSP70) and the co-chaperone BAG3. During physiological stress, aggregation-prone proteins bind to the HSPB8-HSP70-BAG3 chaperone complex making up the molecular scaffold for the Aggresomes formation (Stürner, Behl, 2017). Subsequently, BAG3 mediates the association of the complex with dynein, initiating the microtubule-based retrograde transport of the substrates to the microtubule-organizing center, in order to form Aggresomes (Stürner, Behl, 2017).

Aggresomes are tightly linked to a process called selective autophagy (or Aggrephagy) in fact multiple components recruited in Aggresomes are degraded by this mechanism, in particular in a SQSTM1-dependent manner. SQSTM1, is recognized by the phagosome receptor LC3-II, and with this event a degradation process of the Aggresomes can occur (Takahashi et al., 2018).

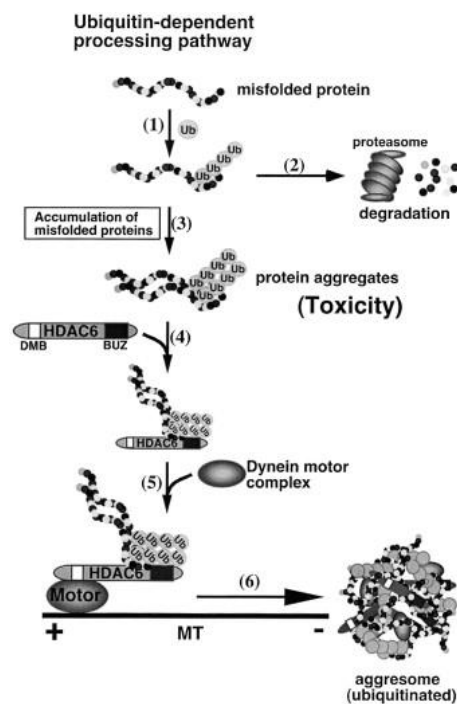


**Figure 1.10 – HDAC6-dependent Aggresome**

(Kawaguchi et al., 2003)

## 1.8 The autophagy-lysosome pathway (ALP)

Autophagy-lysosome pathway (ALP) is a conserved catabolic process, involved in cellular homeostasis and is required to maintain normal cellular physiology under stressful conditions. Autophagy is the preferred degradative route for large, heterogeneous cytoplasmic materials such as protein aggregates, organelles, lipid droplets, and invading bacteria whose size exceed the spatial capacity of proteasomes. This process can be either selective or non-selective: in selective autophagy, the cargo is recognized by specific receptors in order to enable its specific identification, sequestration, and degradation by the autophagosome. In non-specific autophagy, all materials are degraded by the lysosome in a non-specific manner. Several stimuli have been shown to induce autophagy, such as: stress, amino acid and lipid starvation, infectious pathogens and abnormal protein products (such as aggregates or Aggresomes). There are three types of autophagy: macroautophagy, microautophagy, and chaperone-mediated autophagy (CMA). All of these promote proteolytic degradation of



cytosolic components in the lysosome, yet they differ in the way the cargo is directed to this lytic compartment (Khandia et al., 2019). In CMA, cytosolic proteins that expose a pentapeptide signature motif (KFERQ) are recognized by 70 kDa heat shock protein 8 (HSPA8 or HSC70), which in turn binds to a monomer of lysosomal-associated membrane protein 2A (LAMP-2A). This binding triggers the assembly of LAMP-2A multimers that act as the active translocation complex through which the substrates can pass after unfolding. In this way the lysosomal degradation can occur. Microautophagy, on the other hand, refers to the process by which lysosomes directly engulf and digest small volumes of cytosol (Dikic, 2017). The best-characterized form of autophagy is macroautophagy (hereafter called autophagy). It begins with an isolation membrane, also known as a phagophore, likely derived from a lipid bilayer contributed by the ER and/or trans-Golgi and the endosomes. The phagophore engulfs intracellular cargo and sequesters it in a double-membraned structure, called autophagosome (Figure 1.11). The loaded autophagosome matures through fusion with the lysosome, forming the autolysosome and promoting the degradation of autophagosomal contents by lysosomal hydrolytic enzymes. Several permeases and transporters export amino acids and other by-products of degradation back out, into the cytoplasm, where they can be re-used for building macromolecules and for metabolism. One of the most important processes that occurs during the autophagosome formation is the processing of microtubule-associated protein light chain 3 (LC3) (Dikic, 2017). This protein is expressed in most cell types as a full-length cytosolic protein that, upon induction of autophagy, is proteolytically cleaved by a cysteine protease (atg4), to generate LC3-I. The latter, thanks to atg3 activity (another cysteine protease), is then conjugated to phosphatidylethanolamine (PE) to generate the processed LC3-II. The synthesis and processing of LC3 is increased during autophagy, making it a key readout of autophagy levels in cells (Dikic, 2017).

In general, autophagy has been viewed as a random process because it appears to engulf cytosol indiscriminately. However, there is accumulating evidence that the growing phagophore membrane can interact selectively with protein aggregates and organelles. It is proposed that LC3-II, acting as a 'receptor' in the phagophore, interacts with 'adaptor' molecules on the target in order to promote their selective uptake and degradation (Glick et al., 2010). The best-characterized molecule in this regard is p62/SQSTM1, a multi-functional adaptor molecule that binds poly-ubiquitinated protein aggregates with its ubiquitin-binding domain (UBD) promoting their turnover (Glick et al., 2010; Ralston, 2008).

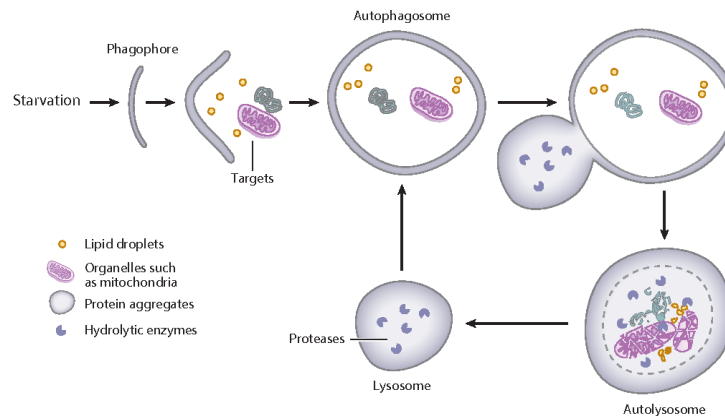


**Figure 1.11 – Autophagosome formation and degradation stages**

(Dikic, 2017)

## 1.9 Sarcoplasmic reticulum architecture

The sarcoplasmic reticulum (SR), a specialized region of the endoplasmic reticulum (ER), is an intracellular membrane system present in cardiac cells that, among other roles, is responsible for the regulation of  $\text{Ca}^{2+}$  transport and the control of excitation-contraction coupling. The SR consists of two structural and functional domains: the so-called non-junctional (or longitudinal) SR and the junctional SR (jSR). In mouse the non-junctional SR is formed by a series of interconnected longitudinal tubules that span the majority of the sarcomere (i.e. between Z-lines), while the junctional SR forms specialized junctions with the T-tubules at the Z-lines, which result in the close juxtaposition ( $\approx 15$  nm) of RyR2s in the jSR and sarcolemmal voltage-gated L-type  $\text{Ca}^{2+}$  channels (Vega et al., 2011).

The Lack of CASQ2 in cardiomyocytes, besides affecting calcium handling, profoundly affects the architecture of the jSR cisternae that appear enlarged and fragmented, potentially modifying CICR (Knollmann et al., 2006) which strongly depends on structural constraints. On the other hand, jSR enlargement has been seen by the same authors as a mechanism to preserve SR calcium content in the absence of CASQ2 (as discussed above).

Given the fact that the SR structure is maintained by microtubule associated SR shaper proteins (Fourest-Lieuvin et al., 2012; Meunier et al., 2009; Osseni et al., 2016; Prosser et al., 2011; Terasaki et al., 1986; Vedrenne, Hauri, 2006; Waterman-Storer, Salmon, 1998), the current Thesis explores the involvement of microtubules and SR structural proteins in our recessive CPVT2 mouse model. We focused on the role of REEP5 and CLIMP63 in shaping the SR in cardiomyocytes in CASQ2-KO mice. The two proteins exert opposite actions: while REEP5 promotes membrane curvature, which helps forming tubules, CLIMP63

promotes the formation of flat cisternal “sheets”. Our results have been published in abstract form at the ESC 2020 congress – The Digital Experience (Bongianino et al., 2020).

CLIMP63 is a transmembrane cytoskeleton-linking membrane protein of 63 kDa, (Schweizer et al., 1993), found in ER sheets where it acts as luminal spacer. This ER-shaping protein participates in the generation and maintenance of the ER sheets through the self-association of the luminal coiled-coil domains in *cis* (between two CLIMP63 proteins of the same ER membrane layer) or in *trans* (between two different ER membrane layers) across the ER lumen (Sandoz et al., 2018; Vedrenne et al., 2005). Furthermore, it was also demonstrated that the cytoplasmic segment of CLIMP63 interacts with microtubules. Experiments with overexpression of this protein have showed a rearrangement of ER and microtubule, suggesting that the protein mediates a direct interaction between ER membranes and cytoskeleton microtubules (Sandoz et al., 2018).

Receptor expression enhancing proteins (REEPs) are members of the DP1/Yop1p family, a cluster of “morphogens” and some of them affect ER structure by establishing its curvature (Lee et al., 2020; Yao et al., 2018). A direct role for REEP5/DP1 in shaping ER tubules has been established by the Chen research group. They demonstrated that REEP5 is the only protein, of the REEPs family, abundant in heart and that colocalizes with the RyR2 in the junctional SR. Lack of REEP5 causes morphological changes in the junctional SR, resulting in a defective connection between the SR and the T-tubules . At the cellular level, REEP5 deficiency reduces the triggering efficiency of L-type  $\text{Ca}^{2+}$  current and decreases  $\text{Ca}^{2+}$  release from the SR (Chiamvimonvat , Song, 2018) that culminates in compromised cardiac contractility (Yao et al., 2018).

## 2. Objectives of the work

Since the first characterization of the *CASQ2-KO mouse model* (Knollmann et al., 2006) it has been described that a *sizable reduction of TRDN occurs at similar mRNA levels than WT cells*. Additionally, *dramatic structural rearrangements of the jSR* have been documented. To this day, the mechanisms that drive these non-arrhythmic phenotypes *have remained unexplored*.

Perhaps, the reason for this lack of exploration has been the clinical evidence itself: CPVT2 patients and mouse models present a structurally normal heart. Such finding has supported the assumption that a radical reduction of CASQ2 is solely accompanied by the development of adrenergically mediated arrhythmias and that further subcellular structural rearrangements remain unimportant from a macroscopic, clinical, point of view. Lack of a large animal model and species differences in cardiac physiology (mouse vs. human) have further fuelled the absence of research in this topic. On the other hand, because of the severity of the arrhythmic phenotype, the research pressure and the resources have been understandably destined to the study of the arrhythmias and their treatment.

With all the above in mind, 15 years later the scientific community possesses a general and well-built understanding of the arrhythmogenic mechanisms of CPVT2. This said, a large percentage of “challenging” patients remain, who are refractory to therapy and so at risk of sudden death. This lack of therapeutical options for such patients has forced us, as translational researchers, to re-evaluate our previous notions about the mechanism(s) and importance of the aforementioned non-arrhythmic CPVT2 phenotypes. *How do these changes contribute to the disease? Is it true that microscopic remodelling has no macroscopic consequence? Can we find new therapeutical targets?* After all, a ventricular cell is much more than calcium channels, DADs and action potentials... *Are we missing the forest for staring at its tallest tree?*

The present study thus re-evaluates our prior assumptions. We tackled the following *two experimental questions: (1) Which is the mechanism that drives reduction of triadin in response to loss of calsequestrine?; and (2) is the loss of triadin part of a maladaptive response to the absence of calsequestrin?*

### 3. Results

#### 3.1 Whole CASQ2-KO hearts Proteomic Analysis

As an initial step, we performed a whole heart Proteomic analysis to understand whether in CASQ2-KO mice, the loss of Calsequestrin 2 leads to a loss of *Proteostasis* and whether the study of abnormal protein expression could further guide our understanding of the mechanisms involved in our animal model of recessive CPVT.

We identified 3638 differentially expressed proteins: an unexpected scenario that indicates that the loss of Calsequestrin not only disrupts Calcium homeostasis but it also modifies the expression of several proteins thus supporting the hypothesis that the heart of CASQ2-KO mice shows a loss of the equilibrium that preserves the physiological balance between synthesis and degradation of proteins (Figure 3.1).

As expected, the most severely downregulated proteins were Triadin ( $Zq = -4.8$ ) and Junctin ( $Zq = -7.3$ ) and when we clustered proteins by functional groups (GO) (Huang et al., 2009) we identified significant alterations of different cell pathways: homophilic cell adhesion via plasmamembrane adhesion molecules ( $Zc = -2.76$ ), respiratory chain ( $Zc = -2.76$ ), smooth endoplasmic reticulum proteins ( $Zc = -2.56$ ), ER-phagy markers ( $Zc = -2.10$ ) and Microtubule associated proteins (MAP) ( $Zc = -2.08$ ) were the most down regulated protein functional groups. The identification of a reduction in the MAP group was crucial for the development of the project. Particularly evident was the reduction in Tau ( $Zq = -3.50$ ) and Dynein light chain 2 ( $Zq = -1.41$ ) protein quantity.

We also report the reduction of Calreticulin ( $Zq = -1.41$ ), Calnexin ( $Zq = -2.56$ ), Reticulon 1 ( $Zq = -1.03$ ) and Peroxiredoxin-4 ( $Zq = -1.30$ ) in Smooth Endoplasmic Reticulum Proteins group ( $Zc = -2.56$ ) that for their role in Calcium homeostasis are worthy of deeper and further studies.

We also observed upregulation of other protein functional groups: Nucleotidyltransferase activity ( $Zc = 3.45$ ), transcription from RNA Pol II protein ( $Zc = 3.29$ ) and especially protein ubiquitination involved in ubiquitin dependent protein catabolic processes ( $Zc = 3.40$ ). From the latter group we would like to emphasize the overexpression of: E3 ubiquitin-protein ligase UBR4 ( $Zq = 3.34$ ) (a proposed regulator of the delivery of cargoes destined to interact with the autophagic machinery), Cullin 1 ( $Zc = 1.00$ ) and Cullin 5 ( $Zc = 1.00$ ) (S. T. Kim et al., 2013).

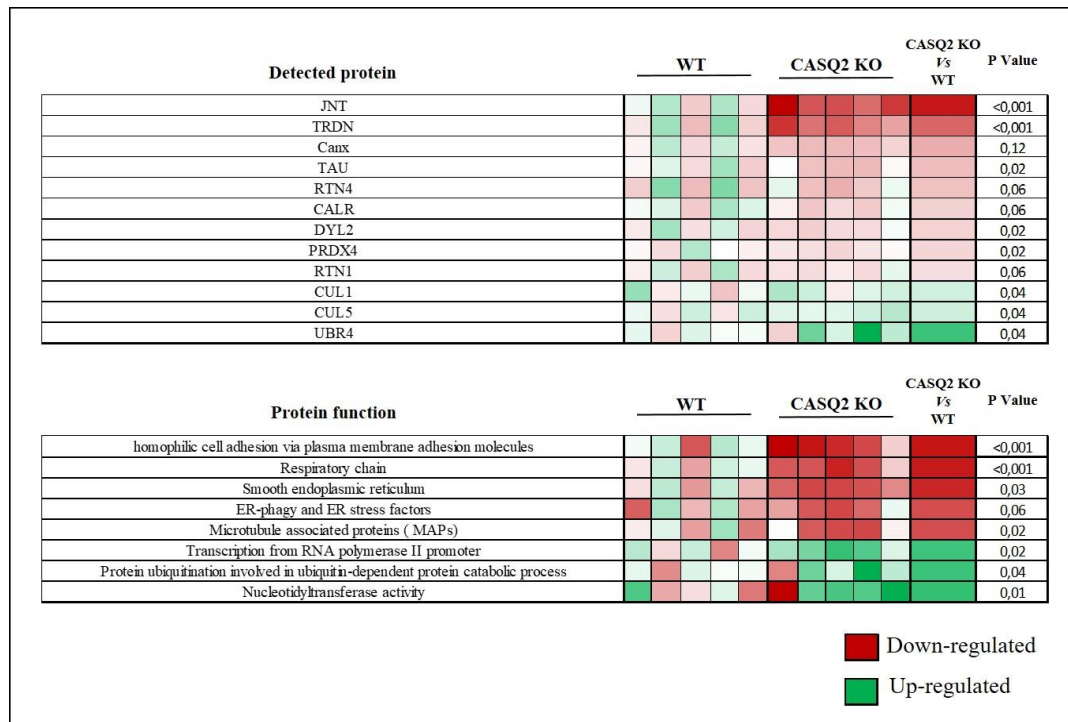


**Figure 3.1 - Proteomic analysis from CASQ2-KO hearts**

(UP) Proteomic analysis of WT and CASQ2-KO heart. Representative downregulated (red) and upregulated (green) proteins found differentially expressed in TRDN-KO (top). The data are expressed in Zq (see methods). (Down) Functional groups found differentially expressed in CASQ2-KO hearts (down). The data are expressed in Zc (see methods) (WT 5 mice, CASQ2-KO 5 mice).

### 3.2 Microtubule structural and molecular alterations in CASQ2-KO cardiomyocytes

Starting from the preliminary Proteomic analysis and the data on MAPs down-regulation we decided to explore the microtubule network in CASQ2-KO cardiomyocytes.

Adult mouse ventricular cardiomyocytes were isolated by aortic perfusion digestion (Sambrano et al., 2002) and prepared for immunofluorescence protocol (see methods). Cells were stained for alpha-Tubulin and Confocal images of microtubules were acquired with a Leica SP8 microscope. The images were processed by a homemade macro routine based on MINA image-J plug-in (Valente et al., 2017). The program was able to successfully detect the microtubule network and measure several geometric parameters. The analysis demonstrated that in CASQ2-KO cardiomyocytes the length of microtubules was significantly reduced compared to cardiomyocytes from WT mice (Figure 3.2A) ( $P < 0.001$ ). Similarly, the branching of the microtubule network was significantly decreased in CASQ2-KO compared to WT cardiomyocytes (Figure 3.2A) ( $P < 0.001$ ).

Given its relevance to this project, the microtubule population related to the junctional Sarcoplasmic Reticulum was also studied. We obtained the colocalization of alpha-Tubulin and RyR2, which we used as junctional Sarcoplasmic Reticulum marker. The colocalization parameter, based on Manders coefficient, showed a

significant decrease in RyR2/alpha-Tubulin spatial overlap in CASQ2-KO mice compared to WT (Figure 3.2B) ( $P=0.002$ ).

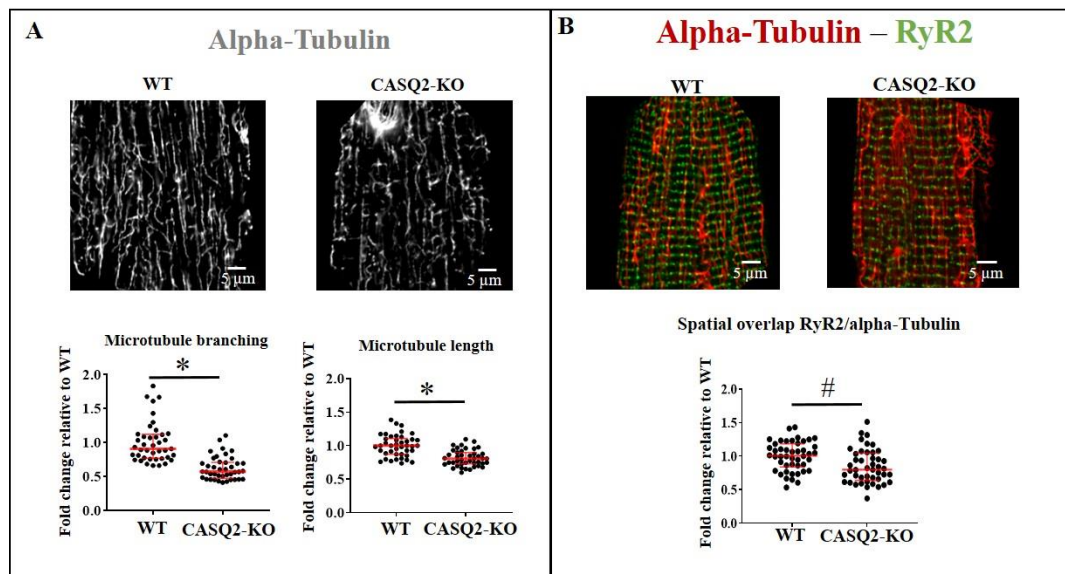


**Figure 3.2 - Structural microtubule alterations**

**A-** Confocal images of isolated cardiomyocytes were stained for alpha-Tubulin (white). **(Left)** The microtubule branching (lower panel), as compared to WT, decreases significantly in CASQ2-KO [Fold change relative to WT, median (p25 - p75): WT: 0.91 (0.77 - 1.12); CASQ2-KO: 0.57 (0.48 - 0.71)]. Mann Whitney test, \*  $P<0.001$  (WT: 3 mice 22 cells 41 ROIs; CASQ2-KO: 3 mice 22 cells 41 ROIs). **(Right)** Similarly, the microtubule length, as compared to WT, decreases significantly in CASQ2-KO [Fold change relative to WT, median (p25 - p75): WT: 1.00 (0.87 - 1.11); CASQ2-KO: 0.81 (0.73 - 0.90)]. Mann Whitney test, \*  $P<0.001$  (WT: 3 mice 22 cells 42 ROIs; CASQ2-KO: 3 mice 22 cells 43 ROIs).

**B-** Confocal images of WT and CASQ2-KO isolated cardiomyocytes double stained for alpha-Tubulin (red) and RyR2 (green). The colocalization quantification, based on Manders coefficient, indicates that the colocalization between RyR2 and alpha-Tubulin in CASQ2-KO is decreased [Fold change relative to WT, median (p25 - p75): WT: 1.00 (0.84 - 1.19); CASQ2-KO: 0.80 (0.64 - 1.05)]. Mann Whitney test, #  $P=0.002$  (WT: 3 mice 22 cells 46 ROIs; CASQ2-KO: 3 mice 22 cells 45 ROIs).

### 3.3 Tau alteration in CASQ2-KO cardiomyocytes

Encouraged by the microtubule alteration data and the preliminary Proteomic result of Tau reduction in CASQ2-KO hearts, we decided to explore possible alterations of this molecule.

Tau is a small protein, better known by its involvement in neurological diseases like Parkinson and Alzheimer, able to wrap around the microtubules and to promote their stabilization and stiffness. Recently the scientific community raised the interest in this protein also for its involvement in other cell types, including cardiomyocytes (Betrie et al., 2017).

The decrease of Tau observed by Proteomic analysis (Figure 3.1), has been validated by Western Blot, showing that Tau protein levels were decreased by ~30% in CASQ2-KO mice hearts compared to WT ( $P=0.041$ ) (Figure 3.3A).

Furthermore, since Tau stabilizes the microtubules by physical contact, we stained isolated cardiomyocytes for Tau and alpha-Tubulin and acquired confocal images for colocalization measurements. The spatial overlap

of Tau with respect to alpha-Tubulin was significantly decreased in CASQ2-KO cardiomyocytes compared to the WT ( $P<0.001$ ) (Figure 3.3B).

After the development of an ImageJ macro based on *find foci* plug-in (Herbert et al., 2014), confocal images of cardiomyocytes stained for Tau were used to measure the number and the dimension of Tau spots within the cells. In line with the observed Tau protein reduction, the Tau spots numerosity was significantly reduced ( $P<0.001$ ) (Figure 3.3C-Left). On the other hand the average of Tau spots dimension within the cardiomyocytes was highly increased in CASQ2-KO compared to the WT ( $P<0.001$ ) (Figure 3.3C-Right). The last results could suggest, as described in literature (Guthrie, Kraemer, 2011), that non-functional Tau could pool together and generate protein aggregates in our model of CPVT2.

The results show that Tau alterations could contribute to the mechanism of microtubule instability and loss of microtubule geometry previously described in CASQ2-KO cardiomyocytes.

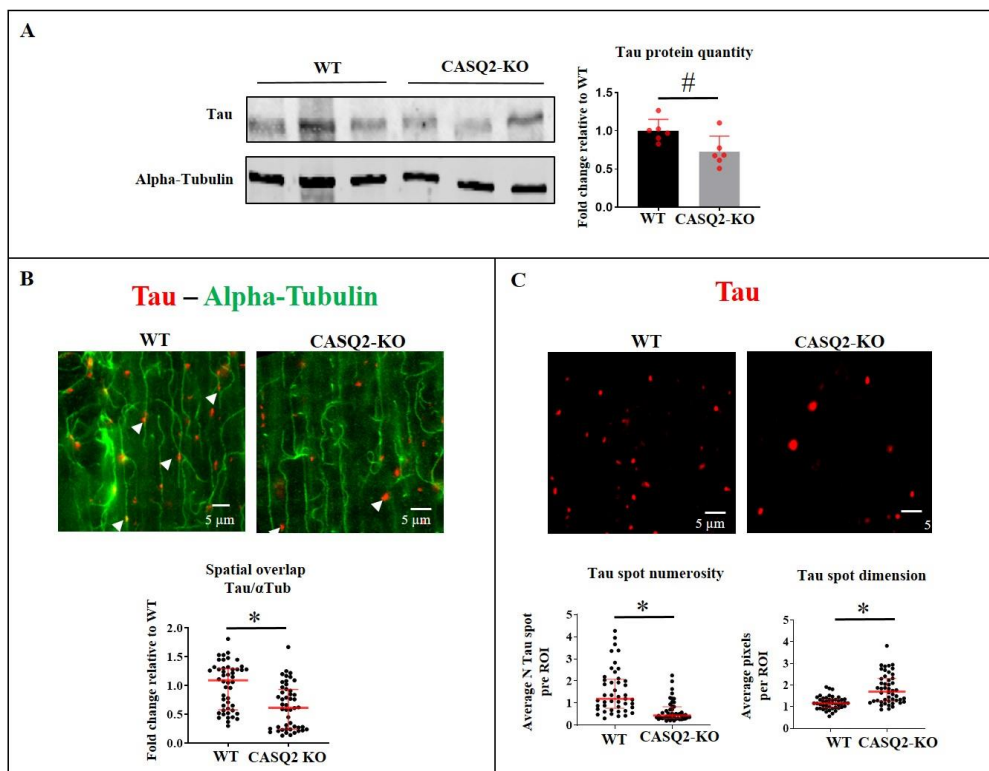


**Figure 3.3 - Tau alterations in CASQ2-KO cardiomyocytes**

**A-** WB from total heart protein homogenate from WT and CASQ2-KO mice. CASQ2-KO hearts present a decrease in Tau protein content (Fold change relative to WT, mean  $\pm$  SD: WT:  $1.00 \pm 0.15$ ; CASQ2-KO:  $0.73 \pm 0.20$ ). Mann-Whitney test, #  $P=0.041$  (WT: 6 mice; CASQ2-KO: 6 mice).  
**B-** Confocal images of isolated cardiomyocytes were stained for Tau (red) and  $\alpha$ Tubulin (green). The analysis showed a decreased co-localization value between the two proteins in CASQ2-KO as compared to the WT (Fold change relative to WT, median (p25 - p75): WT: 1.09 (0.58 - 1.30); CASQ2-KO: 0.62 (0.24 - 0.93). Mann Whitney test, \*  $P<0.001$  (WT: 3 mice 24 cells 48 fields; CASQ2-KO: 3 mice 24 cells 48 fields).  
**C-** (Left) Confocal images of isolated cardiomyocytes stained for Tau (red) were processed using *find foci* imageJ plug-in. the data showed that CASQ2-KO cardiomyocytes are characterized by a significant decrease in Tau spot number as compared to WT (Fold change relative to WT, median (p25 - p75): WT: 1.19 (0.77 - 2.08); CASQ2-KO: 0.44 (0.41 - 0.84). Mann Whitney test, \*  $P<0.001$  (WT: 3 mice 24 cells 45 fields; CASQ2-KO: 3 mice 24 cells 47 fields). (Right), The Tau spot dimension is increased in CASQ2-KO as compared to WT (Fold change relative to WT, median (p25 - p75): WT: 1.16 (0.95 - 1.34); CASQ2-KO: 1.70 (1.26 - 2.31). Mann Whitney test, \*  $P<0.001$  (WT: 3 mice 24 cells 45 fields; CASQ2-KO: 3 mice 24 cells 47 fields).



### 3.4 Alpha-Tubulin deacetylation in CASQ2-KO cardiomyocytes

We hypothesized that the observed microtubule disruption could be mediated by HDAC6-induced deacetylation of alpha-Tubulin. It is known that deacetylation of alpha-Tubulin leads to instability of microtubules (Janke, Montagnac, 2017), thus the presence of deacetylated alpha-Tubulin might account for the disrupted microtubule architecture observed in CASQ2-KO mice. In line with our hypothesis, Western Blot analysis showed that while the levels of alpha-Tubulin did not differ in whole heart homogenates from WT and CASQ2-KO mice ( $P=NS$ ), the levels of acetylated alpha-Tubulin were sharply decreased in CASQ2-KO mice ( $P=0.002$ ) (Figure 3.4)

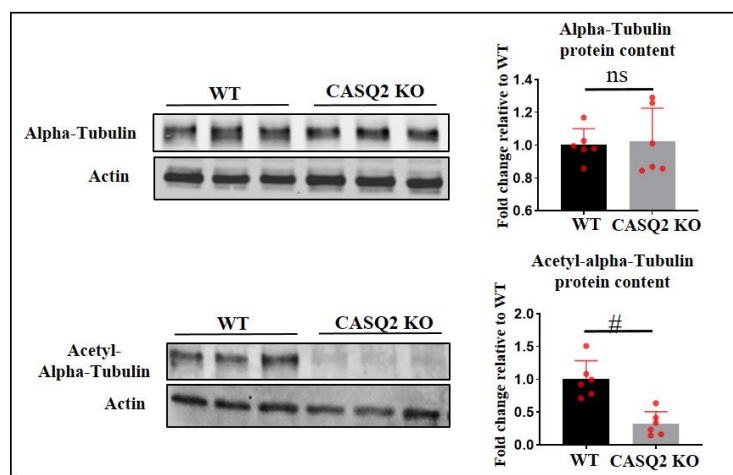


**Figure 3.4 - Alpha-tubulin deacetylation**

WB of total heart protein homogenate from WT and CASQ2-KO mice. (Up) Alpha-Tubulin protein quantity is unchanged in the two groups (Fold change relative to WT, mean  $\pm$  SD: WT:  $1.00 \pm 0.10$ ; CASQ2-KO:  $1.02 \pm 0.21$ ). Mann Whitney test,  $P=NS$  (WT: 6 mice; CASQ2-KO: 6 mice). (Down) CASQ2-KO mice show instead a significant reduction in acetylated alpha-Tubulin (Fold change relative to WT, mean  $\pm$  SD: WT:  $1.00 \pm 0.28$ ; CASQ2-KO:  $0.32 \pm 0.19$ ). Mann Whitney test, #  $P=0.002$  (WT: 6 mice; CASQ2-KO: 6 mice).

### 3.5 HDAC6 involvement in microtubule alterations in CASQ2-KO cardiomyocytes

With the objective of identifying the cause of the observed microtubule disruption in CASQ2-KO, we explored the involvement of the enzyme responsible for alpha-Tubulin deacetylation, Histone deacetylase 6 (HDAC6) (Hubbert et al., 2002).

The molecular trigger responsible for HDAC6 activation is still unclear (D. Zhang et al., 2016), and change in the general cellular *Proteostasis* is the only parameter that is strictly correlated with the activation of this cytosolic deacetylase (Henning, Brundel, 2017; D. Zhang et al., 2016). As previously described by the Proteomic analysis, CASQ2-KO hearts are characterized by an alteration in the *Proteostasis*, supporting the hypothesis of HDAC6 involvement in the microtubule disruption in our model.

Firstly by Western blot analysis from total heart protein extract, we measured HDAC6 protein levels and observed a significant increase in the CASQ2-KO hearts as compared to WT ( $P=0.002$ ) (Figure 3.5A).

The activity of the Histone deacetylase 6 (HDAC6) was evaluated by a fluorometric assay (BioVision). The kit utilizes a synthetic acetylated-peptide substrate, that once processed by HDAC6 results in a release of AFC fluorophore. By analyzing the florescent signal we found that HDAC6 activity ( $P=0.026$ ) (Figure 3.5B) was increased in CASQ2-KO hearts compared to WT.

In order to confirm that HDAC6 is the mediator of the observed microtubule disruption in CASQ2-KO cardiomyocytes, we used Tubostatin A, a well-known HDAC6 specific inhibitor (Z. Wang et al., 2016), to verify whether the reduction of the deacetylase activity would prevent the disruption of microtubules in CASQ2-KO mice. Our hypothesis was confirmed, as exposure to Tubostatin A for 16 hours improved the microtubule's architecture in CASQ2-KO cardiomyocytes. Confocal images of cardiomyocytes stained for alpha-Tubulin and RyR2/ alpha-Tubulin showed that the microtubule branching (WT vs CASQ2-KO + Tubostatin A,  $P=NS$ ) (Figure 3.5C-left), microtubule length (WT vs CASQ2-KO + Tubostatin A,  $P=0.008$ ) (Figure 3.5C-left) and the colocalization of RyR2 with alpha-Tubulin (WT vs CASQ2-KO + Tubostatin A,  $P= NS$ ) were reestablished (Figure 3.5D).

Overall, the results demonstrated the implication of HADAC6 in the process of microtubule breakage in CASQ2-KO hearts.

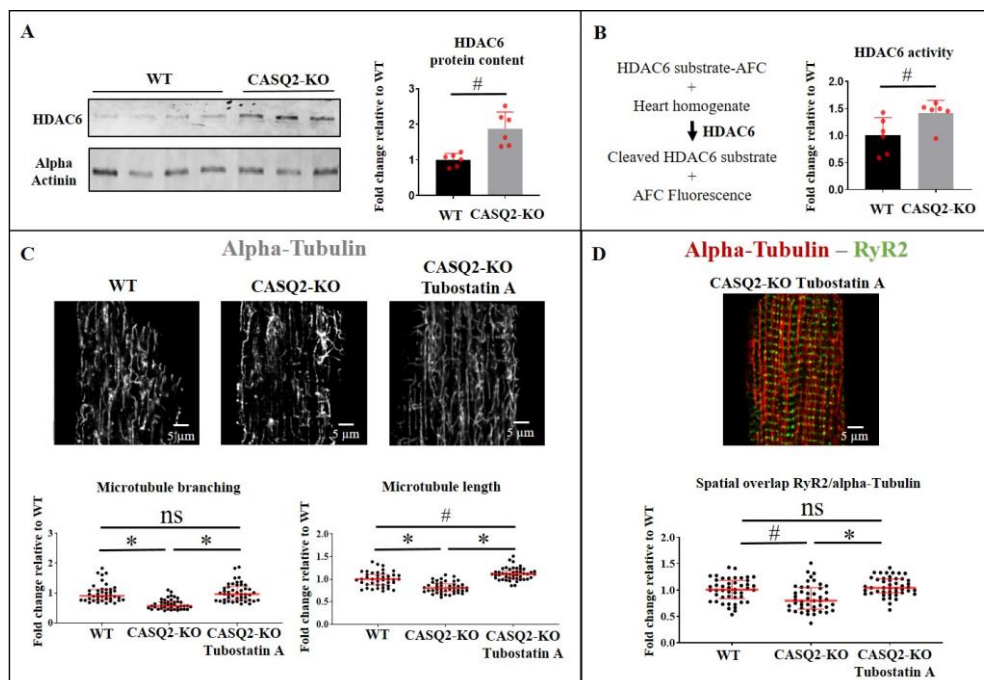


**Figure 3.5 – HDAC6 inhibition by Tubostatin A restore microtubule architecture in CASQ2-KO cardiomyocytes**

**A-** WB of total heart protein homogenate from WT and CASQ2-KO mice. CASQ2-KO hearts presents an increase in HDAC6 protein quantity compared to WT (Fold change relative to WT, mean  $\pm$  SD: WT:  $1.00 \pm 0.18$ ; CASQ2-KO:  $1.88 \pm 0.48$ ). Mann Whitney test, #  $P=0.002$  (WT: 6 mice; CASQ2-KO: 6 mice).

**B-** HDAC6 activity assay. CASQ2-KO presents higher HDAC6 activity compared to WT (Fold change relative to WT, mean  $\pm$  SD: WT:  $1.00 \pm 0.33$ ; CASQ2-KO:  $1.42 \pm 0.24$ ). Mann Whitney test, #  $P=0.026$  (WT: 6 mice; CASQ2-KO: 6 mice).

**C-** Confocal images of isolated cardiomyocytes from WT, CASQ2-KO and CASQ2-KO treated with Tubostatin A stained for alpha-Tubulin (white). The treatment with Tubostatin A reverts the microtubules branching and length scores observed in CASQ2-KO cardiomyocytes to values similar to those of the WT (**Left**) [microtubules branching: fold change relative to WT, median (p25 - p75): WT: 0.90 (0.77 - 1.12); CASQ2-KO: 0.57 (0.47 - 0.71); CASQ2-KO + Tubostatin A: 0.96 (0.77 - 1.22). Kruskal-Wallis test with Dunn's correction, WT vs CASQ2-KO, \* P<0.001; CASQ2-KO vs CASQ2-KO + Tubostatin A, \* P<0.001; WT vs CASQ2-KO + Tubostatin A, P=NS (WT: 3 mice 22 cells 41 ROIs; CASQ2-KO: 3 mice 22 cells 41 ROIs; CASQ2-KO + Tubostatin A: 3 mice 23 Cells 46 ROIs)]; (**Right**) microtubule length: Fold change relative to WT, median (p25 - p75): WT: 1.00 (0.87 - 1.11); CASQ2-KO: 0.81 (0.73 - 0.90); CASQ2-KO + Tubostatin A: 1.12 (1.02 - 1.18)]. Kruskal-Wallis test with Dunn's correction, WT vs CASQ2-KO, \* P<0.001; CASQ2-KO vs CASQ2-KO + Tubostatin A, \* P<0.001; WT vs CASQ2-KO + Tubostatin A, # P=0.008 (WT: 3 mice 22 cells 42 ROIs; CASQ2-KO: 3 mice 22 cells 43 ROIs; CASQ2-KO + Tubostatin A: 3 mice 23 Cells 46 ROIs)].

**D-** Confocal images of CASQ2-KO isolated cardiomyocytes treated with Tubostatin A double stained for alpha-Tubulin (red) and RyR2 (green). The colocalization quantification, based on Manders coefficient, indicates that Tubostatin A exposure rescues the colocalization between RyR2 and alpha-Tubulin in CASQ2-KO [Fold change relative to WT, median (p25 - p75): WT: 1.01 (0.84 - 1.19); CASQ2-KO: 0.80 (0.64 - 1.05); CASQ2-KO + Tubostatin A : 1.04 (0.95 - 1.21)]. Kruskal-Wallis test with Dunn's correction, WT vs CASQ2-KO, # P=0.005; CASQ2-KO vs CASQ2-KO + Tubostatin A, \* P<0.001; WT vs CASQ2-KO + Tubostatin A, P= NS (WT: 3 mice 22 cells 46 ROIs; CASQ2-KO: 3 mice 22 cells 45 ROIs; CASQ2-KO + Tubostatin A: 3 mice 23 Cells 46 ROIs)].

### 3.6 TRDN interacts with the microtubule network

Once established the cause of microtubule disruption in our model of CPVT2, we decided to explore the consequences of this structural alteration.

Following the main objective of the project, the dissection of TRDN reduction in CASQ2-KO, we decided to study the relationship between the defective microtubular network and TRDN.

In order to validate the interaction between the cardiac TRDN and the microtubules we performed a co-immunoprecipitation assay using anti-Alpha-Tubulin antibody processed with magnetic beads. TRDN co-immunoprecipitated in both WT and CASQ2-KO, confirming the interaction between TRDN and the microtubule network (Figure 3.6A).

We also decided to validate the above obtained data by studying the position of TRDN and Tubulin by Confocal microscopy, we found a reduced spatial overlap between the two in CASQ2-KO as compared to WT (P=0.001) (Figure 3.6B). This result indicates that there is less TRDN that shares the same subcellular compartment with alpha-Tubulin in CPVT2 ventricular cells.

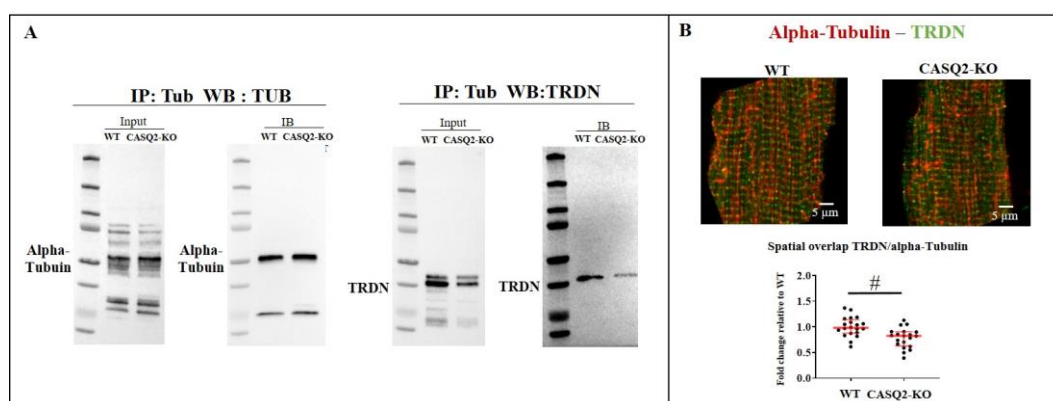


**Figure 3.6 – TRDN takes contact with the microtubule network**

**A-** Co-immunoprecipitation assay. Magnetic beads were processed with anti alpha-Tubulin antibody and they were used to immunoprecipitate TRDN.

**B-** Confocal images of isolated cardiomyocytes double stained for alpha-Tubulin (red) and TRDN (green). The co-localization quantification, based on Manders coefficient, indicates the spatial overlap between alpha-tubulin and TRDN. TRDN/Tub co-localization is decreased in CASQ2-KO [Fold change relative to WT, median (p25-p75): WT: 0.98 (0.88 - 1.14); CASQ2-KO: 0.82 (0.63 - 0.90)]. Mann Whitney test, # P=0.001 (WT: 2 mice 10 Cells 20 fields; CASQ2-KO: 2 mice 10 Cells 20 fields).

### 3.7 Defective TRDN trafficking in CASQ2-KO cardiomyocytes

Since in 2015, Sleiman et al (Sleiman et al., 2015) elegantly demonstrated that Triadin and Calsequestrin jointly travel to the jSR transported by microtubules, we hypothesized TRDN would have defective trafficking since the microtubule network is altered in our model.

We investigated whether, in the heart of CASQ2-KO mice Triadin properly localizes at the Z-lines where the RyR2 and the other dyadic proteins are positioned. Experiments were performed using STED super-resolution microscopy: we compared the co-localization of TRDN with RyR2 in WT and CASQ2-KO mice using Manders's coefficient and demonstrated a loss of colocalization of the two proteins in CASQ2-KO myocytes, therefore proving that TRDN was no longer aligned with the Z-lines ( $P < 0.001$ ) (Figure 3.7-up). To confirm the shift of TRDN to a new localization in between Z-lines, we quantified the density of delocalized TRDN spots (see methods), showing that it was 3.7 times higher in the CASQ2-KO compared to the WT ( $P < 0.001$ ) (Figure 3.7-down).

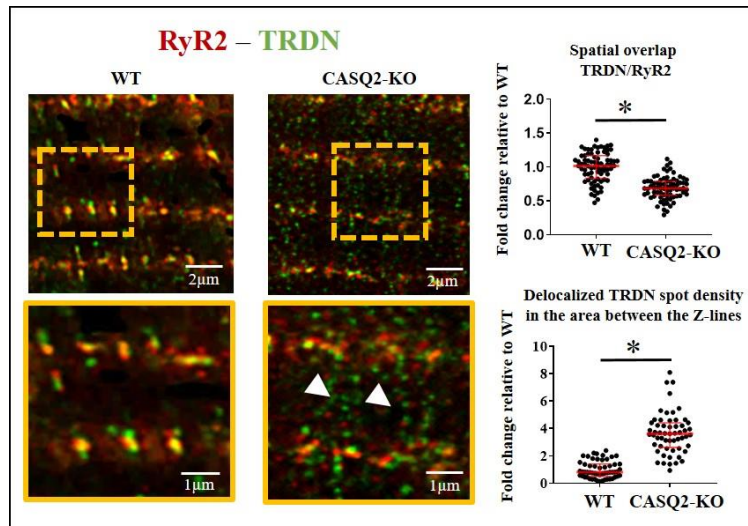


**Figure 3.7 - Triadin delocalization in CASQ2-KO cardiomyocytes**

(Up) STED super-resolution images of isolated cardiomyocytes double stained for RyR2 (red) and TRDN (green) (upper images). Zoomed images show the different distribution of TRDN in WT and CASQ2-KO (bottom image, white arrowheads). The colocalization quantification, based on Manders coefficient, indicates the spatial overlap between TRDN and RyR2. The graph shows a significant decrease in TRDN/RyR2 colocalization in CASQ2-KO [Fold change relative to WT, median (p25-p75): WT: 1.02 (0.83 – 1.17); CASQ2-KO: 0.69 (0.59 – 0.79)]. Mann Whitney test, \*  $P < 0.001$  (WT: 4 mice 24 cells 77 ROIs; CASQ2-KO: 4 mice 24 cells 75 ROIs). (Down). The density of TRDN placed in the area between the Z-lines is significantly increased as compared to WT [Fold change relative to WT, median (p25-p75): WT: 0.81 (0.50 – 1.40); CASQ2-KO: 3.62 (2.62 – 4.42)]. Mann Whitney test, \*  $P < 0.001$  (WT: 3 mice 17 cells 55 ROIs; CASQ2-KO: 3 mice 18 cells 57 ROIs).

### 3.8 Microtubule polymerization modulation affects TRDN position in CASQ2-KO cardiomyocytes

In order to explore whether TRDN delocalization was due to the defective microtubule network, we modulated the microtubule net by treatment with Colchicine, chemical agent which is known to depolymerize microtubules (Vandecandelaere et al., 1997), and Taxol, a microtubule polymerizing agent (Horwitz et al., 1986; Manfredi et al., 1982), and studied TRDN position under these condition.



### 3.8.1 Colchicine treatment

To support our hypothesis that the disruption of microtubules is the cause of the delocalization of TRDN, we tested whether administration of Colchicine to WT mice would lead to the delocalization of TRDN away from the Z lines.

WT mice received an IP injection of Colchicine and after 16 hours, cardiac myocytes were enzymatically isolated and prepared for confocal imaging (see methods). Confocal images showed that, after the exposure to colchicine, WT cardiomyocytes presented fragmented microtubules ( $P < 0.001$ ) (Figure 3.8A). Compared to untreated WT cardiomyocytes, cells from WT animals exposed to colchicine presented a significant decrease in branching ( $P < 0.0001$ ) (Figure 3.8A-Left) and length ( $P < 0.0001$ ) (Figure 3.8A-Right) of microtubules and they also showed a decrease in co-localization (WT vs WT colchicine, \*  $P < 0.001$ ) between alpha-Tubulin and RyR2 (Figure 3.8B).

To test whether the disruption of the geometry of the microtubule network leads to delocalization of TRDN, we assessed whether WT mice treated with Colchicine would present delocalization of TRDN as observed in cardiac myocytes isolated from the heart of CASQ2-KO mice.

The obtained results confirmed our hypothesis, showing a significant decrease of co-localization between TRDN and RyR2 (WT vs WT colchicine,  $P < 0.001$ ) (Figure 3.8C-Left), an increase of TRDN spot density in the area in between the Z-lines in WT myocytes exposed to Colchicine compared to untreated WT (WT vs WT colchicine, \*  $P < 0.001$ ) (Figure 3.8C-Right) and no difference in comparison with the CASQ2-KO.

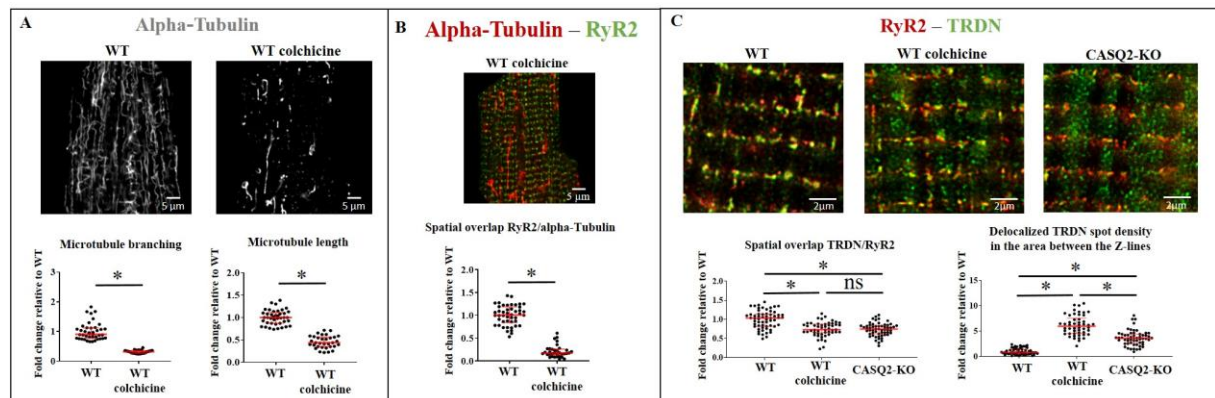


**Figure 3.8 - Microtubule depolymerization causes TRDN delocalization**

**A-** Confocal images of WT isolated cardiomyocytes treated with colchicine stained for alpha-Tubulin. (**Left**) Colchicine treatment in WT causes significant loss of microtubules branching [Fold change relative to WT, median (p25 – p75): WT: 0.90 (0.77 – 1.12); WT + Colchicine: 0.32 (0.27 – 0.36)]. Mann-Whitney test, \*  $P < 0.001$  (WT: 3 mice 22 cells 41 ROIs; WT + Colchicine: 3 mice 17 Cells 33 ROIs). (**Right**) The microtubules length is reduced as well [Fold change relative to WT, median (p25 – p75): WT: 1.00 (0.87 – 1.12); WT + colchicine: 0.44 (0.35 – 0.57). Mann-Whitney test, \*  $P < 0.001$  (WT: 3 mice 22 cells 41 ROIs; WT + colchicine: 3 mice 17 Cells 33 ROIs)].

**B-** Confocal images of WT isolated cardiomyocytes treated with colchicine double stained for alpha-Tubulin (red) and RyR2 (green). The colocalization quantification, based on Manders coefficient, indicates that spatial overlap between RyR2 and alpha-Tubulin is decreased after colchicine exposition [Fold change relative to WT, median (p25 – p75): WT: 1.04 (0.82 – 1.14); WT+ Colchicine: 0.73 (0.66 – 0.88); CASQ2-KO: 0.75 (0.62 – 0.83)]. Kruskal-Wallis test with Dunn's correction, WT vs WT colchicine, \*  $P < 0.001$ ; WT colchicine vs CASQ2-KO,  $P = \text{NS}$ ; WT colchicine vs CASQ2-KO, \*  $P < 0.001$  (WT: 3 mice 22 cells 46 ROIs, WT+ colchicine: 3 mice 17 Cells 34 ROIs)].

**C-** STED super-resolution images of isolated cardiomyocytes treated with colchicine were double stained for RyR2 (red) and TRDN (green). (**Left**) The colocalization parameter, based on Manders coefficient, indicates that colchicine treatment in WT caused a reduction in TRDN/RyR2 colocalization [Fold change relative to WT, median (p25 – p75): WT: 1.04 (0.82 – 1.14); WT+ Colchicine: 0.73 (0.66 – 0.88); CASQ2-KO: 0.75 (0.62 – 0.83)]. Kruskal-Wallis test with Dunn's correction, WT vs WT colchicine, \*  $P < 0.001$ ; WT colchicine vs CASQ2-KO,  $P = \text{NS}$ ; WT colchicine vs CASQ2-KO, \*  $P < 0.001$  (WT: 3 mice 18 cells 59 ROIs; WT+ colchicine: 3 mice 17 cells 51 ROIs; CASQ2-KO: 3 mice 18 cells 57 ROIs)]. (**Right**) The

density of TRDN placed in the area between the Z-lines is significantly increased in the WT treated with Colchicine as compared to WT not treated and with CASQ2-KO [Fold change relative to WT, median (p25-p75): WT: 0.81 (0.50 – 1.40 ); WT + Colchicine : 5.97 (4.54 – 7.55); CASQ2-KO: 3.62 (2.62 – 4.42 )]. Kruskal–Wallis test with Dunn's correction, WT vs WT colchicine, \*  $P < 0.001$ ; WT colchicine vs CASQ2-KO, \*  $P < 0.001$ ; WT colchicine vs CASQ2-KO, \*  $P < 0.001$  (WT: 3 mice 18 cells 55 ROIs; WT+ colchicine: 3 mice 17 cells 50 ROIs; CASQ2-KO: 3 mice 18 cells 57 ROIs).

### 3.8.2 Taxol treatment

To further support our hypothesis, we tested whether the administration of Taxol, could reestablish not only the microtubule network but also TRDN's position in CASQ2-KO.

Taxol was injected intra-peritoneally in CASQ2-KO mice, after 16 hours cardiomyocytes were isolated and prepared for immunofluorescence experiments. Confocal images of the microtubules showed a significant improvement of its network organization. The microtubules length (WT vs CASQ2-KO + Taxol,  $P = \text{NS}$ ) (Figure 3.9A-Left) and ramification (WT vs CASQ2-KO + Taxol,  $P = \text{NS}$ ) (Figure 3.9A-Right) were re-established. STED super resolution images of CASQ2-KO cardiomyocytes treated with Taxol showed that the colocalization of TRDN in respect to RyR2 was improved (WT vs CASQ2-KO + Taxol,  $P = 0.001$ ) (Figure 3.9B-Left) and the delocalized TRDN population was significantly reduced (WT vs CASQ2-KO + Taxol,  $P = \text{NS}$ ) (Figure 3.9B-Right). Therefore, the restoration of microtubule network in CASQ2-KO improves TRDN localization.

Overall, these data confirm that the loss of CASQ2 leads to a disruption of microtubules and that the alteration of the microtubule network impairs the proper localization of TRDN at the Z lines.

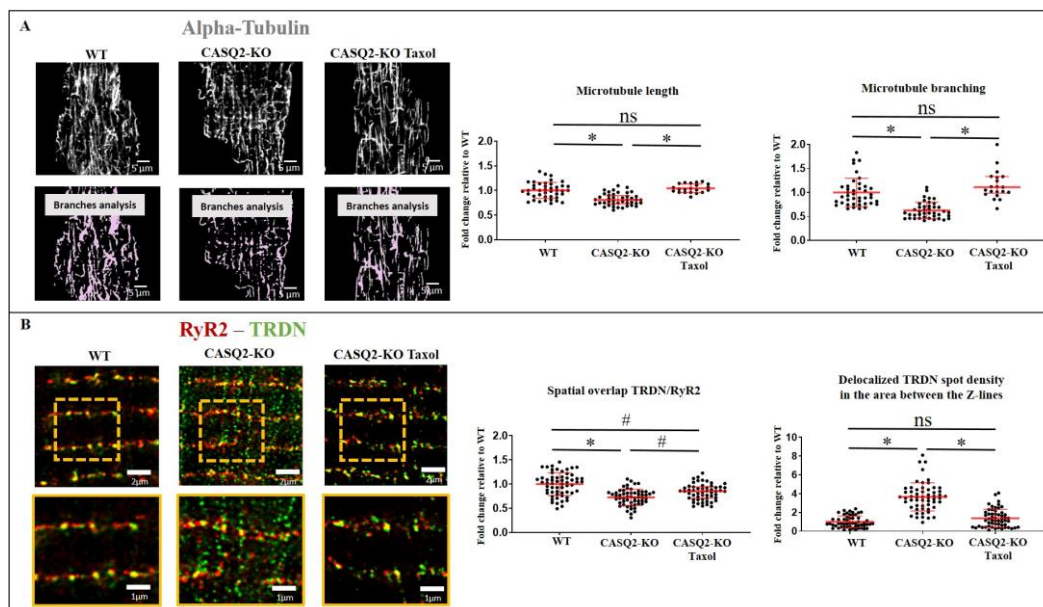


**Figure 3.9 - Taxol treatment restores the microtubule network and TRDN localization**

**A-** Confocal images of isolated cardiomyocytes treated with Taxol stained for alpha-tubulin (white) (upper panel) and mirror binary mask images (MINA, image-J plug in). **(Left)** The treatment with Taxol reverts the microtubules alterations observed in CASQ2-KO cardio myocyte. The branch length mean (Fold change relative to WT, mean  $\pm$  SD: WT:  $1 \pm 0.16$ ; CASQ2-KO:  $0.81 \pm 0.12$ ; CASQ2-KO + Taxol:  $1.04 \pm 0.09$ ). Kruskal–

Wallis test with Dunn's correction, WT vs CASQ2-KO, \*  $P < 0.001$ , CASQ2-KO vs CASQ2-KO + Taxol, \*  $P < 0.001$ , WT vs CASQ2-KO + Taxol,  $P = \text{NS}$ ) (WT: 3 mice 22 cells 42 fields; CASQ2-KO: 3 mice 22 cells 43 fields; CASQ2-KO + Taxol: 2 mice 11 Cells 21 fields). **(Right)** The tubulin branches network mean (ramification) have similar values to the WT (Fold change relative to WT, mean  $\pm$  SD: WT:  $1 \pm 0.30$ ; CASQ2-KO:  $0.63 \pm 0.17$ ; CASQ2-KO + Taxol:  $1.20 \pm 0.38$ . Kruskal–Wallis test with Dunn's correction, WT vs CASQ2-KO, \*  $P < 0.001$ , CASQ2-KO vs CASQ2-KO + Taxol, \*  $P < 0.001$ , WT vs CASQ2-KO + Taxol,  $P = \text{NS}$ ) (WT: 3 mice 22 cells 41 fields; CASQ2-KO: 3 mice 22 cells 41 fields; CASQ2-KO + Taxol: 2 mice 11 Cells 21 fields).

**B-** STED super-resolution images of isolated cardiomyocytes were double stained for RyR2 (red) and TRDN (green) (upper panel) (scale bar 2  $\mu\text{m}$ ). **(Left)** The co-localization parameter, based on Manders coefficient, indicates that CASQ2-KO cardio-myocytes treated with Taxol improved TRDN/RyR2 co-localization by 10% (Manders coefficient, fold change relative to WT, mean  $\pm$  SD: WT:  $1 \pm 0.23$ ; CASQ2-KO:  $0.73 \pm 0.17$ ; CASQ2-KO + Taxol A:  $0.83 \pm 0.17$ . Kruskal–Wallis test with Dunn's correction, WT vs CASQ2-KO, \*  $P < 0.001$ , CASQ2-KO vs CASQ2-KO + Taxol, #  $P = 0.021$ , WT vs CASQ2-KO + Taxol, #  $P = 0.001$ . (WT: 3 mice 22 cells 59 fields; CASQ2-KO: 3 mice 22 cells 57 fields; CASQ2-KO + Taxol: 2 mice 11 Cells 55 fields). **(Right)** STED super-resolution images has been used to calculate the delocalized TRDN density located in the area between the Z-lines. The treatment with Taxol reduces the population of the misplaced TRDN in CASQ2-KO (Fold change relative to WT, mean  $\pm$  SD: WT:  $1 \pm 0.63$ ; CASQ2-KO:  $3.7 \pm 1.5$ ; CASQ2-KO + Taxol:  $1.40 \pm 0.96$ ; Kruskal–Wallis test with Dunn's correction, WT vs CASQ2-KO, \*  $P < 0.001$ , CASQ2-KO vs CASQ2-KO + Taxol, \*  $P < 0.001$ , WT vs CASQ2-KO + Taxol,  $P = \text{NS}$ ) (WT: 3 mice 18 cells 55 fields; CASQ2-KO: 3 mice 18 cells 57 fields; CASQ2-KO + Taxol : 3 mice 21 cells 56 fields).

### 3.9 HDAC6 inhibition improves TRDN localization in CASQ2-KO cardiomyocytes

As previously described, the microtubule disorganization we found is caused by HDAC6 hyperactivity, since the inhibition of this deacetylase by Tubostatin A improved the microtubule net (Figure 3.5). We treated CASQ2-KO mice with Tubostatin A in order to evaluate TRDN's position, expecting similar results as those achieved with Taxol treatment (Figure 3.9). Our hypothesis was fully confirmed, HDAC6 inhibition improved TRDN localization. STED super-resolution images confirmed an improvement on TRDN/RYR2 colocalization (WT vs CASQ2-KO + Tubostatin A,  $P = \text{NS}$ ) (Figure 3.10-Left) and reduction of the delocalized TRDN population in the area between the Z-lines (CASQ2-KO vs CASQ2-KO + Tubostatin A,  $P < 0.001$ ) (Figure 3.10-Right) in CASQ2-KO mice treated with Tubostatin A.

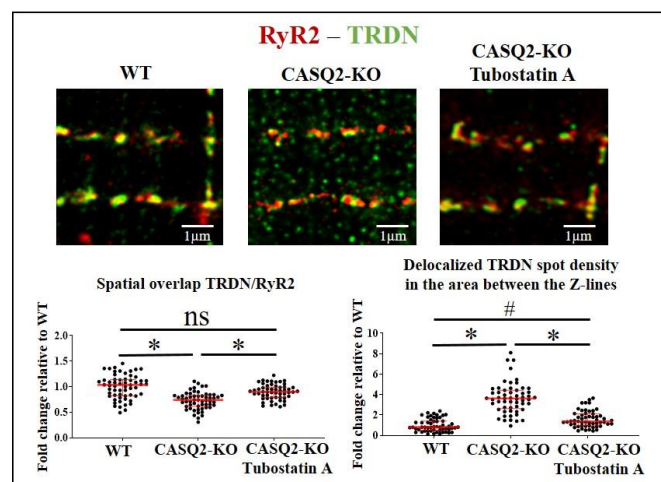


**Figure 3.10 – HDAC6 inhibition by Tubostatin A restores TRDN localization**

STED super-resolution images of isolated cardiomyocytes double stained for RyR2 (red) and TRDN (green). **(Left)** The colocalization parameter, based on Manders coefficient, indicates that CASQ2-KO cardiomyocytes treated with Tubostatin A improved TRDN/RyR2 colocalization [Manders coefficient, fold change relative to WT, median (p25 - p75): WT: 1.04 (0.82 – 1.14); CASQ2-KO: 0.74 (0.62 – 0.83) CASQ2-KO + Tubostatin A: 0.90 (0.79 – 0.99)]. Kruskal–Wallis test with Dunn's correction, WT vs CASQ2-KO, \*  $P < 0.001$ ; CASQ2-KO vs CASQ2-KO + Tubostatin A, \*  $P < 0.001$ ; WT vs CASQ2-KO + Tubostatin A,  $P = \text{NS}$  (WT: 3 mice 18 cells 59 ROIs; CASQ2-KO: 3 mice 18 cells 57 ROIs; CASQ2-KO + Tubostatin A: 3 mice 18 Cells 55 ROIs). **(Right)** STED super-resolution images have been used to calculate the delocalized TRDN density located in the area between the Z-lines. The treatment with Tubostatin A reduces the population of the misplaced TRDN in CASQ2-KO [Fold change relative to WT, median (p25 - p75): WT: 0.80 (0.50 – 1.40); CASQ2-KO: 3.62 (2.62 – 4.42); CASQ2-KO + Tubostatin A: 1.37 (0.95 – 2.11)]; Kruskal–Wallis test with Dunn's correction, WT vs CASQ2-KO, \*  $P < 0.001$ ; CASQ2-KO vs CASQ2-KO + Tubostatin A, \*  $P < 0.001$ ; WT vs CASQ2-KO + Tubostatin A, #  $P = 0.007$  (WT: 3 mice 18 cells 55 ROIs; CASQ2-KO: 3 mice 18 cells 57 ROIs; CASQ2-KO + Tubostatin A: 3 mice 18 Cells 55 ROIs).

### **3.10 Microtubule-associated proteins could be involved in the expansion of CASQ2-KO jSR**

The disruption of the microtubular network and the enlargement of the jSR observed in the heart of CASQ2-KO mice by Electron Microscopy (Knollmann et al., 2006) led us to investigate the pivotal proteins implicated in the regulation of the architecture of the Endoplasmic Reticulum. One of them is the cytoskeleton-linking membrane protein 63 also called CLIMP63. CLIMP63 is known to promote the formation of sheets in the ER at the expenses of tubular structures. Different groups collected experimental evidence, in different cell types, concurring to the hypothesis that CLIMP63 maintains the width of the ER cisternae and that when the protein is downregulated the ER shrinks significantly (Shen et al., 2019). For this reason in 2010 Shibata et al defined CLIMP63 as the “luminal ER spacer” (Shibata et al., 2010). Recently, Dr Marty and coworkers discovered that in skeletal muscle CLIMP63 is the protein that connects Triadin with microtubules (Osseni et al., 2016) but whether the protein serves the same function in the heart is unknown. We therefore compared the protein and mRNA levels of CLIMP 63 in hearts from WT and CASQ2-KO mice and demonstrated that both the protein ( $P<0.001$ ) (Figure 3.11A-Left) and transcript levels ( $P=0.020$ ) (Figure 3.11A-Right) are significantly elevated in CASQ2-KO mice compared to WT mice; supporting the hypothesis that the enlargement of the ER observed in CASQ2-KO mice might be mediated by the increased expression of CLIMP 63. Furthermore, we investigated the interaction between CLIMP63 and alpha-Tubulin and we confirmed by Co-immunoprecipitation (Figure 3.11B) that the protein interaction is doubled in CASQ2-KO mice compared to WT ( $P=0.05$ ).

We also investigated the interplay between RyR2 and CLIMP63 by co-immunoprecipitation and documented that in the heart of CASQ2-KO mice this interaction is doubled compared to the WT. Interestingly, using STED super resolution imaging we observed that in CASQ2-KO cardiomyocytes the co-localization between RyR2 and CLIMP63 is not affected by the absence of CASQ2 ( $P=NS$ ) (Figure 3.11C).

We explored also another SR shaping protein expressed in heart: REEP5. While CLIP63 promotes the formation of flat cisternal “sheets”, REEP5 promotes the membrane curvature that helps forming tubules. Our RT-PCR data showed transcriptional downregulation of REEP5 ( $P<0.001$ ) (Figure 3.11D).



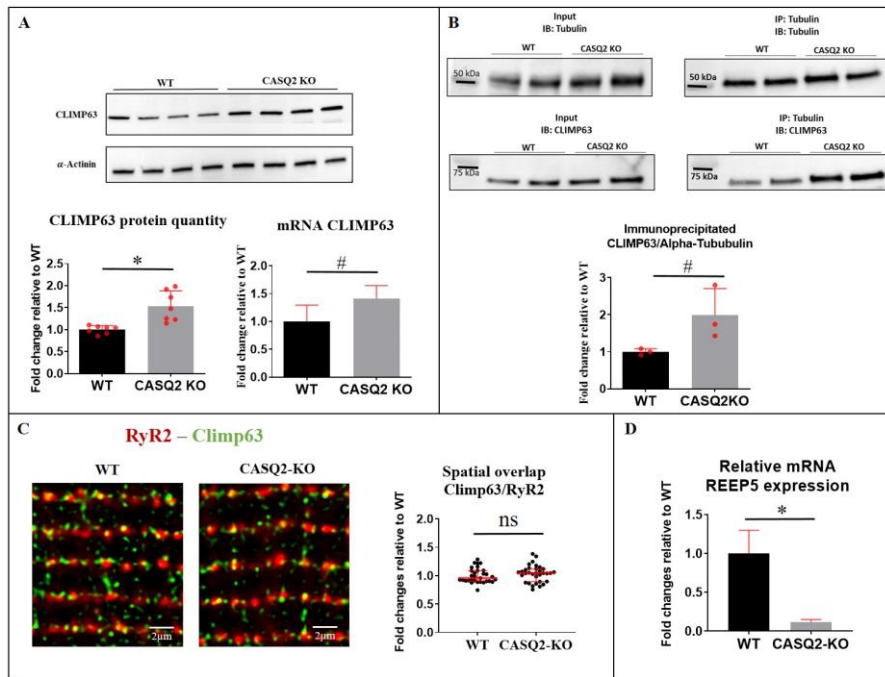


**Figure 3.11 – SR associated proteins alterations (Climp63-REEP5)**

**A-** (Left) WB from total heart protein homogenate from WT and CASQ2-KO mice. CASQ2-KO hearts present an increase in Climp63 protein content (Fold change relative to WT, mean  $\pm$  SD: WT:  $1.00 \pm 0.09$ ; CASQ2-KO:  $1.75 \pm 0.35$ ). Mann-Whitney test, \*  $P < 0.001$  (WT: 7 mice; CASQ2-KO: 7 mice). (Right) Real-time PCR analysis of Climp63 mRNA expression normalized on GAPDH. CASQ2-KO hearts show a significant increase Climp63 mRNA expression as compared to WT (fold change relative to WT, mean  $\pm$  SD: WT:  $1.00 \pm 0.30$ ; CASQ2-KO:  $1.41 \pm 0.23$ ); Mann Whitney test, #  $P = 0.020$  (WT: 6 mice; CASQ2-KO: 7 mice).

**B-** Co-immunoprecipitation assay. Magnetics beads were processed with anti alpha-tubulin antibody and they were used to immunoprecipitated Climp63. The quantity of co-immunoprecipitated Climp63 is higher in the CASQ2-KO as compared to WT. (Fold change relative to WT, mean  $\pm$  SD: WT:  $1.00 \pm 0.08$ ; CASQ2-KO:  $1.99 \pm 0.72$ ). Mann-Whitney test, #  $P = 0.05$  (WT: 3 mice; CASQ2-KO: 3 mice).

**C-** STED super-resolution images of isolated cardiomyocytes double stained for RyR2 (red) and Climp63 (green). The colocalization parameter shows that WT and CASQ2-KO have no difference on Climp63/RyR2 colocalization [Fold change relative to WT, median (p25 - p75): WT: 0.96 (0.90 - 1.09); CASQ2-KO: 1.05 (0.90 - 1.12). Mann-Whitney test,  $P = \text{NS}$  (WT: 2 mice 10 cells 31 ROIs; CASQ2-KO: 2 mice 11 cells 33 ROIs).

**D-** Real-time PCR analysis of REEP5 mRNA expression normalized on GAPDH. CASQ2-KO hearts show a significant decrease REEP5 mRNA expression as compared to WT (fold change relative to WT, mean  $\pm$  SD: WT:  $1.00 \pm 0.3$ ; CASQ2-KO:  $0.12 \pm 0.03$ ); Mann Whitney test, \*  $P < 0.001$  (WT: 7 mice; CASQ2-KO: 7 mice).

### 3.11 Microtubule derangement explains the expansion of the jSR in CASQ2-KO

To further, demonstrate the involvement of microtubules in SR morphology, and that their alteration could cause a concomitant alteration of SR geometry, we tested whether the modulation of microtubule polymerization could affect the SR structuring.

First, we tested whether the delivery of Colchicine, that as previously demonstrated causes important destructing of the microtubule network, would cause an expansion of the SR in WT cardiomyocytes. Experiments fully confirmed our expectations demonstrating how the perturbation of the microtubule network influences SR architecture. Transmitted Electron Microscopy (TEM) of WT colchicine heart showed a significant increase of The JSR width (WT vs WT + Colchicine,  $P < 0.001$ ) (Figure 3.12-Left) and he SR area (WT vs WT + Colchicine,  $P = 0.023$ ) (Figure 3.12-Right) compared to WT.

In parallel, we demonstrated the importance of a stable microtubule network for SR morphology by exposing CASQ2-KO mice to Taxol. The Inhibition of microtubule depolymerization by Taxol is able to shrink the expanded JSR cisternae: The JSR width (CASQ2-KO vs CASQ2-KO + Tubostatin A,  $P<0.001$ ) (Figure 3.12-Left) and the SR area (CASQ2-KO vs CASQ2-KO + Tubostatin A,  $P<0.001$ ) (Figure 3.12-Right) were significantly increased in comparison with the non-treated mice.

Since HDAC6 is involved in the mechanism of microtubules alteration in CASQ2-KO mice, we tested whether the reestablishment of microtubule network conveyed by Tubostatin A would correspond to an improvement of SR morphology in CASQ2-KO. TEM images of Tubostatin A treated mice heart demonstrated that the JSR width (CASQ2-KO vs CASQ2-KO + Tubostatin A:  $P<0.001$ ) (Figure 3.12-Left) and SR area (CASQ2-KO vs CASQ2-KO + Tubostatin A:  $P<0.001$ ) (Figure 3.12-Right) significantly improved compared to the CASQ2-KO non-treated mice.

The results showed how microtubules play a crucial role on SR architecture and that the reported SR expansion in CASQ2-KO hearts (Knollmann et al., 2006) is caused by the altered microtubule network.

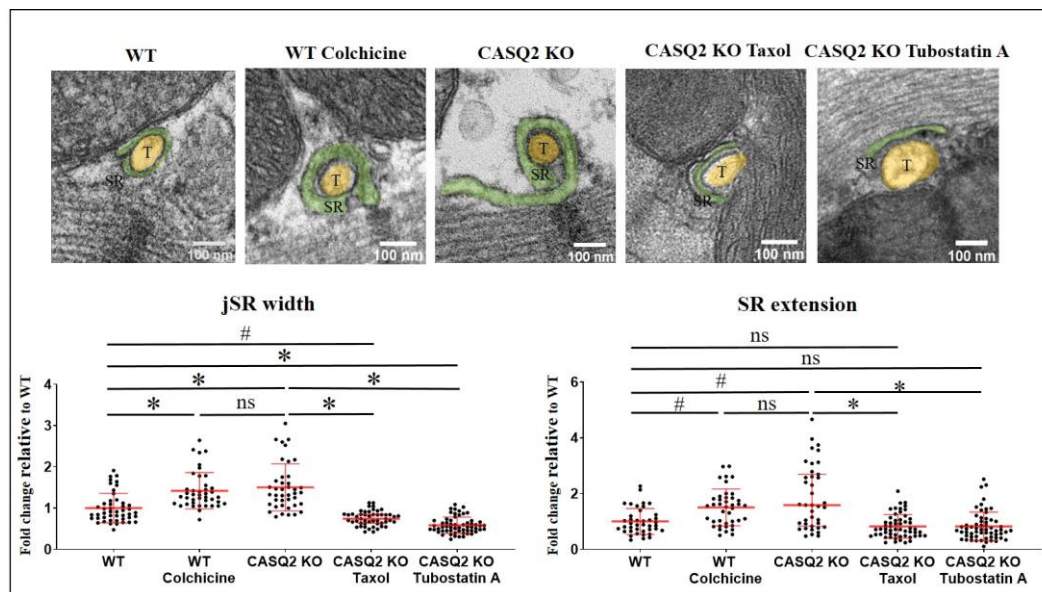


**Figure 3.12 – The SR expansion in CASQ2-KO heart is caused by microtubules alterations**

TEM images of WT hearts treated with microtubule modulating agents (highlighted in yellow: T-tubule, in green : Sarcoplasmic reticulum). (Left) Colchicine treatment in WT causes the increase of junctional SR width, while repolymerisation of the microtubule network by Taxol and Tubostatin reduce the JSR width (Fold change relative to WT, median (p25 - p75): WT: 0.89 (0.75 - 1.12); WT + Colchicine: 1.28 (1.11 - 1.52); CASQ2-KO: 1.36 (1.08 - 1.70); CASQ2-KO + Taxol: 0.74 (0.63 - 0.85); CASQ2-KO + Tubostatin A: 0.54 (0.45 - 0.69). Kruskal–Wallis test with Dunn's correction, WT vs CASQ2-KO, \*  $P<0.001$ ; WT vs WT + Colchicine, \*  $P<0.001$ ; WT + Colchicine vs CASQ2-KO:  $P=NS$ , CASQ2-KO vs CASQ2-KO + Taxol: \*  $P<0.001$ ; CASQ2-KO vs CASQ2-KO + Tubostatin A: \*  $P<0.001$ ; WT vs CASQ2-KO + Taxol: #  $P=0.035$ ; WT vs CASQ2-KO + Tubostatin A: \*  $P<0.001$  (WT : 2 mice 47 fields; WT + Colchicine : 2 mice 41 fields CASQ2-KO: 2 mice 41 fields; CASQ2-KO + Taxol: 3 mice 50 fields; CASQ2-KO + Tubostatin A: 3 mice 59 fields). (Right) Similarly, the SR extension follows the same trends, after Colchicine treatment in WT the SR volume increases and Taxol and Tubostatin A treatment in CASQ2-KO reduces it (Fold change relative to WT, median (p25 - p75): WT : 0.88 (0.66 - 1.23); WT + Colchicine: 1.56 (0.96 - 1.85); CASQ2-KO: 1.59 (0.83 - 2.69); CASQ2-KO + Taxol: 0.72 (0.49 - 1.06); CASQ2-KO + Tubostatin A : 0.69 (0.45 - 1.00). Kruskal–Wallis test with Dunn's correction, WT vs CASQ2-KO, #  $P=0.016$ ; WT vs WT + Colchicine, #  $P=0.023$ ; WT + Colchicine vs CASQ2-KO:  $P=NS$ , CASQ2-KO vs CASQ2-KO + Taxol: \*  $P<0.001$ ; CASQ2-KO vs CASQ2-KO + Tubostatin A: \*  $P<0.001$ ; WT vs CASQ2-KO + Taxol: #  $P=0.035$ ; WT vs CASQ2-KO + Tubostatin A: \*  $P<0.001$  (WT: 2 mice 40 fields; WT + Colchicine : 2 mice 41 fields; CASQ2-KO: 2 mice 39 fields; CASQ2-KO + Taxol: 3 mice 50 fields; CASQ2-KO + Tubostatin A: 3 mice 60 fields).

### 3.12 TRDN degradation in CASQ2-KO

Since the first characterizations of CASQ2-KO models, it was known that the absence of CASQ2 caused a significant reduction of TRDN protein quantity (Chopra et al., 2009) [our data confirmed TRDN downregulation in CASQ2-KO hearts,  $P=0.05$  (Figure 3.13)] but the mechanism of this decrease has remained unknown for decades.

### 3.13 TRDN mRNA content in CASQ2-KO heart

First of all, we decided to test if TRDN reduction was associated with changes in its expression. By RT-PCR we quantified the *Trdn* mRNA quantity and found that TRDN reduction is not associated with a direct reduction of *Trdn* mRNA expression ( $P=NS$ ) (Figure 3.13-Right) (Knollmann et al., 2006). Therefore, we hypothesized that TRDN could undergo degradation processes in CASQ2-KO mice.

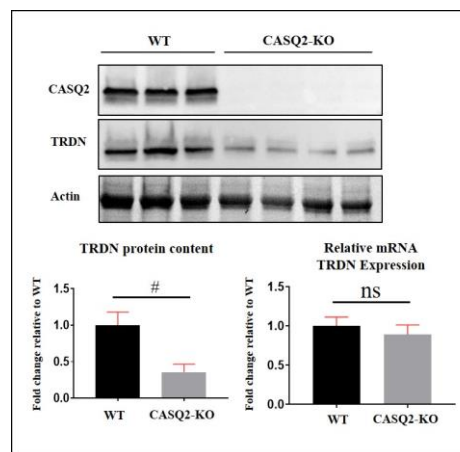


**Figure 3.13 –Protein and mRNA TRDN levels are reduced in CASQ2-KO hearts**

(Left) WB of total heart protein homogenate from WT and CASQ2-KO mice. CASQ2-KO hearts presents an decrease in TRDN protein quantity compared to WT (Fold change relative to WT, mean  $\pm$  SD: WT:  $1.00 \pm 0.18$ ; CASQ2-KO:  $0.36 \pm 0.11$ ). Mann Whitney test, #  $P=0.05$  (WT: 3 mice; CASQ2-KO: 4 mice). (Right) Real-time PCR analysis of TRDN mRNA expression normalized on GAPDH. CASQ2-KO hearts do not show changes in TRDN mRNA expression as compared to WT (fold change relative to WT, mean  $\pm$ SD: WT:  $1.00 \pm 0.2341$ ; CASQ2-KO:  $0.8366 \pm 0.1320$ ); Mann Whitney test,  $P=NS$  (WT: 5 mice; CASQ2-KO: 5 mice).

### 3.14 Proteasome inhibition

We tested whether TRDN protein levels could be increased by inhibition of the Proteasome, since is one of the principal degradation machinery within the cells. After 16 hours of exposure of isolated ventricular cardiomyocytes to the proteasome inhibitor MG132, we tested the efficacy of the treatment by studying the accumulation of the total poly-ubiquitinated proteins as a consequence of proteasome machinery blockage. Although the drug was efficiently blocking the Proteasome, as shown by an overall increase in the level of undegraded ubiquitinated proteins, TRDN protein levels were not increased in CASQ2-KO ( $P=NS$ ) (Figure 3.14).

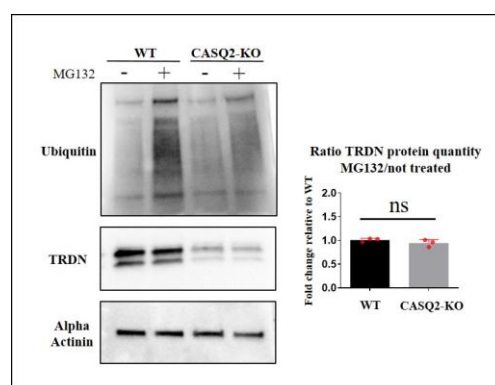


**Figure 3.14 – TRDN is not degraded by the proteasome machinery in CASQ2-KO hearts**

Western blot analysis of total protein homogenate from isolated cardiomyocytes exposed to MG132. Effect on proteasome inhibition has been checked by ubiquitin bands densitometry. The MG132/not treated ratio of TRDN protein quantity does not change between WT and CASQ2-KO (fold change relative to WT, mean  $\pm$ SD: WT:  $1.00 \pm 0.0367$ ; CASQ2-KO:  $0.9455 \pm 0.07729$ ). Mann Whitney test,  $P=NS$  (WT: 3 mice; WT+MG132: 3 mice; CASQ2-KO: 3 mice; CASQ2-KO + MG132: 3 mice).

### 3.15 Autophagy flux in CASQ2-KO heart

Another widespread mechanism of degradation in different cell types, including cardiomyocytes, is Autophagy.

Thus, we performed a series of experiments to assess whether TRDN was degraded by autophagy. We first determined the global autophagic flux in WT and CASQ2-KO cardiomyocytes. To this end, we exposed cardiomyocytes to the inhibitors of autophagosome-lysosome fusion chloroquine (CQ) or hydroxychloroquine (HCQ) and measured the accumulation of autophagolysosomes using the autophagosomes marker LC3 (Klionsky et al., 2016). We measured the autophagy flux by Western Blot, which showed that CQ induces an increase in the LC3 II/LC3 I ratio in CASQ2-KO compared to WT ( $P=0.028$ ) (Figure 3.15A). Both drugs also produced an accumulation of the autophagosome marker LC3 in both WT and CASQ2-KO cardiomyocytes, indicating that in both genotypes the autophagic flux is present. We confirmed the observation by measuring the LC3 signal by confocal microscopy and found an increased LC3 accumulation signal in CASQ2-KO cardiomyocytes ( $P<0.001$ ) (Figure 3.15B), suggesting autophagy hyper-activation in response to CASQ2 deficiency.

Moreover, we tested the presence of a second autophagic marker, Lamp1, in an attempt to confirm the previous result by independent means. This protein is contained within the lysosome's membranes and its increase correlates with an elevated autophagy flux (Cheng et al., 2018; Eskelinen, 2006; Klionsky et al., 2016). Confocal images of cardiomyocytes stained for Lamp1 showed higher accumulation of these bodies in CASQ2-KO mice ( $P<0.001$ ) (Figure 3.15C). Thus, 2 separate markers confirmed that autophagy is hyper-activated in the absence of CASQ2.

In order to understand whether an augmented activation of autophagy was associated with TRDN degradation, first, we studied TRDN-LC3 colocalization following autophagy inhibition. We acquired STED images of cardiomyocytes from mice treated with CQ and stained for LC3 and TRDN and found that the linear intensity correlation (Pearson coefficient) (see methods) was higher in CASQ2-KO than in WT mice ( $P < 0.001$ ) (Figure 3.15D) The data suggested the enhanced recruitment of TRDN to the autophagy pathway in CASQ2 mutant cells.

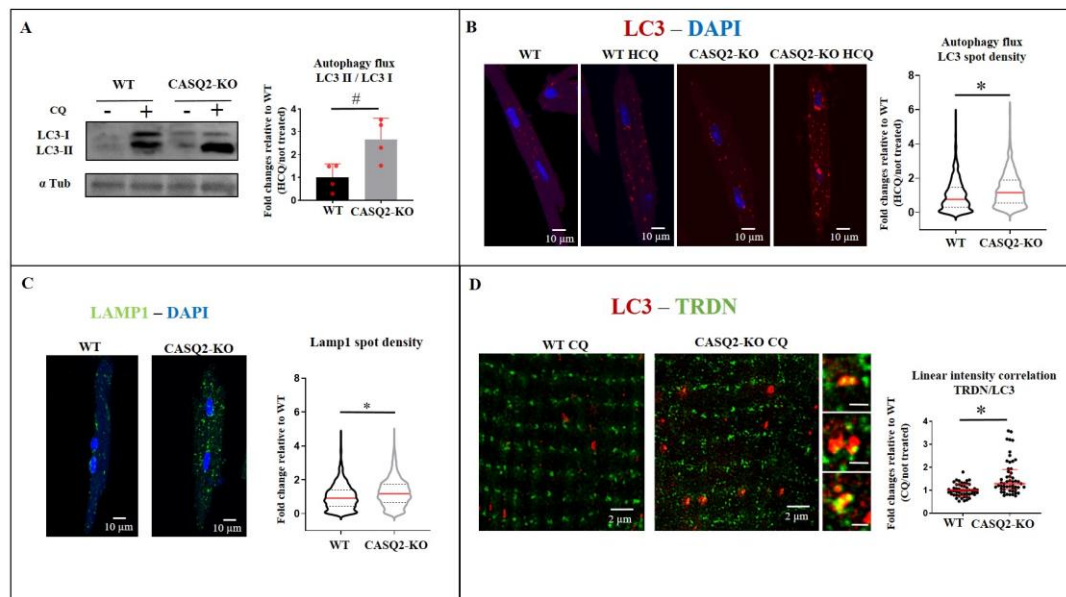


**Figure 3.15 – Autophagy Flux is increased in CASQ2-KO cardiomyocytes**

**A-** WB of isolated cardiomyocytes protein homogenate from WT and CASQ2-KO mice after HCQ treatment. Autophagy flux has been calculated as the ratio between LC3II, mature autophagic isoform, and LC3I, immature cytoplasmic isoform and we observed that LC3II/LC3I increased in CASQ2-KO cardiomyocytes (Fold change relative to WT, mean  $\pm$  SD: WT:  $1.00 \pm 0.60$ ; CASQ2-KO:  $2.67 \pm 0.93$ ). Mann Whitney test, #  $P = 0.028$  (WT: 4 mice; WT + HCQ: 4 mice; CASQ2-KO: 4 mice; CASQ2-KO + HCQ: 4 mice).

**B-** Confocal images of isolated cardiomyocytes treated with HCQ stained for LC3 (red) and DAPI (blue) (upper panel). The autophagy flux in the CASQ2-KO cardiomyocytes is increased compared to WT (Fold change relative to WT, median (p25 - p75): WT: 0.77 (0.31 - 1.48); CASQ2-KO: 1.16 (0.56 - 1.90). Mann Whitney test, \*  $P < 0.001$  (WT: 3 mice 989 cells; WT+HCQ: 3 mice 748 cells; CASQ2-KO: 3 mice 730; CASQ2-KO+HCQ: 3 mice 877 cells).

**C-** Confocal images of isolated cardiomyocytes stained for LAMP1 (green) and DAPI (blue). In CASQ2-KO cardiomyocytes LAMP1 spot density increases as compared to WT [Fold change relative to WT, median (p25 - p75): WT: 0.91 (0.43 - 1.41); CASQ2-KO: 1.18 (0.67 - 1.75)]. Mann Whitney test, \*  $P < 0.001$  (WT: 3 mice 989 cells; CASQ2-KO: 3 mice 730 cells).

**D-** STED super-resolution images of isolated cardiomyocytes double stained for LC3 (red) and TRDN (green). Zoomed images show the accumulation of LC3 and TRDN in the same region in CASQ2-KO after autophagy inhibition (lower panel) (scale bar 100 nm). In CASQ2-KO cardiomyocytes the colocalization between LC3 and TRDN increases (CQ/not treated Pearson coefficients, fold change relative to WT median (p25 - p75): WT: 0.98 (0.83 - 1.18); CASQ2-KO: 1.28 (1.04 - 1.90). Mann-Whitney test, \*  $P < 0.001$  (WT+CQ: 3 mice 18 cells 51 ROIs; CASQ2-KO+CQ: 3 mice 19 cells 52 ROIs).

### 3.16 Inhibition of early autophagosome formation in CASQ2-KO cardiomyocytes

The specific autophagy pathway involved in TRDN degradation was studied by treating cardiomyocytes with 3-Methyladenine (3MA), a specific inhibitor of macroautophagy that prevents early autophagosome formation (Klionsky et al., 2016). 3MA treatment restores TRDN/RyR2 colocalization (WT vs CASQ2-KO + 3MA,



P=NS) (Figure 3.16A-Left) and reduces the TRDN spot density at the Z-line in CASQ2-KO cardiomyocytes (WT vs CASQ2-KO + 3MA, P=NS) (Figure 3.16A-Right)

Autophagosome formation inhibition by 3MA rescues the localization of TRDN along the Z-lines in CASQ2 mutant cardiomyocytes. These observations suggest that the nucleation phase of autophagy could prime TRDN's aggregation.

In order to understand if the delocalization of TRDN is primarily due to microtubules alteration or autophagy activation, we treated WT cardiomyocytes with both Colchicine and 3MA. STED super resolution images of Cardiomyocytes stained for TRDN and RyR2 showed that TRDN colocalization with RyR2 is reduced, compared to the non-treated WT ( $P < 0.001$ ), and no difference was observed in comparison to CASQ2-KO ( $P = \text{NS}$ ). The population of delocalized TRDN in the area in between the Z- line follows the same trend: the Colchicine + 3MA treatments in the WT cause an important increase of TRDN spot density in the area between the Z-lines compared to the WT ( $P < 0.001$ ), and no difference with CASQ2-KO ( $P = \text{NS}$ ). TRDN delocalizes after microtubular disruption despite the inhibition of autophagosomes formation: the microtubular alterations are the cause of TRDN misplacement confirming that TRDN is delocalized due to the defect in trafficking and targeting. Autophagy is not the primary cause of TRDN delocalization.

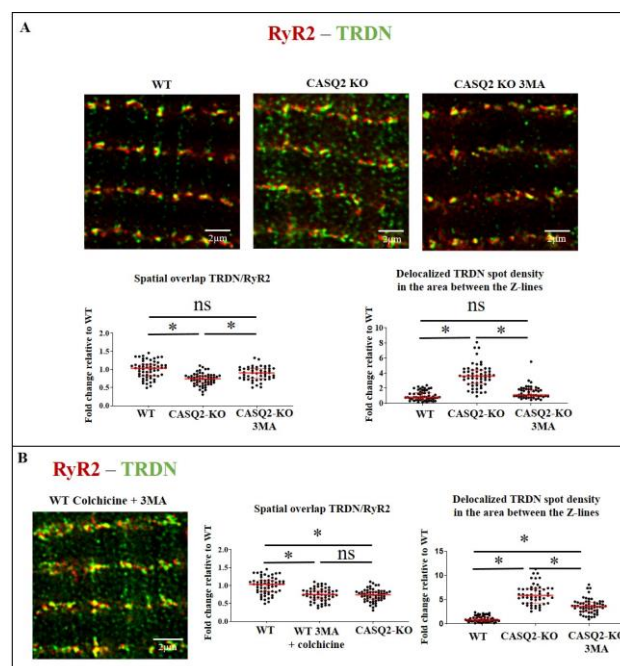


**Figure 3.16 – Nucleation phase of autophagy primes TRDN aggregation**

**A- (Left)** Isolated cardiomyocytes stained for RyR2 and TRDN after 3MA. Spatial overlap 3MA treatment (Fold change relative to WT, median (p25 - p75): WT: 1.04 (0.82 – 1.14); CASQ2-KO: 0.74 (0.62 – 0.83); CASQ2-KO + 3MA: 0.90 (0.75 – 1.03). Kruskal–Wallis test; WT vs CASQ2-KO, \*  $P < 0.001$ ; CASQ2-KO vs CASQ2 + 3MA, \*  $P < 0.001$ ; WT vs CASQ2-KO + 3MA,  $P = \text{NS}$ . (WT: 3 mice 18 cells 57 fields; CASQ2-KO: 3 mice 18 cells 57 fields; CASQ2-KO + 3MA: 3 mice 17 cells 49 fields). **(Right)** The density of TRDN placed in the area between the Z-lines (Fold change relative to WT, median (p25 - p75): WT: 0.81 (0.50 – 1.40); CASQ2-KO: 3.62 (2.62 – 4.42); CASQ2-KO + 3MA: 1.11 (0.87 – 1.86). Kruskal–Wallis test,

WT vs CASQ2-KO, \*  $P < 0.001$ ; CASQ2-KO vs CASQ2 +3 MA, \*  $P < 0.001$ ; WT vs CASQ2-KO + 3MA,  $P = NS$  (WT:3 mice 17 cells 55 fields; CASQ2-KO: 3 mice 18 cells 57 fields; CASQ2-KO + 3MA: 3 mice 17 cells 48 fields).

**B-** (Left) Isolated cardiomyocytes stained for RyR2 and TRDN after 3MA + Colchicine. Spatial overlap 3MA + colchicine (Manders coefficient, fold change relative to WT, median (p25 - p75): WT: 1.06 (0.82 - 1.14); CASQ2-KO: 0.74 (0.62 - 0.83); CASQ2-KO + 3MA: 0.75 (0.61 - 0.86). Kruskal-Wallis test, WT vs CASQ2-KO, \*  $P < 0.001$ ; CASQ2-KO vs CASQ2 +3MA+ colchicine,  $P = NS$ ; WT vs CASQ2-KO + 3MA+ colchicine, \*  $P < 0.001$ . (WT:3 mice 18 cells 59 fields; CASQ2-KO: 3 mice 18 cells 57 fields CASQ2-KO+ 3MA+ colchicine: 3 mice 18 cells 54 fields). (Right) The density of TRDN placed in the area between the Z-lines (Fold change relative to WT, median (p25 - p75): 0.81 (0.50 - 1.40); CASQ2-KO: 3.62 (2.62 - 4.42); CASQ2-KO + 3MA + Colchicine: 5.87 (4.27 - 11.35). Kruskal-Wallis test, WT vs CASQ2-KO, \*  $P < 0.001$ ; CASQ2-KO vs CASQ2 +3MA+ colchicine, \*  $P < 0.001$ ; WT vs CASQ2-KO + 3MA+ colchicine, \*  $P < 0.001$  (WT:3 mice 17 cells 55 fields; CASQ2-KO: 3 mice 18 cells 57 fields; CASQ2-KO + 3MA + Colchicine: 3 mice 18 cells 52 fields).

### 3.17 TRDN is degraded by autophagy in CASQ2-KO

Our experiments so far have shown that a close relationship exists between TRDN and autophagy. We next explored the autophagic degradation of TRDN by Western blot. Mice were treated with autophagy inhibitor CQ in vivo and TRDN accumulation measured by WB at different time-points. First, we treated CASQ2-KO mice with 10 mg/kg/day of CQ, autophagy inhibitor, for 7 days through osmotic mini-pumps (Alzlet, 2001) implanted subcutaneously. The results showed that autophagy inhibition caused a significant increase in TRDN protein quantity in CASQ2-KO ( $P = 0.015$ ) (Figure 3.17A). We decided to reduce the CQ exposition using an acute treatment 50mg/kg for 24h and similarly the TRDN quantity were significant increased ( $P = 0.015$ ) (Figure 3.17B).

The results demonstrated the involvement of autophagy in TRDN degradation: both acute and chronic treatment doubled TRDN's protein quantity in CASQ2 KO mice. Contrarily, in WT cardiomyocytes TRDN levels were not altered upon autophagy inhibition (data not shown), indicating that either autophagy does not play a role in the homeostatic degradation of TRDN or that the homeostatic turnover is too slow to be detected with these approaches.

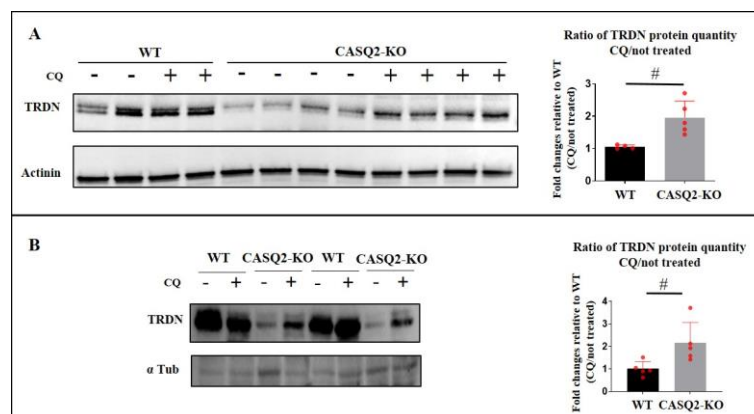


**Figure 3.17 – chronic and acute autophagy inhibition causes TRDN accumulation**

**A-** WB of isolated cardiomyocyte protein homogenate from WT and CASQ2-KO mice after chronic (7 days) CQ treatment. Autophagy inhibition in the KO mice causes an increase of TRDN quantity in the ratio CQ/not treated (Fold change relative to WT, mean ± SD: WT: 1.05 ± 0.06; CASQ2-KO: 1.95 ± 0.5). Mann-Whitney test, #  $P = 0.015$  (WT: 4 mice; WT + CQ: 4 mice; CASQ2-KO: 6 mice; CASQ2-KO + CQ: 5 mice).

**B-** WB of isolated cardiomyocyte protein homogenate from WT and CASQ2-KO mice after Acute CQ treatment (24h). Autophagy inhibition in the KO mice causes an increase of TRDN quantity in the ratio CQ/not treated (Fold change relative to WT, mean  $\pm$  SD: WT:  $1.00 \pm 0.33$ ; CASQ2-KO:  $2.15 \pm 0.91$ ). Mann Whitney test, # P=0.015 (WT: 5 mice; WT + CQ: 5 mice; CASQ2-KO: 5 mice; CASQ2-KO + CQ: 5 mice).

### 3.18 Aggrephagy drives TRDN degradation in CASQ2-KO cardiac myocytes

In order to investigate the connection between microtubule alterations and TRDN degradation by autophagy, we explored Aggrephagy, a form of macroautophagy that degrades aggregates of mislocalized proteins (or misfolded, damaged, unused proteins) (Dikic, 2017).

Isolated cardiomyocytes were stained with a fluorescent reactive (Proteostat, Enzo Life Sciences) able to specifically detect Aggresomes. Confocal microscopy images showed a higher accumulation of protein aggregates in CASQ2-KO cells ( $P < 0.001$ ) (Figure 3.18A). Although the aggresomes' cellular localization has been reported to be in the perinuclear area (Stürner, Behl, 2017), our results showed a scatter organization of the aggresomes along the cardiomyocytes. We believe that this peculiar aggresomes organization could be caused by trafficking failure driven by the disruption of the microtubule architecture, responsible for their transport to the perinuclear microtubule organization center (Garcia-Mata et al., 2002).

Furthermore, in order to validate the formation of TRDN aggregates in CASQ2-KO, we used a proximity ligation assay (PLA) (Duolink PLA technology, MERK). The technique allows to determine the protein-to-protein proximity by Confocal images. The assay relies on secondary Antibodies conjugated with a complementary oligonucleotide sequences able to pair only if in close distance. After a rolling circle amplification process the paired oligonucleotide sequences give a fluorescent signal. The incidence of PLA bright positive spots is higher in our model than in WT cells ( $P < 0.001$ ), indicating that TRDNs are pooled together in specific cellular areas of the cell (Figure 3.18B). Proteins that enter in the Aggresome formation/degradation pathway need to be ubiquitinated and recruited by HSP70 before being wrapped by the auto-phagosome membranes (Stürner, Behl, 2017). CASQ2-KO co-immunoprecipitation demonstrates that TRDN is ubiquitinated ( $P = 0.018$ ) and associated with HSP70 to a larger extent than in WT cells ( $P = 0.026$ ) (Figure 3.18C). Moreover, the treatment of mice with CQ to inhibit auto-phagosome fusion with lysosomes, increased the accumulation of ubiquitinated protein and HSP70-associated TRDN (Ubiquitin, WT vs. CASQ KO + CQ,  $P = 0.001$ ; HSP70, WT vs CASQ KO + CQ  $P = 0.036$ ) (Figure 3.18C), which confirmed that the degradation of TRDN is mediated by the Aggrephagy pathway. P62 promotes selective autophagy, and is degraded when this pathway is activated (Stürner, Behl, 2017). Confocal images of CASQ2-KO cardiomyocytes stained for p62 showed a reduced accumulation of p62 spot density vs. their WT counterparts ( $P < 0.001$ ) (Figure 3.18D). Furthermore, in dilated cardiomyopathy, p62 has been proposed to act as a proteotoxic stress sensor that promotes the selective degradation of misfolded and/or aggregated proteins by



autophagy (Su, Wang, 2011). Our results suggest that TRDN is degraded through selective macroautophagy in CASQ2-KO cardiomyocytes.

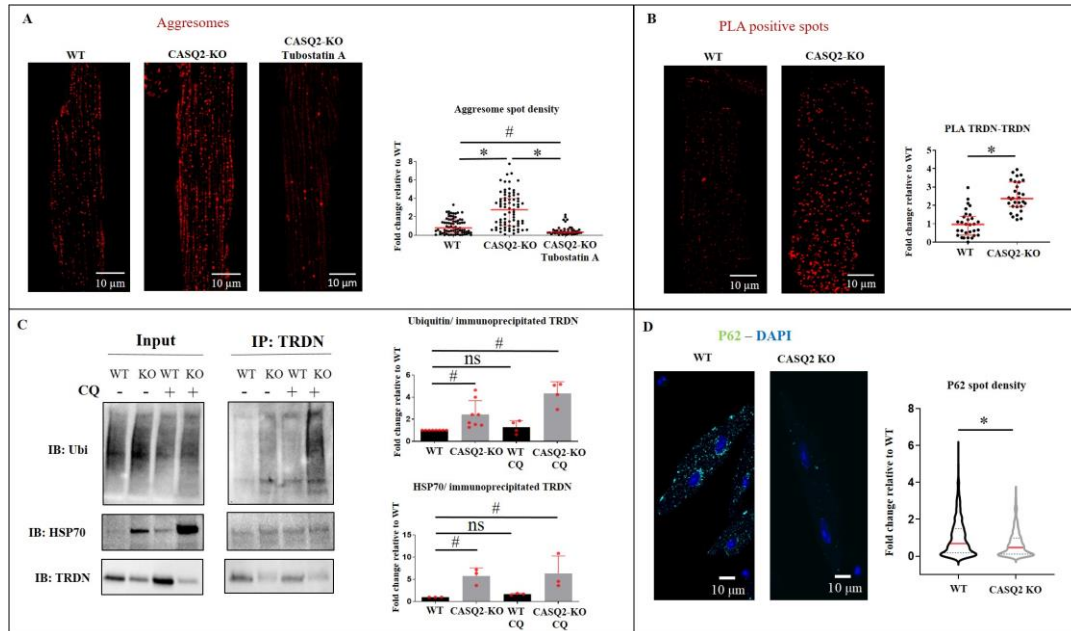


**Figure 3.18 – Aggresomes in CASQ2-KO cardiomyocytes**

**A-** Isolated cardiomyocytes have been stained with Proteostat kit to detect Aggresomes within the cells. The Aggresomes spot density is significantly increased in CASQ2-KO cardiomyocytes [Fold change relative to WT, median (p25 - p75): WT: 0.78 (0.30 – 1.68); CASQ2-KO: 2.77 (1.03 – 4.03)]. Kruskal–Wallis test with Dunn's correction, \* P<0.001 (WT: 5 mice, 75 Cells; CASQ2-KO: 5 mice, 75 cells).

**B-** The aggregation between TRDN monomers was calculated by Proximity ligation assay (PLA). The PLA spot density is significantly increased in CASQ2-KO cardiomyocytes [Fold change relative to WT, median (p25 - p75): WT: 0.97 (0.38 – 1.40); CASQ2-KO: 2.37 (1.94 – 3.28)]. Mann-Whitney test, \* P<0.001 (WT: 3 mice, 30 Cells; CASQ2-KO: 3 mice, 30 cells).

**C-** Using Co-immunoprecipitation assay we compared the quantity of ubiquitinated TRDN and TRDN in contact with HSP70 in WT, CASQ2-KO untreated heart and in WT and CASQ2-KO heart from mice exposed to Chloroquine (CQ). In CASQ2-KO mice TRDN is both ubiquitinated and labelled by HSP70 proteins in a higher extent compared to WT. When the Aggresome degradation pathway is interrupted by Chloroquine treatment both ubiquitinated and HSP70 tagged TRDN are accumulated significantly in CASQ2-KO group compared to controls (**Up**) Ubiquitin densitometry normalized on immunoprecipitated TRDN, fold change relative to WT, mean ± SD: WT: 1.00; CASQ2-KO: 2.43±1.25; WT + CQ: 1.28±0.58; CASQ2-KO: 4.34±1.05. Kruskal–Wallis test with Dunn's correction, WT vs . CASQ KO, # P=0.018; WT vs . CASQ KO + CQ, # P=0.001; WT vs WT + CQ, P= NS (WT: 8 mice; CASQ2-KO: 8 mice; WT + CQ: 4 mice CASQ2-KO + CQ: 4 mice). (**Down**) HSP70 densitometry normalized on immunoprecipitated TRDN (fold change relative to WT, mean ± SD: WT: 1.00; CASQ2-KO: 5.73 ± 1.85; WT + CQ: 1.66 ± 0.21; CASQ2-KO: 6.35 ± 3.93). Kruskal–Wallis test with Dunn's correction, WT vs . CASQ KO, # P=0.026; WT vs . CASQ KO + CQ, # P=0.036; WT vs WT + CQ, P= NS (WT: 3 mice; CASQ2-KO: 3 mice; WT + CQ: 3 mice CASQ2-KO + CQ: 3 mice).

**D-** Confocal images of isolated cardiomyocytes stained for p62 (green) and DAPI (blue). In CASQ2-KO cardiomyocytes p62 spot density decreases as compared to WT [Fold change relative to WT, median (p25 - p75): WT: 0.91 (0.43 – 1.41); CASQ2-KO: 1.18 (0.67 – 1.75)]. Mann-Whitney test, \* P<0.001 (WT: 3 mice 981 cells; CASQ2-KO: 3 mice 731 cells).

### 3.19 Protein proximity by FRET microscopy in CASQ2-KO cardiomyocytes

Since the first characterization of CASQ2 KO mouse model, Knollman and co-workes provided the interpretation that the reduction of TRDN could be compensatory mechanisms activated to compensate CASQ2 absence and maintain a balance between RyR2's regulatory proteins (Faggioni, Knollmann, 2012;

Knollmann et al., 2006). Instead, CASQ2 is able to reduce RyR2 open probability ( $P_0$ ), while TRDN increases it (Györke et al., 2004; Terentyev et al., 2005b). In this context, the absence of the RyR2 negative regulator (CASQ2) should be compensated by a reduction of the activator (TRDN). Given that the regulation on RyR2 open probability is performed by physical contact, we decided to explore if the absence of CASQ2 would be also associated with a reduction on TRDN proximity to RyR2.

Here, we study the proximity of proteins with a fluorescence-resonance-energy-transfer (FRET)-based approach. The technique relies on the physical property of the fluorophores, the resonance. When two fluorophores are in a distance equal or minor than 7 nm, one fluorophore (donor) transfers part of its energy to the other fluorophore (acceptor). Here we measure the FRET efficiency (FRET%) that is a value in function of the donor energy decay (Figure 3.19A). Isolated cardiomyocytes were labelled for TRDN and RyR2 with suitable fluorophores (Alexa fluor 514 and Alexa fluor 568) and data were acquired by ALBA microscope for FFS/FLIM (ISS).

First, we wanted to investigate if RyR2 organization in clusters was maintained in a model where CASQ2 is absent and Triadin is partially absent. RyR2 to RYR2 proximity did not differ between WT and CASQ2-KO cardiomyocytes ( $P=NS$ ) (Figure 3.19B-Up). Afterwards, Triadin/RyR2 proximity was studied. FRET data showed a significant reduction in TRDN proximity to RyR2 in CASQ2-KO cardiomyocytes ( $P<0.001$ ) (Figure 3.19B-Middle).

If Triadin is separated from the RyR2, does it stay in the jSR or does it diffuse away from it? In order to study the distribution of TRDN in SR area in CASQ2-KO cardiomyocytes, we studied the proximity of TRDN with a marker of the non-junctional SR: SERCA. Those two proteins have not been reported to be in proximity in WT mice and indeed the FRET efficiency results showed 0 FRET% in WT cardiomyocytes. Interestingly, the CASQ2-KO cardiomyocytes showed 50% FRET% between TRDN and SERCA ( $P<0.001$ ) (Figure 3.19B-Down). The last result was also validated by STED microscopy of cardiomyocytes stained for TRDN and SERCA since the colocalization of TRDN with SERCA was higher in CASQ2-KO cardiomyocytes ( $P=0.011$ ) (Figure 3.19C).

Overall, the FRET results show that the absence of CASQ2, lead a loss on TRDN-RYR2 interaction, and TRDN diffuses to non-junctional SR regions.

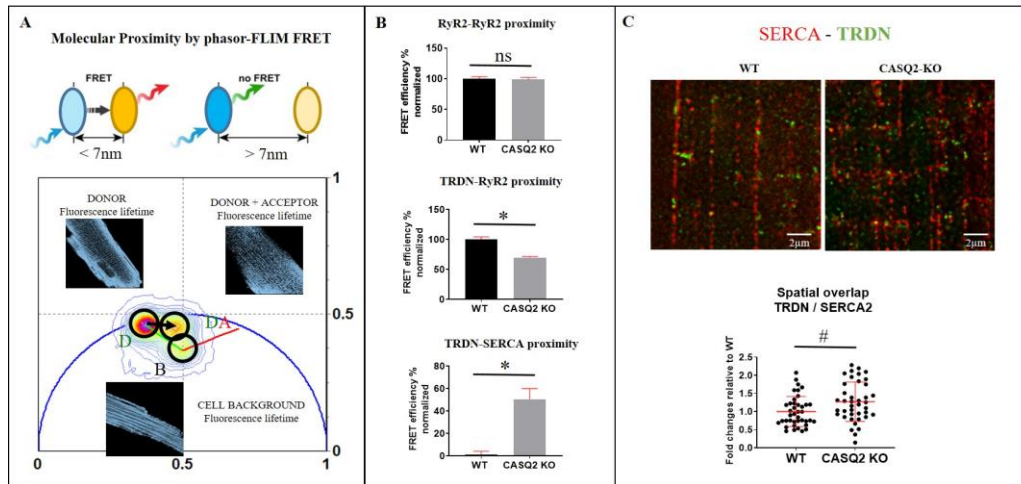


**Figure 3.19 – TRDN diffuses to the non-junctional SR.**

**A-** Representative images of phasor plot from isolated cardiomyocytes stained for TRDN and RyR2. Black arrow from D (donor) to DA (donor-Acceptor) represents the FRET % efficiency.

**B-** FRET efficiency percentage results. **(Up)** The proximity between RyR2s showed no changes between WT and CASQ2-KO (FRET% relative to WT, mean ± SD: WT: 100.0 ± 3.5 ; CASQ2-KO: 98.9 ± 3.2). Mann-Whitney test, P=NS (WT: 3 mice, 16 Cells; CASQ2-KO: 3 mice, 14 cells). **(Middle)** TRDN proximity to RyR2 is reduced in CASQ2-KO cardiomyocytes (FRET% relative to WT, mean ± SD: WT: 100.3 ± 4.2 ; CASQ2-KO: 69.9 ± 1.8). Mann-Whitney test, \* P<0.001 (WT: 3 mice 15 cells; CASQ2-KO: 3 mice 17 cells). **(Down)** TRDN proximity to the not junctional Sarcoplasmic reticulum, SERCA is increased in CASQ2-KO cardiomyocytes (FRET% relative to WT, mean ± SD: WT: 1.0 ± 3.2 ; CASQ2-KO: 50.5 ± 9.5). Mann-Whitney test, \* P<0.001 (WT: 3 mice 10 cells; CASQ2-KO: 3 mice 12 cells).

**C-** STED super-resolution images of isolated cardiomyocytes double stained for SERCA (red) and TRDN (green). The colocalization results showed an increased spatial overlap between SERCA and TRDN in CASQ2-KO cardiomyocytes. (fold changes relative to WT: WT: 0.91 (0.72-1.22); CASQ2-KO: 1.22 (0.92-1.76). Mann-Whitney test, # P=0.011 (WT: 3 mice, 13 cells, 41 ROI; CASQ2-KO: 3 mice 12 cells 36 ROI))

### 3.20 AAV9-CASQ2 infection in CASQ2-KO mice

In order to finally validate if the aforementioned findings described in the CASQ2-KO model were triggered by CASQ2 absence, we used an Adeno-associated viral vector serotype 9 (AAV9) containing cDNA of *CASQ2* wild-type (AAV9-CASQ2) tagged with the *green fluorescent protein (GFP)* gene to infect pups (P8) CASQ2-KO mice.

This approach had already been performed by our group (Denegri et al., 2012; Lodola et al., 2016), demonstrating that the overexpression of WT-CASQ2 in CASQ2-KO mice restored the reduced Couplon proteins (TRDN, JNT), the SR morphology and the electrophysiological behavior. Here we explore the other molecular pathological defects found by this study.

CASQ2-KO mice infected with WT-CASQ2 were used for cardiomyocytes isolation and image acquisition. Cardiomyocytes stained for alpha-Tubulin demonstrated a full restoration of the microtubules network: the microtubule branching (P=NS) (Figure 3.20A-Left) and the microtubule length (P=NS) (Figure 3.20A-Right) were not different from the WT.

Coupled to the restoration of the microtubule network was the repositioning of TRDN. STED super resolution images of cardiomyocytes stained for RyR2 and TRDN showed recovery of colocalization between TRDN and RyR2 (P=NS) (Figure 3.20B-Left) and a complete re-localization of TRDN to the Z-lines (P=NS) (Figure

3.20B-Right).CASQ2-KO mice infected with WT-CASQ2 also showed a significant decrease on HDAC6 protein quantity to similar values than WT mice (WT vs CASQ2-KO+AAV9-CASQ2, P= NS) (Figure 3.20C) demonstrating that the upregulation of HDAC6 is a consequence of CASQ2 in our CPVT2 model.

Overall, the results proved that the microtubule-HDAC6 mediated disorganization and the consequent TRDN delocalization and HDAC6 upregulation are phenomena triggered by the absence of CASQ2.

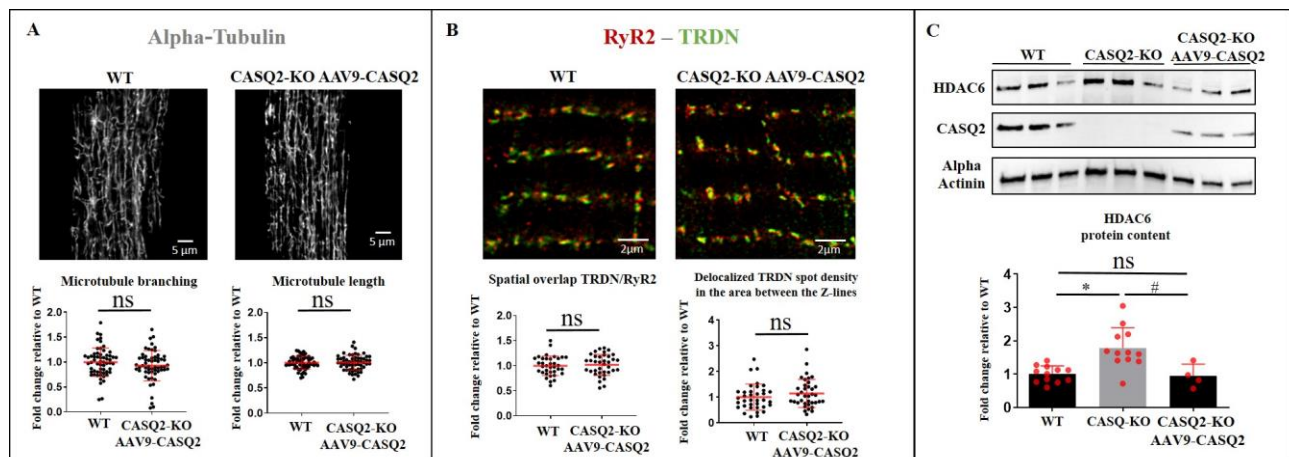


**Figure 3.20 - AAV9-CASQ2 infection in CASQ2-KO mice restores microtubular network, TRDN localization and HDAC6 protein levels**

**A-** Confocal images of CASQ2-KO infected with AAV9-CASQ2 for alpha-Tubulin. The restoration of CASQ2 in CASQ2 mice reverts the microtubule network alteration in CASQ2-KO cardiomyocytes (**Left**) [microtubule branching, WT: 1.00 (0.80-1.13); CASQ2-KO+AAV9-CASQ2: 0.92 (0.81-1.10)]. Mann-Whitney test, P=NS (**Right**).[microtubule length, WT: 0.98 (0.93-1.10); CASQ2-KO+AAV9-CASQ2: 1.00 (0.89-1.09)]. Mann-Whitney test, NS P=0.90. (WT: 3 mice, 30 cells, 60 ROIs; CASQ2-KO+AAV9-CASQ2 3 mice, 30Cells, 60 ROIs).

**B-** STED super-resolution images of isolated cardiomyocytes from CASQ2-KO infected AAV9-CASQ2 mice were double stained for RyR2 (red) and TRDN (green). (**Left**). The colocalization parameter shows that the restoration of CASQ2 in CASQ2 mice reverts TRDN/RYR2 spatial overlap [WT: 0.99 (0.87-1.15); CASQ2-KO+AAV9-CASQ2: 1.07 (0.87-1.19)]. Mann-Whitney test, NS P=0.55. (WT: 3 mice, 12 cells, 36 ROIs; CASQ2-KO+AAV9-CASQ2 3 mice, 12 Cells, 37 ROIs). (**Right**) Similarly the density of TRDN placed in the area between the Z-lines was not different between WT and CASQ2-KO+AAV9-CASQ2 [WT: 0.89 (0.63 - 1.22); CASQ2-KO+AAV9-CASQ2: 1.05 (0.78-1.44)]. Mann-Whitney test, P=NS (WT: 3 mice, 12 cells, 36 ROIs; CASQ2-KO+AAV9-CASQ2 3 mice, 12 Cells, 37 ROIs).

**C-** WB of total heart protein homogenate from WT CASQ2-KO and CASQ2-KO infected with AAV9-CASQ2. The expression of CASQ2 in CASQ2-KO hearts restores the HDAC6 protein quantity (WT: 1.00±0.25; CASQ2-KO: 1.79±0.61; CASQ2-KO+AAV9-CASQ2: 0.94±0.35). Kruskal-Wallis test with Dunn's correction, WT vs CASQ2-KO, # P=0.002; CASQ2-KO vs CASQ2-KO+AAV9-CASQ2, # P=0.028; WT vs CASQ2-KO+AAV9-CASQ2, P= NS (WT: 12 mice; CASQ2-KO: 12 mice; CASQ2-KO+AAV9-CASQ2: 4 mice).

## 4. METHODS

### 4.1 Proteomic study

#### 4.1.1 Preparation of mouse tissue protein extracts

Protein extraction was carried out from mouse tissue samples (5 WT and 5 CASQ2-KO animals) in the presence of 50 mM iodoacetamide (for alkylating free thiols from reduced Cys residues), boiled for 10 min, sonicated and incubated with agitation for 30 min at room temperature in the dark. Cell lysates were centrifuged at 13,000 g for 15 min to eliminate cell debris, and protein concentration in the supernatant was determined by using the RCDC Protein Assay Kit (Bio-Rad). The protein extracts were stored at -80°C.

#### 4.1.2 Protein digestion of protein extracts

The 10 samples were digested following the FASILOX protocol (Bonzon-Kulichenko et al., 2020). Briefly, the protein extracts (100 micrograms) were diluted with denaturing buffer (8 M urea in 100 mM Tris-HCl pH 8.5) and concentrated on Nanosep 30 K Omega Centrifugal Devices (Pall) by 10 min centrifugation at 14,000 g. After on-filter protein reduction with 40 mM dithiothreitol, the nascent free thiols were alkylated by incubation with 50 mM S-methyl methanethiosulfonate in the dark. Then protein samples were digested overnight at 37°C with sequencing grade trypsin (Promega) at 1:40 (w/w) trypsin: protein ratio. The resulting tryptic peptides from each sample were recovered by centrifugation at 10,000 rpm for 5 min after addition of 40 ul of 50 mM ammonium bicarbonate (twice), after which 50 ul of 500 mM NaCl were added and the filters centrifuged for 15 min at 10,000 rpm. Trifluoroacetic acid was added to a final concentration of 1% and the peptides were desalted on OASIS HLB extraction cartridges (Waters) and dried-down.

#### 4.1.3 Stable isotope labelling of peptides

The dried peptides were taken up in 100 mM triethylammonium bicarbonate and peptide concentration was determined using a Direct Detect IR spectrometer (Millipore). Equal amounts of each peptide sample were isobarically labeled with tandem mass tag (TMT) reagents (Thermo Fisher) according to the manufacturer's instructions and mixed together. The mixture was desalted using OASIS HLB extraction cartridges (Waters) and dried-down for later LC-MS/MS analysis.

#### **4.1.4 LC-MS/MS analysis**

The TMT-labelled peptides were infused to an Ultimate 3000 nano-flow HPLC system (Thermo Fisher Scientific) coupled on-line with a Q Exactive HF hybrid quadrupole-Orbitrap mass spectrometer (Thermo Fisher Scientific). C18-based reversed phase separation was used with a 50-cm analytical column (EASY-Spray, Thermo Fisher Scientific). Peptides were loaded in buffer A (0.1% formic acid (v/v)) and eluted with a 300-min linear gradient of buffer B (90% ACN, 0.1% formic acid (v/v)) at 200 nL/min flow. Mass spectra were acquired in a data-dependent manner, with an automatic switch between MS and MS/MS using a top 15 method and 45 s dynamic exclusion. The MS spectra were acquired in the orbitrap analyzer with a mass range of 400–1500 m/z and 120,000 resolution, while HCD MS/MS was performed at 29 normalized collision energy with 30,000 resolution.

#### **4.1.5 Database searching**

LC-MS/MS data were analyzed with Proteome Discoverer (version 2.1, Thermo Fisher Scientific) using SEQUEST-HT (Thermo Fisher Scientific). The data were searched against a Uniprot database containing all sequences from mouse (February 13, 2019; 77,204 entries). For database searching, parameters were set as follows: trypsin digestion with two maximum missed cleavage sites, precursor mass tolerance of 800 ppm, fragment mass tolerance of 20 mmu. Variable modifications were Met oxidation, Cys carbamidomethylation and Cys methylthiolation. Lys and peptide N-terminal modification of +229.1629 as fixed modifications from TMT labelling. The MS/MS spectra were searched in parallel against the corresponding inverted databases for false discovery rate (FDR) calculation. Peptide identification from MS/MS data was performed using the probability ratio method (Martínez-Bartolomé et al., 2008). FDR of peptide identifications were calculated using the refined method (Bonzon-Kulichenko et al., 2015; Navarro , Vazquez, 2009), taking 1% FDR as a threshold for peptide identification. Peptides were assigned only to the best protein proposed by Proteome Discoverer.

#### **4.1.6 Quantification at the peptide, protein and category levels**

The quantitative information extracted from the MS/MS spectra by Proteome Discoverer was integrated from the spectrum level to the peptide level, then to the protein level and finally to the functional category level on the basis of the WSPP model (Navarro et al., 2014) and the systems biology triangle algorithm (García-Marqués et al., 2016) using the SanXoT software package (Trevisan-Herraz et al., 2019). The validity of the null hypothesis was carefully checked at every level (spectrum, peptide, protein and category) by plotting the

cumulative distributions with zero mean and unit variance (Navarro et al., 2014), and the outliers at the peptide, protein and category level were detected at 1% FDR as described in (Navarro et al., 2014).

#### **4.1.7 Protein functional annotation**

For the integration of LC-MS/MS data to the functional category level based on the WSPP model (Navarro et al., 2014) and the systems biology triangle (García-Marqués et al., 2016), the proteins quantified were functionally annotated using DAVID (Huang et al., 2009), which comprises such functional databases as KEGG, REACTOME, Gene Ontology and Panther.

### **4.2 Animal procedures**

#### **4.2.1 Ethical aspects**

Animals were bred and housed at the Centro Nacional de Investigaciones Cardiovasculares Carlos III (CNIC) and treated according to the European Directive 2010/63/EU and the Guide for the Care and Use of Laboratory Animals (National Institute of Health, USA). Experimental protocols were approved by the ethical committee of the Universidad Autónoma de Madrid.

#### **4.2.2 Choice of mouse model**

The CASQ2-KO null strain was chosen for this study due to (Leenhardt et al., 1995a) its highly penetrant phenotypical CPVT manifestations; (Rosen, Danilo, 1980) it is a classical and established model of recessive CPVT used by several competent groups in CPVT research; and (S G Priori et al., 2001) prior knowledge that the phenotype is reversible via gene-replacement therapy (Denegri et al., 2012).

#### **4.2.3 Drug treatments**

In some experiments, CASQ2-KO mice were treated with different drugs (depending on the experiment) prior to isolation of ventricular myocytes. In all cases, intra-peritoneal injection was the method of choice. Dosage used: Chloroquine (CQ) (Sigma) 50mg/kg (24h); colchicine (Sigma) 1mg/kg (16h); Tubostatin A hydrochloride (Sigma Aldrich) 40mg/kg (16h). TRDN-KO mice were treated with Tubostatin A with 25mg/Kg for 3 days (Z. Wang et al., 2016). The evaluation of TRDN accumulation after autophagy inhibition was also

performed by chronic treatment: Chloroquine (CQ) (Sigma) was administered at 10 mg/kg/day for a period of 7 days through osmotic mini-pumps (Alzet, 2001) implanted subcutaneously.

#### **4.2.4 Isolation of ventricular myocytes**

Retrograde aortic perfusion and enzymatic digestion were applied to isolate ventricular myocytes from male animals, 8-12 weeks of age. The method is a modified version of that from Sambrano et al. (Sambrano et al., 2002) in use in our laboratory (Bongianino et al., 2017; Denegri et al., 2012; Rizzi et al., 2008).

#### **4.2.5 AAV9-CASQ2 viral construct and infection procedure in CASQ2-KO mice**

We used an adeno-associated serotype-9 vector containing the cDNA of the murine CASQ2 gene. The cDNA was cloned into a bicistronic (pIRES) eukaryotic expression vector and subcloned into the multiple cloning site of pAAV2.1-CMV-eGFP containing the cytomegalovirus promoter and the green fluorescent protein (eGFP) as reporter gene (Denegri et al., 2012). The AAV recombinant virus (AAV9-CASQ2) were produced by the AAV Vector Core of the Telethon Institute of Genetics and Medicine (TIGEM, Napoli, Italy). The infection was performed by intraperitoneal injection on postnatal day 8 (P8) pups with  $2.6 \times 10^{11}$  GC. Mice were studied 3 months after the infection.

### **4.3 Two-Color confocal and stimulated emission depletion (STED) microscopy in immunostained ventricular myocytes**

#### **4.3.1 Immunostaining protocol**

Isolated mouse ventricular myocytes, previously adapted to physiological  $\text{Ca}^{2+}$  levels for at least 30 minutes, were fixed with PBS + 4% paraformaldehyde for 10 minutes. To remove fixative-dependent mitochondrial autofluorescence, cells were incubated with PBS + 100 mM glycine for 1h. Cells were permeabilized using 0,2% Triton X100 for 10 minutes, then kept for 1 hour in blocking medium (PBS + 4% BSA + 0,1% Triton X100). The proteins pairs under investigation were labelled by incubation with blocking medium + primary antibody pairs (1:50 - 1:200, see below) for 2 hours at room temperature in a shaker at 15 rpm, and then the



reaction continued overnight at 4 °C with no shaking. The next morning, cells were incubated in blocking medium + secondary antibody pairs (1:200, see below) for 2 hours at room temperature in a shaker at 15 rpm. Cells were mounted using Abberior Mount Liquid antifade (refraction index = 1.38). Between steps, 3 washes were given in the appropriate solution.

#### **4.3.2 Colocalization (STED) and microtubule extension (confocal) experiments**

Secondary antibody pairs were coupled to Alexa 514 and Alexa 568 dyes, as both are amenable to STED using a single 660 nm depletion laser. This avoided calibrations and re-alignment procedures (Hebisch et al., 2017). We verified no bleed-through of the emitted fluorescence at the selected spectral windows, and the specificity of the antibodies for their target (Figure 4.1). Images were acquired using a gated STED-3X-WLL SP8 confocal microscope with spectral detection (Leica Microsystems, Germany). At least 3 high magnification square Regions of interest (ROI) of approximately 20x20 µm were acquired within the same cell, thus sampling the entire cell. STED Images were captured with a HCPL APO CS2 100x/1.40NA oil-immersion objective, setting the focal plane 2-4 µm above the coverslip (and within the cell) to minimize oil/cytosol diffraction index-related artefacts while still having good and periodic subcellular structure. Between frame images of 744x744 pixels with pixel size 26.08 nm (zoom 6) were collected at a speed of 400 Hz (unidirectional mode) and pinhole 1 A.U (Ex/Em:514/525-562, 568/584-632). We used a photon-counting hybrid detector applying a gating interval of 2.37-10.69 to remove autofluorescence and reflections. The number of average scans per line and of accumulated frames varied from 2 to 6, depending on fluorophore and experiment. The 660 nm depletion laser was set at 90% of its full power, and 2D-STED depletion at 100%. Confocal images for the microtubule extension study were captured similarly: between frame images of 744x744 pixels with pixel size 52 nm (zoom 3) were collected at a speed of 400 Hz (unidirectional mode) and pinhole 1 A.U (Ex/Em:514/525-562, 568/584-632). The number of average scans per line was set at 2 and the number of accumulated frames was set at 3.

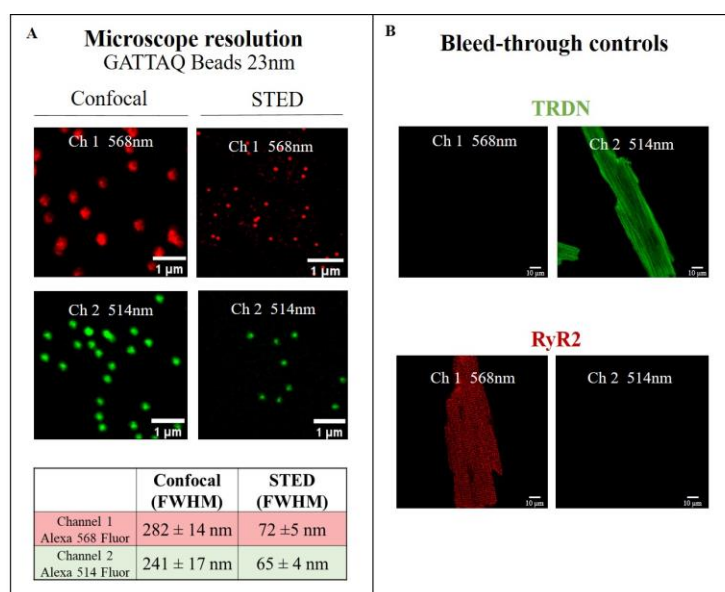


**Figure 4.1 – technical controls**

**A-** Comparison of confocal vs. STED resolution in the SP8 microscope. GATTAQ Beads (Gattaquant DNA Nanotechnologies), 23 nm in size, were imaged as close as possible to the coverslip level in confocal vs. STED modes, using similar settings to those for our immunostaining experiments. Resolution is described as the full width at half magnitude (FWHM) of the Gaussian fit to an average of 50 beads from different fields.

**B-** Bleed-through controls. Fixed ventricular myocytes were stained (see methods) either with an anti-Triadin antibody plus a secondary antibody conjugated to Alexa 514 (top) or with an anti-RyR2 primary antibody plus a secondary antibody conjugated to Alexa 568 (bottom). It was verified that, using our STED single depletion donut protocol, no significant bleed-through was observed between the 2 channels.

### 4.3.3 Colocalization analysis

STED images were deconvoluted using Huygens Professional software (Scientific Volume Imaging). The colocalization was calculated using ImageJ software (<https://imagej.nih.gov/ij/>) and the JACOP plug-in (Just Another Colocalization Plug-in) (Bolte, Cordelières, 2006). Co-localization analysis was based on *whole image analysis* relying on Mander's coefficient (*co-occurrence*) and Pearson's coefficient (*Linear intensity Correlation*). *Co-occurrence*, based on Mander's coefficient, defines the spatial overlap of two proteins within the cell, irrespective of whether their quantities are related or not. Mander's coefficient uses as reference the image pixels occupied by one protein and quantifies the fraction of pixels co-existing with the other protein. It can only take values from 0 to 1. *Linear correlation*, based on Pearson coefficient, describes whether the proteins are not only at the same subcellular structures, but their quantities are related to each other. It can take values from 1 (quantities and localization co-vary) to 0 (if unrelated) or even to -1 (if localization is the same, but protein quantities co-vary inversely) (Dunn et al., 2011). Pearson coefficient has been used during LC3-TRDN colocalization analysis. Pearson coefficient allowed us to study not only the spatial overlap between TRDN and LC3 pixel population but also the concomitant accumulation of TRDN and LC3 fluorescent signal in the specific cellular compartment in the cells.

#### **4.3.4 Analysis of delocalized Triadin**

Spot density analysis was performed on STED images using an in-house coded macro for ImageJ, which made use of the *Analyze Particles* tool. Briefly, the RyR2 image was used as a reference to trace the approximate location of the Z-lines. This area was enlarged by 0.65 nm and excluded from the Triadin image. The number of Triadin spots in the remainder of the image was normalized by the non-excluded area.

#### **4.3.5 Microtubule extension analysis**

We adapted the Mitochondrial Network Analysis (MiNA) ImageJ plug-in to our alpha-Tubulin confocal images (Valente et al., 2017). The plug-in is based on combining the plug-in Analyze Skeleton and Ridge Detection generating a tool able to detect and measure with high precision linear networks, branches and individual structures. We quantified the length of the branches (i.e. the average length of the lines used to represent the microtubule structures) and how ramified is the network (i.e. the average number of branches).

#### **4.3.6 Autophagy inhibition experiments in living cardiomyocytes**

Autophagy was determined evaluating autophagic flux, i.e. a comparison of the number of LC3-positive autophagosomes in the absence and presence of the autophagy inhibitor Hydroxychloroquine (HCQ, Sigma). To this end, isolated cardiomyocytes were maintained in culture for 6 hours with/without 30  $\mu$ M HCQ.

After culture, cardiomyocytes were fixed overnight at 4°C in 2% paraformaldehyde in PBS. After fixation, immunofluorescence was made following standard procedures: fixation in methanol at 4°C for 10 min, permeabilized with 0.5% Triton X-100 and blocked in PBS containing 10% goat serum and 0.1% Triton X-100.

Isolated cardiomyocytes were then imaged with a Leica SP5 confocal microscope using 20  $\times$  /0.75 dry and 63  $\times$  /1.30 oil objectives. Confocal images for the autophagy study were captured with the following settings: Between frame images of 775x775 pixels, with pixel size 758 nm (zoom 1) were collected at a speed of 400 Hz (unidirectional mode) and pinhole 1 A.U (Ex/Em:488/500-543, 568/583-647, 647/645-703). The number of average scans per line was set at 2 and the number of accumulated frames was set at 3. Nuclei were co-stained with DAPI. Data analysis was made using an in-house coded macro for ImageJ, which automatically detected individual cardiomyocytes and quantified the number of LC3, Lamp1 and p62 spots per cell.

#### **4.3.7 Sample preparation for FLIM-FRET microscopy**

Isolated adult ventricular myocytes were plated into 35mm glass bottom plate (Ibidi) previously coated with Laminin (Sigma) and fixed with PBS + 4% paraformaldehyde for 10 minutes. Autofluorescence was removed by 1h incubation in PBS + 100 mM glycine . Cells were permeabilized as previously described and then kept for 1 hour in blocking medium (see above). The proteins pairs under investigation were labelled by incubation with blocking medium + primary antibody pairs (1:50) for 2 hours at room temperature in a shaker at 15 rpm. Cells were incubated in blocking medium + secondary antibody pairs (1:200, donor Alexa fluor 514, acceptor Alexa fluor 568) for 2 hours at room temperature in a shaker at 15 rpm. Images were acquired using Alba FLIM/FCS (ISS) confocal microscope. The data were collected analyzed by the CNIC microscopy unit (<https://www.cnic.es/en/investigacion/microscopy>) using an already published fluorescence lifetime imaging analysis approach (Caiolfa et al., 2007; Digman et al., 2008).

#### **4.4 Quantitative Real Time PCR**

Total RNA from WT and CASQ2-KO hearts were purified with RNeasy mini kit (Qiagen). Real-Time assay was run employing 1 µg template RNA using iScript cDNA Synthesis kit (BIORAD). Triadin and the reference GAPDH mRNAs were amplified by CFX96 detection module (BIORAD) in optical 96-well plates. Samples were analyzed with SsoFast EvaGreen Supermix using the specific primer mix and 20 ng of cDNA template using the following primers: mTRDNfor: 5'GGCTTCTTGTCATCGCTCTGA 3', mTRDNrev : 5' CAATCTTGGAATGGAGCTTG 3', mGAPDHfor: 5' GAAAGCTGTGGCGTGATG 3', mGAPDHrev: 5' GCCCAAGATGCCCTTCAGTG 3' RT-PCR results were evaluated using the Bio-Rad CFX Manager software package (BIORAD). Values for Fold Expression, normalized over GAPDH amplification, were automatically generated by the BIORAD CFX Manager software 1.5.

#### **4.5 Western Blot Analysis**

Hearts were excised, washed in ice cold PBS to remove excess of blood and immediately flash-frozen in liquid nitrogen. Total tissue homogenates were obtained by pulverization using a mortar and a pestle in presence of liquid nitrogen. Further homogenization of the dry pellet proceeded in a buffer containing (mM) KH<sub>2</sub>PO<sub>4</sub> 30, NAF 40, EDTA 5, Sucrose 300, DTT 0.5, protease inhibitor (Sigma), at pH 7.30. After 1 cycle sonication the sample was solubilized in one volume of 100 mM TRIS-HCL pH 7.4 + 6% SDS for 1 hour at room temperature. The sample was centrifuged at 21000 g for 10 minutes at 4°C and the supernatant was stored. Protein quantification was performed by Pierce BSA Protein Assay kit (Thermo). Protein samples were suspended in SDS-PAGE loading buffer (30 µg of proteins + β-Mercaptoethanol + 4x Laemmli Sample Buffer,

BIORAD) and heated at 90°C for 5 minutes. Proteins were separated in a 4%-15% SDS-PAGE precast gradient gel (Mini-PROTEAN TGX Stain free, BIORAD). Proteins were transferred to PVDF membrane (Trans-blot Turbo, BIORAD) by semidry transfer system (Trans-Blot turbo transfer system, BIORAD). The membrane was blocked with 5% milk in TBS-T buffer (20 mM Tris, 137 mM NaCl, 0.1% Tween-20 at pH 7.4). Primary antibodies were incubated overnight at 4°C. Membranes were incubated with suitable HRP or fluorophore-coupled secondary antibodies for 1 hour and the bands were detected by Li-Cor Odyssey fluorescence scanner or ChemiDoc MP Image System (BIORAD). Band intensity was quantified by Imagej software. The Western Blot data come from the average of 3 technical replicates for each used mouse.

#### **4.6 Proteasome inhibition**

Isolated ventricular myocytes were exposed for 16 hours to the proteasome inhibitor MG132 (10µM). Cells were harvested and total protein homogenate was extracted for Western Blot analysis (see above). MG132 effect on proteasome activity was evaluated by testing the total quantity of poly-ubiquitinated proteins.

#### **4.7 HDAC6 activity assay**

The activity of the Histone deacetylase 6 (HDAC6) has been evaluated by a fluorometric assay (BioVision). The kit utilizes a synthetic acetylated-peptide substrate, that once processed by HDAC6 results in a release of AFC fluorophore. Florescent signal was detected by multiwell-spectrofluorimeter (Fluoroskan Ascent, Thermo labsystems). Sample preparation, measurement and reactivity calculations were performed following the manufacturer's guidelines.

#### **4.8 Co-Immunoprecipitation assay**

Hearts were flash-frozen and pulverized as above until a homogeneous powder was formed. Dry pellet was subsequently lysed in 9 volumes of extraction buffer (1X IP buffer (ThermoScientific), 50 mM NaCl, 0.5% Triton X-100, 1X protease inhibitors cocktail (Sigma) in ice for 10 minutes. Lysed tissue was then sonicated for 10 seconds and centrifuged at 2600 g for 10 minutes. The amount of protein in the supernatant was quantified using BCA assay (Thermo Scientific) and 2 mg of total protein were incubated with 1.5 mg of anti-TRDN antibody anti-alpha-tubulin antibody conjugated M-270 Epoxy magnetic beads (Thermo Scientific) for 1 hour at 4°C on a rolling wheel. After incubation, beads were washed 4 times with the Extraction buffer and protein complexes were collected using elution buffer (125mM Tris-HCl,pH 6.8, 4%SDS). For Ubiquitination experiments 5 µg of Triadin antibody were conjugated for each mg of M-270 Epoxy magnetic beads (Thermo

Scientific) used in immunoprecipitation and extraction buffer was supplemented with 10mM *N*-Ethylmaleimide (NEM) to inhibit deubiquitinating enzymes. The final detection of interacting proteins was performed using SDS-PAGE electrophoresis and subsequently by performing Western Blot (see above).

#### **4.9 Protein aggregation assay**

Aggresomes were detected by confocal microscopy using *Proteostat* protein aggregation assay (Enzo Life Sciences). Isolated adult cardio-myocytes were processed following the manufacturer's guidelines. Spot detection from confocal images was performed by an ImageJ macro based on find maxima plug in. Aggresomes spot density was calculated by normalizing the number of spots detected with the cells area.

#### **4.10 Proximity ligation assay (PLA)**

TRDN aggregates were assessed by Duolink PLA technology (MERK). Isolated adult cardiomyocytes were processed following the manufacturer's guidelines. The kit requires primary antibody (anti-TRDN, see below antibodies section) and relies on secondary Antibodies conjugated with complementary oligonucleotides sequences able to pair only if in close distance. After a rolling circle amplification process the paired oligonucleotides sequences give a fluorescent signal that was detected by confocal microscopy. The brighter spots were detected by an Image J macro based on find maxima plug in and normalized over the cell area.

#### **4.11 Generation of the viral construct**

The cDNA sequence encoding the murine protein CASQ2-WT (NM\_009814.2), without 3' and 5' UTR was amplified by PCR and inserted by TA cloning into the pGEM-T-Easy vector (Promega). By enzymatic digestion with EcoRI, the fragment corresponding to the gene of interest has been excised from the vector and subcloned into the pIRES vector (BD Clontech). The resulting functional cassette mCASQ2-IRES was then amplified by specific primers containing adapters for the restriction enzyme NotI: NotI-CASQ2 Forward:

5'\_CACAGCGGCCGCACAATGAAGAGGATTACCTGCTCATGG\_3' and NotI-IRES Reverse: 5'\_CGAAGCATTAACCCTCACTAAAGG\_3' and inserted by NotI enzymatic digestion into the pAAV-2.1-eGFP. This plasmid is functional and necessary for the production of AAV particles because it contains Inverted Terminal Repeats of the Adeno Associated Virus genome.

All the used plasmids were sequenced to control the integrity of the cloned sequences. The AAV production was done in collaboration with the Tigem core facility (<http://www.tigem.it/core-facilities/adeno-associated-virus-aav-vector-core>). The AAV vectors were produced using a transient transfection of three plasmids in

HEK293 cells: pAd helper, pAAV rep-cap (packaging), pAAV Cis (including our inserts, cloned in the pAAV2.1 Multi Cloning Site (MCS). The vectors were purified by CsCl centrifugation and underwent quality control such as Real Time PCR and Dot Blot analysis for physical titer, or Coomassie staining of SDS PAGE to evaluate the presence and purity of capsid proteins, the infectivity (eGFP+ cells/ml) and the sterility. The service returned us a viral preparation in PBS with a total yield  $2.6 \times 10^{12}$  genome copies/ml (GC/ml). All AAV stocks were frozen at  $-80^{\circ}\text{C}$  in single vial and thawed during the surgical procedure.

#### **4.12 Antibodies**

In the current study, immunostainings (IF), Western Blots (WB), co-immunoprecipitations (Co-IP) and Proximity ligation assay (PLA) relied on the following primary and secondary antibodies: Anti-RyR (Invitrogen, MA3-925, IF) (Marck, HPA020028, IF), anti-CASQ2 (Sigma-aldrich, C3868, IF, WB), anti-TRDN32 (custom made rabbit Ab developed by Isabel Marty's lab, IF, WB, PLA), anti-alpha-Tubulin (Invitrogen, 62204, IF, WB), anti-LC3 (Nanotools, LC3-5F10, IF, WB), anti-Lamp1 (Hybridoma bank, 1D4B, IF), anti-alpha-Tubulin antibody (Abcam, ab7291, Co-IP), anti HDAC6 (Assay BioTec, C0226, WB), anti-p62 (Progen, GP62-C, IF), anti-Climp 63 (Abcam, ab223774, WB) anti-Triadin (Invitrogen, MA3-927, Co-IP), anti-Ubiquitin (Invitrogen, 13-1600, WB), anti HSP70 (Enzo Life Sciences, BML-SA660; WB) anti-p62 (Progen, GP62-C, IF), anti- $\alpha$  Actinin (Santa Cruz Biotechnology, sc-17829, WB), anti-mouse Alexa Fluor 568 nm (Invitrogen, A11004, IF), anti-rabbit Alexa Fluor 514 nm (Invitrogen, A31558, IF), goat anti-guinea pig Alexa fluor 647 (A21450, Invitrogen, IF), anti-rat Alexa fluor 488 (A11006, Invitrogen, IF), anti-rabbit DyLight 800 nm (Rockland, 611-145-122, WB) and anti-mouse Alexa Fluor 680 nm (Invitrogen, A-21057, WB), anti-mouse HRP (Promega, W402B, WB), anti-rabbit HRP (Promega, W401B, WB).

#### **4.13 Statistics**

Statistical analyses were performed with GraphPad Prism 7.0 (GraphPad Software, San Diego, CA, USA). Continuous data were reported as median (p25 - p75) or mean  $\pm$  SD and compared using non-parametric tests (Mann-Whitney's test for 2-groups comparison and Kruskal-Wallis test with Dunn's correction for multi-group comparisons). The symbol (#) was used to define  $0.05 > P > 0.001$ ; the symbol (\*) was used to define  $P < 0.001$ .

The number of mice and cells used in individual experiments are detailed in the legend of each figure. On the plots, data for mutants and treated have been normalized for the mean of the WT group. Statistical significance was set at  $P < 0.05$  (two tails).

## 5. Discussion

In 2006 the early characterizations of the CASQ2-KO mouse model of CPVT2 (Knollmann et al., 2006), reported the reduction of the levels of Triadin (TRDN). In the past 15 years, the mechanisms that drive these changes have remained unknown.

In the last ten years, we have dedicated extensive efforts to contribute to the comprehension of the arrhythmogenic mechanisms underpinning recessive CPVT (Rizzi et al., 2008) and to develop gene-therapy strategies that would prevent their occurrence (Bongianino et al., 2017; Denegri et al., 2012; Lodola et al., 2016). Here we set out to unravel the mechanisms that drive the reduction of TRDN.

Our initial consideration originated from the evidence that cardiac cells heavily rely on mechanisms that preserve *Proteostasis* because of their long-lasting lifespan and absence of cellular regeneration. We therefore hypothesized that the loss of a pivotal protein like Calsequestrin would likely be the ignition of homeostatic processes dedicated to restraining maladaptive responses, and that loss of Triadin could be the expression of such a defensive process.

### 5.1 Disruption of microtubules drives the delocalization of TRDN

The first point that we elaborated was whether loss of TRDN could be related to an abnormal targeting of the protein that, by preventing its localization at the Z-lines, would promote its degradation. We therefore used stimulated emission depletion microscopy (STED) to establish the colocalization of TRDN and the cardiac Ryanodine Receptor (RyR2) a large protein of the dyadic complex, which also localizes at the Z-lines. The data supported our hypothesis showing a highly significant loss of proximity between TRDN and RyR2. Based on the evidence that CASQ2 and TRDN localization is mediated by microtubules, as demonstrated by the Cala's laboratory in two elegant studies (McFarland et al., 2010; Sleiman et al., 2015), we thought that a microtubular dysfunction could be responsible for the misplacing of the protein.

In the heart, microtubules localize in four specific regions: the intercalated discs, the nucleus, the mitochondria and the dyad/ Z-discs. This fine-tuned localization suggests that their role is highly specialized and tightly regulated (Matthew A. Caporizzo et al., 2019). Furthermore, it is known that modifications of the density and of the dynamics of microtubules is part of the response in several heart diseases. In heart failure, modifications of the density of microtubules is mediated by post-translational modifications and it parallels the progression of left ventricular dysfunction (Chen et al., 2018). Recently, it has been shown that loss of function mutations in the Myosin Binding Protein C gene in hypertrophic cardiomyopathy patients, associates with a proliferation of the microtubular network and with an increase in alpha-Tubulin quantity and acetylated alpha-Tubulin (Dorsch, Schuldt, Remedios, et al., 2019). We therefore hypothesized that lack of CASQ2 could elicit post-translational modifications that, by altering microtubular organization, would lead to an abnormal TRDN



localization. Using confocal microscopy, we demonstrated that the length of the branches of the alpha-Tubulin network was strongly reduced, leading to the disruption of the microtubule architecture. Our data also showed that while levels of alpha-Tubulin were not modified in the heart of CASQ2-KO mice compared to WT, the levels of acetylated alpha-Tubulin were significantly reduced in mutant animals. The link between the reduction of acetylated alpha-Tubulin and the loss of resilience of microtubules has been demonstrated in an elegant study by Xu and coworkers in 2017 (Z. Xu et al., 2017), who provided compelling evidence that acetylation of alpha-Tubulin at Lysin 40 ( $\alpha$ K40) is critical for the protection of microtubules from mechanical breakage and for the preservation of their integrity.

Additionally, our observation was reminiscent of the study published by Macquart et al. (Macquart et al., 2019) who reported that mice carriers of the homozygous mutation of the Lamin A/C gene LMNA<sup>H222P/H222P</sup> manifested dilated cardiomyopathy and conduction disorders that occurred alongside a decreased expression of acetylated alpha-Tubulin and microtubule derangement. We therefore hypothesized that post-translational modification of alpha-Tubulin could be mediated by HDAC6 or Sirtuin (D. Zhang et al., 2016). We reviewed the literature to assess the role of the two acetylases in cardiac physiology and realized that the published data supported the view that in the setting in which cardiac *Proteostasis* is altered, in response to genetic or acquired pathologies, de-acetylation or hyper-acetylation of alpha-Tubulin has been observed.

An interesting example of the activation of HDAC6-mediated alpha-Tubulin deacetylation in the heart is represented by the response to rapid atrial pacing that causes progressive ventricular dilatation and reduces contractility, leading to a specific type dilated cardiomyopathy called “Tachycardiomyopathy” (D. Zhang et al., 2014). The authors demonstrate that in HL1 atrial cells (Claycomb et al., 1998) and in the heart of *Drosophila pupae* tachypacing induces a contractile dysfunction that is associated with HDAC6-mediated alpha-Tubulin deacetylation and microtubule degradation. Of relevance, in analogy with what we observed in our CASQ2 model, the authors show that preventive treatment with the HDAC6 inhibitor Tubostatin A is able to rescue ventricular contractility in tachypaced dogs. Overall, the study demonstrates that rapid pacing drives an HDAC6-mediated maladaptive remodeling able to disrupt contractility.

Similarly, we demonstrated that in our CASQ2 knock out mice the protein levels and the activity of HDAC6 are increased. To further prove the link between microtubule alteration and TRDN delocalization we demonstrated that cardiac myocytes isolated from wild type mice treated with colchicine (a known microtubules disruption promoter) lose the localization of TRDN at the Z-line. Furthermore, we also demonstrated that HDAC6 inhibition by Tubostatin A recovers TRDN localization at the Z-lines in CASQ2-KO mice, therefore confirming the involvement of HDAC6 in the process.

This set of experiments provides the proof of concept that in the absence of CASQ2 a post-translational response mediated by HDAC6 undermines the stability of the microtubular network by reducing acetylated

alpha-Tubulin driving delocalization of TRDN. Whether this adaptive response to a loss of CASQ2 should be regarded as a further adverse consequence or a compensatory mechanism remains an intriguing question. Considering that CASQ2 is a pleiotropic protein and aside from acting as a luminal  $\text{Ca}^{2+}$  buffer it also modulates RyR2's closure at low luminal  $\text{Ca}^{2+}$ , thus acting as a luminal  $\text{Ca}^{2+}$  sensor. Loss of CASQ2 therefore increases the opening probability of the RyR2 channel, while the concomitant delocalization of TRDN, which enhances  $\text{Ca}^{2+}$  release from the SR, may be regarded as a favorable consequence of HDAC6-mediated remodeling.

## **5.2 CASQ2 gene transfer in CASQ2-KO mice**

To investigate whether in our experimental model the loss of CASQ2 is the trigger for the adaptive response that leads to degradation of Triadin, we tested whether normalizing the levels of CASQ2 would reduce HDAC6 levels. We therefore infected CASQ KO mice with a cardiotropic adeno-associated viral vector-serotype 9 (AAV9) containing the wild type cDNA of murine CASQ2 driven by a Cytomegalovirus promoter. In the experiment we used a dose able to restore 80% of the CASQ2 levels in CASQ2-KO mice (Denegri et al., 2012). Data showed that the expression of CASQ2 normalized the levels of HDAC6, prevented fragmentation of microtubules, and promoted TRDN localization at the Z lines.

This set of experiments provides the proof-of-concept that the absence of CASQ2 activates a post-translational response mediated by an increase in HDAC6 abundancy and a concomitant enhancement of its activity. This cascade of events promotes de-acetylation of alpha-Tubulin and undermines the stability of the microtubule network leading to delocalization of TRDN. As a final step we dissected the mechanism by which TRDN is degraded.

## **5.3 Autophagy is the pathway for TRDN degradation**

Here we show that autophagy, and not the proteasome, is involved in TRDN degradation in CASQ2-KO mice. This mechanism correlates with the activation of autophagy in mutant cardiomyocytes, a phenomenon already reported in several cardiac diseases (Dorsch, Schuldt, Knežević, et al., 2019; Tannous, Zhu, Johnstone, et al., 2008; Tannous, Zhu, Nemchenko, et al., 2008).

The finding of increased TRDN aggregation and Aggresome hypertrophy in CASQ2-KO cardiomyocytes, together with TRDN poly-ubiquitination and TRDN/HSP70 binding, indicates that the mechanism of TRDN degradation relies on its aggregation and recruitment into the Aggresomes. Aggresome formation involves the selective recruitment of misfolded aggregated proteins in a process that requires ubiquitination of the target proteins and their transport to the Aggresome through a mechanism that comprise the activity of HDAC6, p62 and microtubule dynamics (Kawaguchi et al., 2003a; Sandri, Robbins, 2014; Su, Wang, 2011b). Ubiquitinated

aggregates interact directly with adaptor proteins like p62 and NBR1, which associate to LC3 in the autophagosome membrane, thus allowing the aggregate's delivery to autophagosomes (Sandri , Robbins, 2014). In addition to the regulatory role in the transport of proteins to form Aggresomes, HDAC6 is essential for the formation of auto-phagosomes at the Aggresome, thereby facilitating the autophagic degradation of aggregates (Iwata et al., 2005; Zheng , Wang, 2010). In CASQ2-KO, we found that the increased HDAC6 activity is essential for TRDN aggregation, Aggresome hypertrophy and microtubule disorganization, while p62 was found downregulated in CASQ2-KO cardiomyocytes. These findings thus suggest that TRDN accumulation provokes its aggregation, which activates its ubiquitination and the HDAC6-p62 pathway for their recruitment into the Aggresomes and degradation by autophagy. Interestingly, both HDAC6 inhibition and autophagosome formation inhibition by 3MA rescue the localization of TRDN to the Z-lines in CASQ2 mutant cardiomyocytes. These observations suggest that the nucleation phase of autophagy could prime TRDN aggregation.

These novel findings suggest that selective autophagy represents a corrective mechanism to eliminate the excess of TRDN unbound to CASQ2. This hypothesis agrees with the evidence provided by Teng and co-workers that Phospholamban, a protein that also regulates intracellular  $\text{Ca}^{2+}$  located in the SR membrane, is degraded by Aggresome formation and macro-autophagy (Teng et al., 2015), therefore suggesting that this pathway might be the common regulator of  $\text{Ca}^{2+}$  handling proteins levels in the cardiac SR. Taken together, these data indicate that autophagy is activated as a safeguard mechanism to degrade TRDN aggregates, thereby trying to protect the cardiomyocytes from proteotoxicity.

The findings previously described are summarized in this figure 5.1.

#### **5.4 Microtubule derangement explains expansion of the jSR**

The disruption of the microtubular network and the enlargement of the jSR observed in the heart of CASQ2-KO mice by Electron Microscopy led us to investigate one of the pivotal proteins implicated in the regulation of the architecture of the Endoplasmic Reticulum: the cytoskeleton-linking membrane protein 63 also called CLIMP63. CLIMP63 is known to promote the formation of sheets in the ER at the expenses of tubular structures. Different groups collected experimental evidence in different cell types concurring to the interpretation that CLIMP63 maintains the width of the ER cisternae and that when the protein is down-regulated the ER shrinks significantly (Shen et al., 2019). For this reason in 2010 Shibata et al defined CLIMP63 as the “luminal ER spacer” (Shibata et al., 2010). Recently, Dr Marty and coworkers discovered that CLIMP63 in skeletal muscle is the protein that connects Triadin and microtubules (Osseni et al., 2016) : whether the protein serves the same function in heart is unknown. We therefore compared the mRNA and protein levels of CLIMP 63 in hearts derived from WT and CASQ2-KO mice and demonstrated that both the

transcript and the protein levels are significantly elevated in CASQ2-KO mice, supporting the theory that the enlargement of the ER observed might be mediated by the increased expression of CLIMP 63. We also observed a reduction of mRNA content of REEP5, responsible of the curved tubular membranes in the SR (Yao et al., 2018), hence demonstrating a protein expression unbalance of SR- shaper proteins. Moreover, we investigated the interaction between CLIMP63 and tubulin, and we confirmed by co-immunoprecipitation that the co-localization is doubled in CASQ2-KO mice compared to WT. To demonstrate this interpretation of our results, we tested whether a disassembly of the microtubules, obtained by treating WT mice with Colchicine, would lead to the expansion of the SR in WT cardiomyocytes. Experiments fully confirmed our expectations demonstrating to what extent a perturbation of the microtubular network might influence the jSR architecture. Moreover, CASQ2-KO heart were treated with Taxol (Horwitz et al., 1986; Manfredi et al., 1982), and this experiment demonstrated that the restoration of microtubule network reduced the dimension the expanded SR.

Our data represent the first evidence that the loss of SR homeostatic environment and SR integrity in CPVT mice may be caused by a disturbance in balance between REEP5 and CLIMP63, therefore reducing the formation of curved tubular membranes in favour of the flat sheet morphology. Moreover, given the strict relationship between CLMP63 and microtubules (Osseni et al., 2016; Vedrenne et al., 2005; Vedrenne, Hauri, 2006), our data also demonstrated the importance of an orderly microtubule network for the maintenance of a structured SR.

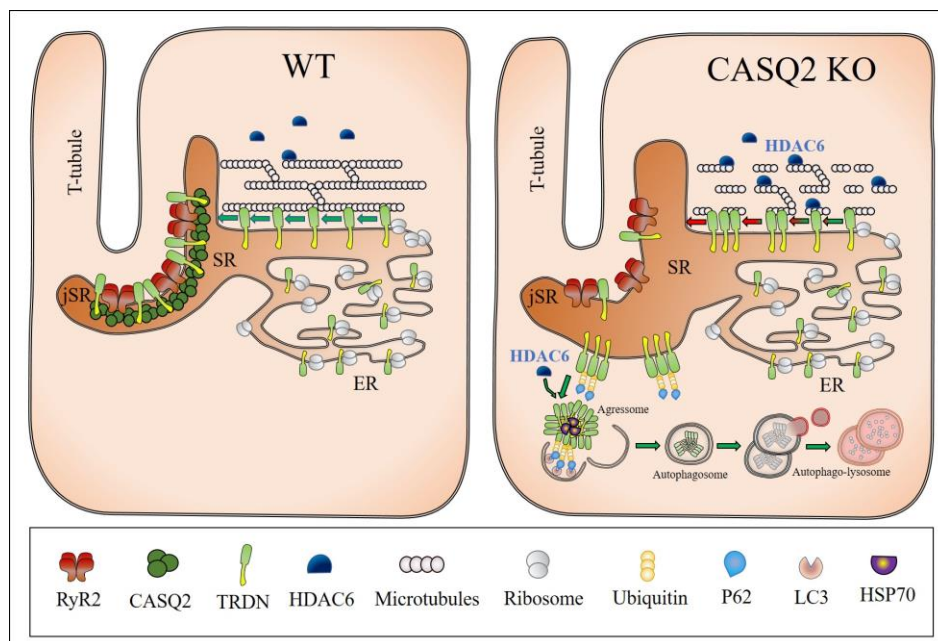


**Figure 5.1 Graphical summary CASQ2-KO**

The image represents WT and CASQ2-KO cardiomyocytes, summarizing the results of the study. CASQ2-KO cardiomyocytes show higher quantity and activity of HDAC6, that by deacetylating alpha-Tubulin destabilizes the microtubule network leading to delocalization of TRDN far from the Junctional SR (Z lines of the cardiac myocytes). Delocalized TRDN binds p62 and HSP70 and forms aggregates that lead to the development of Aggresomes that enter into the autophagy degradative pathway

## 6. Conclusions

We have demonstrated how the loss of the dyadic protein Calsequestrin 2 elicits a major and unexpected microscopic remodeling in the hearts of CASQ2-KO mice. This finding re-evaluates the current view that the loss of Calsequestrin 2 only increases the propensity of RyR2 to spontaneous diastolic release of  $\text{Ca}^{2+}$ . The simplified vision of the consequence of a loss of CASQ2 has hampered for decades the mechanistic importance of dissecting the link between the loss of CASQ2 and the decrease in TRDN levels. Our investigation opens to a new and intriguing view of the pathophysiology of recessive CPVT that might also be applicable to other inherited cardiac diseases.

For the first time we implicate post-translational modifications of proteins, that at first glance appear unrelated to the disease, that induce an activation of corrective measures to mitigate the systemic manifestations in cardiomyocytes. In CASQ2-KO mice the de-acetylation of alpha-Tubulin, by fragmenting the microtubules and reducing the targeting of Triadin to the dyad, may attenuate the facilitation of RyR2 opening mediated by TRDN thus reducing the severity of arrhythmias.

As a final consideration, it is important to highlight that in the clinical setting patients who carry compound heterozygous nonsense CASQ2 mutations have been described (Postma et al., 2002). These patients are affected by a severe form of the disease and it is likely that the mechanisms that we have described in the CASQ2 null mice also occur in such group of patients that are devoid of cardiac Calsequestrin making our observations relevant to the pathophysiology of the disease in humans.

## 7. Conclusiones

Hemos demostrado que la pérdida de la proteína de la díada, Calsecuestrina 2, provoca un gran e inesperado remodelado en el corazón de los ratones CASQ2-KO. Este descubrimiento revalora a la visión actual según la cual la pérdida de Calsecuestrina 2 únicamente incrementa la propensión del RyR2 a liberaciones espontáneas de  $\text{Ca}^{2+}$  durante la diástole. La visión simplificada de la consecuencia de la una pérdida de CASQ2 ha obstaculizado durante décadas la importancia mecanicista de estudiar la conexión entre la pérdida de CASQ2 y la disminución en los niveles de TRDN. Nuestra investigación abre una novedosa e intrigante visión a cerca de la patofisiología del CPVT recesivo, que podría ser aplicado también a otras enfermedades cardíacas hereditarias.

Por primera vez, hemos podido demostrar que las modificaciones post-translacionales de las proteínas, que a primera vista parecían no estar implicadas con la enfermedad, son capaces de inducir una serie de medidas correctivas para mitigar las manifestaciones sistémicas en los cardiomiocitos. En los ratones CASQ2-KO la deacetilación de la  $\alpha$ -tubulina, la fragmentación de los microtúbulos y la reducción de localización de la Triadina, podrían atenuar la capacidad de apertura de RyR2 mediada por la TRDN y, por tanto, reduciendo la severidad de las arritmias.

Como consideración final, cabe destacar que en el entorno clínico se han descrito pacientes que carecen de la proteína CASQ2 a causa de diferentes mutaciones sin sentido en el gen *CASQ2* (Postma et al., 2002).

Estos pacientes se ven afectados por una forma severa de la enfermedad y es probable que los mecanismos que hemos descrito en los ratones CASQ2 null ocurran también en dicho grupo de pacientes desprovistos de Calsecuestrina cardíaca; haciéndose relevantes nuestras observaciones a nivel patofisiológico en la enfermedad en humanos.

## 8. Bibliography

- Bal, N. C., Sharon, A., Gupta, S. C., Jena, N., Shaikh, S., Gyorke, S., & Periasamy, M. (2010). The catecholaminergic polymorphic ventricular tachycardia mutation R33Q disrupts the N-terminal structural motif that regulates reversible calsequestrin polymerization. *Journal of Biological Chemistry*, 285(22), 17188–17196. <https://doi.org/10.1074/jbc.M109.096354>
- Bar-Nun, S., & Glickman, M. H. (2012). Proteasomal AAA-ATPases: Structure and function. In *Biochimica et Biophysica Acta - Molecular Cell Research* (Vol. 1823, Issue 1, pp. 67–82). Elsevier. <https://doi.org/10.1016/j.bbamcr.2011.07.009>
- Bers, D. M. (2002). Cardiac excitation-contraction coupling. In *Nature* (Vol. 415, Issue 6868, pp. 198–205). Nature. <https://doi.org/10.1038/415198a>
- Betrie, A. H., Ayton, S., Bush, A. I., Angus, J. A., Lei, P., & Wright, C. E. (2017). Evidence of a Cardiovascular Function for Microtubule-Associated Protein Tau. *Journal of Alzheimer's Disease*, 56(2), 849–860. <https://doi.org/10.3233/JAD-161093>
- Bodakuntla, S., Jijumon, A., Villablanca, C., Gonzalez-Billault, C., & Janke, C. (n.d.). *Microtubule-associated proteins: structuring the cytoskeleton*. <https://doi.org/10.1016/j.tcb.2019.07.004i>
- Bolte, S., & Cordelières, F. P. (2006). A guided tour into subcellular colocalization analysis in light microscopy. In *Journal of Microscopy* (Vol. 224, Issue 3, pp. 213–232). Blackwell Publishing Ltd. <https://doi.org/10.1111/j.1365-2818.2006.01706.x>
- Bongianino, R., Denegri, M., Mazzanti, A., Lodola, F., Vollero, A., Boncompagni, S., Fasciano, S., Rizzo, G., Mangione, D., Barbaro, S., Di Fonso, A., Napolitano, C., Auricchio, A., Protasi, F., & Priori, S. G. (2017). Allele Specific Silencing of Mutant mRNA Rescues Ultrastructural and Arrhythmic Phenotype in Mice Carriers of the R4496C Mutation in the Ryanodine Receptor Gene (RYR2). *Circulation Research*. <https://doi.org/10.1161/CIRCRESAHA.117.310882>
- Bongianino, R., Foroni, B. ., Cancemi, A., Sperindio, R., Fasciano, S., Denegri, M., & Priori, S. . (2020). Disruption of the architecture of the junctional sarcoplasmic reticulum in recessive catecholaminergic polymorphic ventricular tachycardia is caused by the er-shaping proteins reep5 and climp63. *European Heart Journal*, 41(Supplement\_2). <https://doi.org/10.1093/ehjci/ehaa946.3578>
- Bonzon-Kulichenko, E., Camafeita, E., López, J. A., Gómez-Serrano, M., Jorge, I., Calvo, E., Núñez, E., Trevisan-Herraz, M., Bagwan, N., Bárcena, J. A., Peral, B., & Vázquez, J. (2020). Improved integrative analysis of the thiol redox proteome using filter-aided sample preparation. *Journal of Proteomics*, 214. <https://doi.org/10.1016/j.jprot.2019.103624>
- Bonzon-Kulichenko, E., Garcia-Marques, F., Trevisan-Herraz, M., & Vázquez, J. (2015). Revisiting peptide identification by high-accuracy mass spectrometry: Problems associated with the use of narrow mass

- precursor windows. *Journal of Proteome Research*, 14(2), 700–710. <https://doi.org/10.1021/pr5007284>
- Brandt, N. R., Caswell, A. H., Wen, S. R., & Talvenheimo, J. A. (1990). Molecular interactions of the junctional foot protein and dihydropyridine receptor in skeletal muscle triads. *The Journal of Membrane Biology*, 113(3), 237–251. <https://doi.org/10.1007/BF01870075>
- Butler, K. V., Kalin, J., Brochier, C., Vistoli, G., Langley, B., & Kozikowski, A. P. (2010). Rational design and simple chemistry yield a superior, neuroprotective HDAC6 inhibitor, tubastatin A. *Journal of the American Chemical Society*, 132(31), 10842–10846. <https://doi.org/10.1021/ja102758v>
- Cacheux, M., Fauconnier, J., Thireau, J., Osseni, A., Brocard, J., Roux-Buisson, N., Brocard, J., Fauré, J., Lacampagne, A., & Marty, I. (2019). Interplay between Triadin and Calsequestrin in the Pathogenesis of CPVT in the Mouse. *Molecular Therapy*, 28(1). <https://doi.org/10.1016/j.ymthe.2019.09.012>
- Caiolfa, V. R., Zama, M., Malengo, G., Andolfo, A., Madsen, C. D., Sutin, J., Digman, M. A., Gratton, E., Blasi, F., & Sidenius, N. (2007). Monomer-dimer dynamics and distribution of GPI-anchored uPAR are determined by cell surface protein assemblies. *Journal of Cell Biology*, 179(5), 1067–1082. <https://doi.org/10.1083/jcb.200702151>
- Campbell, K. P., MacLennan, D. H., Jorgensen, A. O., & Mintzer, M. C. (1983). Purification and characterization of calsequestrin from canine cardiac sarcoplasmic reticulum and identification of the 53,000 dalton glycoprotein. *Journal of Biological Chemistry*, 258(2), 1197–1204. [https://doi.org/10.1016/s0021-9258\(18\)33178-8](https://doi.org/10.1016/s0021-9258(18)33178-8)
- Caporizzo, Matthew A., Chen, C. Y., & Prosser, B. L. (2019). Cardiac microtubules in health and heart disease. In *Experimental Biology and Medicine* (Vol. 244, Issue 15, pp. 1255–1272). SAGE Publications Inc. <https://doi.org/10.1177/1535370219868960>
- Caporizzo, Matthew Alexander, Chen, C. Y., Salomon, A. K., Margulies, K. B., & Prosser, B. L. (2018). Microtubules Provide a Viscoelastic Resistance to Myocyte Motion. *Biophysical Journal*, 115(9), 1796–1807. <https://doi.org/10.1016/j.bpj.2018.09.019>
- Chen, C. Y., Caporizzo, M. A., Bedi, K., Vite, A., Bogush, A. I., Robison, P., Heffler, J. G., Salomon, A. K., Kelly, N. A., Babu, A., Morley, M. P., Margulies, K. B., & Prosser, B. L. (2018). Suppression of deetyrosinated microtubules improves cardiomyocyte function in human heart failure. *Nature Medicine*, 24(8), 1225–1233. <https://doi.org/10.1038/s41591-018-0046-2>
- Cheng, X. T., Xie, Y. X., Zhou, B., Huang, N., Farfel-Becker, T., & Sheng, Z. H. (2018). Revisiting LAMP1 as a marker for degradative autophagy-lysosomal organelles in the nervous system. In *Autophagy* (Vol. 14, Issue 8, pp. 1472–1474). Taylor and Francis Inc. <https://doi.org/10.1080/15548627.2018.1482147>
- Chiamvimonvat, N., & Song, L. S. (2018). LRRC10 (Leucine-rich repeat containing protein 10) and REEP5 (Receptor accessory protein 5) as novel regulators of cardiac excitation-contraction coupling structure and function. In *Journal of the American Heart Association* (Vol. 7, Issue 3, p. e008260). American Heart Association Inc. <https://doi.org/10.1161/JAHA.117.008260>



- Chopra, N., Kannankeril, P. J., Yang, T., Hlaing, T., Holinstat, I., Ettensohn, K., Pfeifer, K., Akin, B., Jones, L. R., Franzini-Armstrong, C., & Knollmann, B. C. (2007). Modest reductions of cardiac calsequestrin increase sarcoplasmic reticulum Ca<sup>2+</sup> leak independent of luminal Ca<sup>2+</sup> and trigger ventricular arrhythmias in mice. *Circulation Research*, 101(6), 617–626.  
<https://doi.org/10.1161/CIRCRESAHA.107.157552>
- Chopra, N., Yang, T., Asghari, P., Moore, E. D., Huke, S., Akin, B., Cattolica, R. A., Perez, C. F., Hlaing, T., Knollmann-Ritschel, B. E. C., Jones, L. R., Pessah, I. N., Allen, P. D., Franzini-Armstrong, C., & Knollmann, B. C. (2009). Ablation of triadin causes loss of cardiac Ca<sup>2+</sup> release units, impaired excitation-contraction coupling, and cardiac arrhythmias. *Proceedings of the National Academy of Sciences of the United States of America*, 106(18), 7636–7641.  
<https://doi.org/10.1073/pnas.0902919106>
- Claycomb, W. C., Lanson, N. A., Stallworth, B. S., Egeland, D. B., Delcarpio, J. B., Bahinski, A., & Izzo, N. J. (1998). HL-1 cells: A cardiac muscle cell line that contracts and retains phenotypic characteristics of the adult cardiomyocyte. *Proceedings of the National Academy of Sciences of the United States of America*, 95(6), 2979–2984. <https://doi.org/10.1073/pnas.95.6.2979>
- Clemens, D. J., Tester, D. J., Giudicessi, J. R., Bos, J. M., Rohatgi, R. K., Abrams, D. J., Balaji, S., Crotti, L., Faure, J., Napolitano, C., Priori, S. G., Probst, V., Rooryck-Thambo, C., Roux-Buisson, N., Sacher, F., Schwartz, P. J., Silka, M. J., Walsh, M. A., & Ackerman, M. J. (2019). International Triadin Knockout Syndrome Registry: The Clinical Phenotype and Treatment Outcomes of Patients with Triadin Knockout Syndrome. *Circulation: Genomic and Precision Medicine*, 12(2), 65–75.  
<https://doi.org/10.1161/CIRCGEN.118.002419>
- Collins, G. A., & Goldberg, A. L. (2017). The Logic of the 26S Proteasome. In *Cell* (Vol. 169, Issue 5, pp. 792–806). Cell Press. <https://doi.org/10.1016/j.cell.2017.04.023>
- Cooper IV, G. (2006). Cytoskeletal networks and the regulation of cardiac contractility: Microtubules, hypertrophy, and cardiac dysfunction. In *American Journal of Physiology - Heart and Circulatory Physiology* (Vol. 291, Issue 3). Am J Physiol Heart Circ Physiol.  
<https://doi.org/10.1152/ajpheart.00132.2006>
- Coumel P FJ, Lucet V, Attuel P, B. Y. (1978). Catecholamine-induced severe ventricular arrhythmias with Adams-Stokes syndrome in children: report of four cases. *Br Heart*, 40(suppl), 28–37.
- Denegri, M., Avelino-Cruz, J. E., Boncompagni, S., De Simone, S. A., Auricchio, A., Villani, L., Volpe, P., Protasi, F., Napolitano, C., & Priori, S. G. (2012). Viral gene transfer rescues arrhythmogenic phenotype and ultrastructural abnormalities in adult calsequestrin-null mice with inherited arrhythmias. *Circulation Research*, 110(5), 663–668. <https://doi.org/10.1161/CIRCRESAHA.111.263939>
- Desai, A., & Mitchison, T. J. (1997). Microtubule polymerization dynamics. In *Annual Review of Cell and Developmental Biology* (Vol. 13, pp. 83–117). Annu Rev Cell Dev Biol.

<https://doi.org/10.1146/annurev.cellbio.13.1.83>

- Devalla, H. D., Gélinas, R., Aburawi, E. H., Beqqali, A., Goyette, P., Freund, C., Chaix, M., Tadros, R., Jiang, H., Le Béhec, A., Monshouwer-Kloots, J. J., Zwetsloot, T., Kosmidis, G., Latour, F., Alikashani, A., Hoekstra, M., Schlaepfer, J., Mummery, C. L., Stevenson, B., ... Passier, R. (2016). TECRL , a new life-threatening inherited arrhythmia gene associated with overlapping clinical features of both LQTS and CPVT . *EMBO Molecular Medicine*, 8(12), 1390–1408.  
<https://doi.org/10.15252/emmm.201505719>
- Dhindwal, S., Lobo, J., Cabra, V., Santiago, D. J., Nayak, A. R., Dryden, K., & Samsó, M. (2017). A cryo-EM-based model of phosphorylation- and FKBP12.6-mediated allosterism of the cardiac ryanodine receptor. *Science Signaling*, 10(480). <https://doi.org/10.1126/scisignal.aai8842>
- Di Barletta, M. R., Viatchenko-Karpinski, S., Nori, A., Memmi, M., Terentyev, D., Turcato, F., Valle, G., Rizzi, N., Napolitano, C., Gyorke, S., Volpe, P., & Priori, S. G. (2006). Clinical phenotype and functional characterization of CASQ2 mutations associated with catecholaminergic polymorphic ventricular tachycardia. *Circulation*, 114(10), 1012–1019.  
<https://doi.org/10.1161/CIRCULATIONAHA.106.623793>
- Digman, M. A., Caiolfa, V. R., Zamai, M., & Gratton, E. (2008). The phasor approach to fluorescence lifetime imaging analysis. *Biophysical Journal*, 94(2). <https://doi.org/10.1529/biophysj.107.120154>
- Dikic, I. (2017). Proteasomal and autophagic degradation systems. In *Annual Review of Biochemistry* (Vol. 86, pp. 193–224). Annual Reviews Inc. <https://doi.org/10.1146/annurev-biochem-061516-044908>
- Dinchuk, J. E., Henderson, N. L., Burn, T. C., Huber, R., Ho, S. P., Link, J., O'Neil, K. T., Focht, R. J., Scully, M. S., Hollis, J. M., Hollis, G. F., & Friedman, P. A. (2000). Aspartyl  $\beta$ -hydroxylase (Asph) and an evolutionarily conserved isoform of Asph missing the catalytic domain share exons with junctin. *Journal of Biological Chemistry*, 275(50), 39543–39554. <https://doi.org/10.1074/jbc.M006753200>
- Dorsch, L. M., Schuldt, M., Knežević, D., Wiersma, M., Kuster, D. W. D., van der Velden, J., & Brundel, B. J. J. M. (2019). Untying the knot: protein quality control in inherited cardiomyopathies. In *Pflugers Archiv European Journal of Physiology* (Vol. 471, Issue 5, pp. 795–806). Springer Verlag.  
<https://doi.org/10.1007/s00424-018-2194-0>
- Dorsch, Schuldt, Remedios, Schinkel, Jong, Michels, Kuster, Brundel, & Velden. (2019). Protein Quality Control Activation and Microtubule Remodeling in Hypertrophic Cardiomyopathy. *Cells*, 8(7), 741.  
<https://doi.org/10.3390/cells8070741>
- Dries, E., Santiago, D. J., Johnson, D. M., Gilbert, G., Holemans, P., Korte, S. M., Roderick, H. L., & Sipido, K. R. (2016). Calcium/calmodulin-dependent kinase II and nitric oxide synthase 1-dependent modulation of ryanodine receptors during  $\beta$ -adrenergic stimulation is restricted to the dyadic cleft. *Journal of Physiology*, 594(20), 5923–5939. <https://doi.org/10.1113/JP271965>
- Du, G. G., Sandhu, B., Khanna, V. K., Guo, X. H., & MacLennan, D. H. (2002). Topology of the Ca<sup>2+</sup>

- release channel of skeletal muscle sarcoplasmic reticulum (RyR1). *Proceedings of the National Academy of Sciences of the United States of America*, 99(26), 16725–16730.  
<https://doi.org/10.1073/pnas.012688999>
- Dunn, K. W., Kamocka, M. M., & McDonald, J. H. (2011). A practical guide to evaluating colocalization in biological microscopy. In *American Journal of Physiology - Cell Physiology* (Vol. 300, Issue 4). Am J Physiol Cell Physiol. <https://doi.org/10.1152/ajpcell.00462.2010>
- Eberharter, A., & Becker, P. B. (2002). Histone acetylation: A switch between repressive and permissive chromatin. Second in review on chromatin dynamics. *EMBO Reports*, 3(3), 224–229.  
<https://doi.org/10.1093/embo-reports/kvf053>
- Eisner, D. A., Caldwell, J. L., Kistamás, K., & Trafford, A. W. (2017). Calcium and Excitation-Contraction Coupling in the Heart. In *Circulation Research* (Vol. 121, Issue 2, pp. 181–195). Lippincott Williams and Wilkins. <https://doi.org/10.1161/CIRCRESAHA.117.310230>
- Eshun-Wilson, L., Zhang, R., Portran, D., Nachury, M. V., Toso, D. B., Löhr, T., Vendruscolo, M., Bonomi, M., Fraser, J. S., & Nogales, E. (2019). Effects of  $\alpha$ -tubulin acetylation on microtubule structure and stability. *Proceedings of the National Academy of Sciences of the United States of America*, 116(21), 10366–10371. <https://doi.org/10.1073/pnas.1900441116>
- Eskelinen, E. L. (2006). Roles of LAMP-1 and LAMP-2 in lysosome biogenesis and autophagy. In *Molecular Aspects of Medicine* (Vol. 27, Issues 5–6, pp. 495–502). Mol Aspects Med.  
<https://doi.org/10.1016/j.mam.2006.08.005>
- Fabiato, A., & Fabiato, F. (1975). Contractions induced by a calcium-triggered release of calcium from the sarcoplasmic reticulum of single skinned cardiac cells. *The Journal of Physiology*, 249(3), 469–495.  
<https://doi.org/10.1113/jphysiol.1975.sp011026>
- Fabiato, Alexandre, & Fabiato, F. (1979). Use of chlorotetracycline fluorescence to demonstrate  $\text{Ca}^{2+}$ -induced release of  $\text{Ca}^{2+}$  from the sarcoplasmic reticulum of skinned cardiac cells [14]. In *Nature* (Vol. 281, Issue 5727). <https://doi.org/10.1038/281146a0>
- Faggioni, M., & Knollmann, B. C. (2012). Calsequestrin 2 and arrhythmias. In *American Journal of Physiology - Heart and Circulatory Physiology* (Vol. 302, Issue 6, p. H1250). American Physiological Society. <https://doi.org/10.1152/ajpheart.00779.2011>
- Fassett, J. T., Xu, X., Kwak, D., Wang, H., Liu, X., Hu, X., Bache, R. J., & Chen, Y. (2013). Microtubule Actin Cross-Linking Factor 1 Regulates Cardiomyocyte Microtubule Distribution and Adaptation to Hemodynamic Overload. *PLoS ONE*, 8(9). <https://doi.org/10.1371/journal.pone.0073887>
- Fassett, J., Xu, X., Kwak, D., Zhu, G., Fassett, E. K., Zhang, P., Wang, H., Mayer, B., Bache, R. J., & Chen, Y. (2019). Adenosine kinase attenuates cardiomyocyte microtubule stabilization and protects against pressure overload-induced hypertrophy and LV dysfunction. *Journal of Molecular and Cellular Cardiology*, 130, 49–58. <https://doi.org/10.1016/j.yjmcc.2019.03.015>

- Feriotto, G., Finotti, A., Volpe, P., Treves, S., Ferrari, S., Angelelli, C., Zorzato, F., & Gambari, R. (2005). Myocyte Enhancer Factor 2 Activates Promoter Sequences of the Human A $\beta$ H-J-J Locus, Encoding Aspartyl- $\beta$ -Hydroxylase, Junctin, and Junctate. *Molecular and Cellular Biology*, 25(8), 3261–3275. <https://doi.org/10.1128/mcb.25.8.3261-3275.2005>
- Fourest-Lieuvin, A., Rendu, J., Osseni, A., Pernet-Gallay, K., Rossi, D., Oddoux, S., Brocard, J., Sorrentino, V., Marty, I., & Fauré, J. (2012). Role of triadin in the organization of reticulum membrane at the muscle triad. *Journal of Cell Science*, 125(14), 3443–3453. <https://doi.org/10.1242/jcs.100958>
- Franke, W. W., Schumacher, H., Borrmann, C. M., Grund, C., Winter-Simanowski, S., Schlechter, T., Pieperhoff, S., & Hofmann, I. (2007). The area composita of adhering junctions connecting heart muscle cells of vertebrates - III: Assembly and disintegration of intercalated disks in rat cardiomyocytes growing in culture. *European Journal of Cell Biology*, 86(3), 127–142. <https://doi.org/10.1016/j.ejcb.2006.11.003>
- Franzini-Armstrong, C., Kenney, L. J., & Varriano-Marston, E. (1987). The structure of calsequestrin in triads of vertebrate skeletal muscle: a deep-etch study. *The Journal of Cell Biology*, 105(1), 49–56. <https://doi.org/10.1083/jcb.105.1.49>
- Franzini-Armstrong, Clara, Protasi, F., & Tijskens, P. (2005). The assembly of calcium release units in cardiac muscle. *Annals of the New York Academy of Sciences*, 1047, 76–85. <https://doi.org/10.1196/annals.1341.007>
- Froemming, G. R., Murray, B. E., & Ohlendieck, K. (1999). Self-aggregation of triadin in the sarcoplasmic reticulum of rabbit skeletal muscle. *Biochimica et Biophysica Acta - Biomembranes*, 1418(1), 197–205. [https://doi.org/10.1016/S0005-2736\(99\)00024-3](https://doi.org/10.1016/S0005-2736(99)00024-3)
- Ganong. *Fisiologia Medica | Enhanced Reader*. (n.d.). Retrieved April 14, 2021, from moz-extension://5957c67c-f053-48a5-ba87-d8bb11659888/enhanced-reader.html?openApp&pdf=http%3A%2F%2Fwww.untumbes.edu.pe%2Fvcs%2Fbiblioteca%2Fdocument%2Fvarioslibros%2F0440.%2520Ganong.%2520Fisiolog%25C3%25ADa%2520m%25C3%25A9dica.pdf
- García-Marqués, F., Trevisan-Herraz, M., Martínez-Martínez, S., Camafeita, E., Jorge, I., Lopez, J. A., Méndez-Barbero, N., Méndez-Ferrer, S., Del Pozo, M. A., Ibáñez, B., Andrés, V., Sánchez-Madrid, F., Redondo, J. M., Bonzon-Kulichenko, E., & Vázquez, J. (2016). A novel systems-biology algorithm for the analysis of coordinated protein responses using quantitative proteomics. *Molecular and Cellular Proteomics*, 15(5), 1740–1760. <https://doi.org/10.1074/mcp.M115.055905>
- Garcia-Mata, R., Gao, Y. S., & Sztul, E. (2002). Hassles with taking out the garbage: Aggravating aggresomes. In *Traffic* (Vol. 3, Issue 6, pp. 388–396). Traffic. <https://doi.org/10.1034/j.1600-0854.2002.30602.x>
- Gittes, F., Mickey, B., Nettleton, J., & Howard, J. (1993). Flexural rigidity of microtubules and actin

- filaments measured from thermal fluctuations in shape. *Journal of Cell Biology*, 120(4), 923–934.  
<https://doi.org/10.1083/jcb.120.4.923>
- Glick, D., Barth, S., & Macleod, K. F. (2010). Autophagy: Cellular and molecular mechanisms. In *Journal of Pathology* (Vol. 221, Issue 1, pp. 3–12). J Pathol. <https://doi.org/10.1002/path.2697>
- Gu, Y., Oyama, F., & Ihara, Y. (1996).  $\tau$  Is widely expressed in rat tissues. *Journal of Neurochemistry*, 67(3), 1235–1244. <https://doi.org/10.1046/j.1471-4159.1996.67031235.x>
- Guthrie, C. R., & Kraemer, B. C. (2011). Proteasome inhibition drives HDAC6-dependent recruitment of tau to aggresomes. *Journal of Molecular Neuroscience*, 45(1), 32–41. <https://doi.org/10.1007/s12031-011-9502-x>
- Györke, I., Hester, N., Jones, L. R., & Györke, S. (2004). The Role of Calsequestrin, Triadin, and Junctin Conferring Cardiac Ryanodine Receptor Responsiveness to Luminal Calcium. *Biophysical Journal*, 86(4), 2121–2128. [https://doi.org/10.1016/S0006-3495\(04\)74271-X](https://doi.org/10.1016/S0006-3495(04)74271-X)
- Hakamata, Y., Nakai, J., Takeshima, H., & Imoto, K. (1992). Primary structure and distribution of a novel ryanodine receptor/calcium release channel from rabbit brain. *FEBS Letters*, 312(2–3), 229–235.  
[https://doi.org/10.1016/0014-5793\(92\)80941-9](https://doi.org/10.1016/0014-5793(92)80941-9)
- Hao, R., Nanduri, P., Rao, Y., Panichelli, R. S., Ito, A., Yoshida, M., & Yao, T. P. (2013). Proteasomes Activate Aggresome Disassembly and Clearance by Producing Unanchored Ubiquitin Chains. *Molecular Cell*, 51(6), 819–828. <https://doi.org/10.1016/j.molcel.2013.08.016>
- Hayashi, M., Denjoy, I., Extramiana, F., Maltret, A., Buisson, N. R., Lupoglazoff, J. M., Klug, D., Hayashi, M., Takatsuki, S., Villain, E., Kamblock, J., Messali, A., Guicheney, P., Lunardi, J., & Leenhardt, A. (2009). Incidence and risk factors of arrhythmic events in catecholaminergic polymorphic ventricular tachycardia. *Circulation*, 119(18), 2426–2434.  
<https://doi.org/10.1161/CIRCULATIONAHA.108.829267>
- Hebisch, E., Wagner, E., Westphal, V., Sieber, J. J., & Lehnart, S. E. (2017). A protocol for registration and correction of multicolour STED superresolution images. *Journal of Microscopy*, 267(2), 160–175.  
<https://doi.org/10.1111/jmi.12556>
- Henning, R. H., & Brundel, B. J. J. M. (2017). Proteostasis in cardiac health and disease. In *Nature Reviews Cardiology* (Vol. 14, Issue 11, pp. 637–653). Nature Publishing Group.  
<https://doi.org/10.1038/nrcardio.2017.89>
- Herbert, A. D., Carr, A. M., Hoffmann, E., & Lichten, M. (2014). FindFoci: A focus detection algorithm with automated parameter training that closely matches human assignments, reduces human inconsistencies and increases speed of analysis. *PLoS ONE*, 9(12), e114749.  
<https://doi.org/10.1371/journal.pone.0114749>
- Hong, C. S., Kwak, Y. G., Ji, J. H., Chae, S. W., & Han Kim, D. (2001). Molecular cloning and characterization of mouse cardiac junctate isoforms. *Biochemical and Biophysical Research*

*Communications*, 289(4), 882–887. <https://doi.org/10.1006/bbrc.2001.6056>

- HORWITZ, S. B., LOTHSTEIN, L., MANFREDI, J. J., MELLADO, W., PARNES, J., ROY, S. N., SCHIFF, P. B., SORBARA, L., & ZEHEB, R. (1986). Taxol: Mechanisms of Action and Resistance. *Annals of the New York Academy of Sciences*, 466(1), 733–744. <https://doi.org/10.1111/j.1749-6632.1986.tb38455.x>
- Houle, T. D., Ram, M. L., & Cala, S. E. (2004). Calsequestrin mutant D307H exhibits depressed binding to its protein targets and a depressed response to calcium. *Cardiovascular Research*, 64(2), 227–233. <https://doi.org/10.1016/j.cardiores.2004.09.009>
- Huang, D. W., Sherman, B. T., Zheng, X., Yang, J., Imamichi, T., Stephens, R., & Lempicki, R. A. (2009). Extracting biological meaning from large gene lists with DAVID. In *Current Protocols in Bioinformatics: Vol. Chapter 13* (Issue SUPPL. 27). Curr Protoc Bioinformatics. <https://doi.org/10.1002/0471250953.bi1311s27>
- Hubbert, C., Guardiola, A., Shao, R., Kawaguchi, Y., Ito, A., Nixon, A., Yoshida, M., Wang, X. F., & Yao, T. P. (2002). HDAC6 is a microtubule-associated deacetylase. *Nature*, 417(6887), 455–458. <https://doi.org/10.1038/417455a>
- Iwata, A., Riley, B. E., Johnston, J. A., & Kopito, R. R. (2005). HDAC6 and microtubules are required for autophagic degradation of aggregated Huntingtin. *Journal of Biological Chemistry*, 280(48), 40282–40292. <https://doi.org/10.1074/jbc.M508786200>
- Jacobson, A. D., Zhang, N. Y., Xu, P., Han, K. J., Noone, S., Peng, J., & Liu, C. W. (2009). The lysine 48 and lysine 63 ubiquitin conjugates are processed differently by the 26 S proteasome. *Journal of Biological Chemistry*, 284(51), 35485–35494. <https://doi.org/10.1074/jbc.M109.052928>
- Janke, C., & Montagnac, G. (2017a). Causes and Consequences of Microtubule Acetylation. In *Current Biology* (Vol. 27, Issue 23, pp. R1287–R1292). Cell Press. <https://doi.org/10.1016/j.cub.2017.10.044>
- Janke, C., & Montagnac, G. (2017b). Causes and Consequences of Microtubule Acetylation. In *Current Biology* (Vol. 27, Issue 23, pp. R1287–R1292). Cell Press. <https://doi.org/10.1016/j.cub.2017.10.044>
- Jia, S., VanDusen, W. J., Diehl, R. E., Kohl, N. E., Dixon, R. A. F., Elliston, K. O., Stern, A. M., & Friedman, P. A. (1992). cDNA cloning and expression of bovine aspartyl (asparaginy)  $\beta$ -hydroxylase. *Journal of Biological Chemistry*, 267(20), 14322–14327. [https://doi.org/10.1016/s0021-9258\(19\)49715-9](https://doi.org/10.1016/s0021-9258(19)49715-9)
- Jiang, D., Xiao, B., Yang, D., Wang, R., Choi, P., Zhang, L., Cheng, H., & Chen, S. R. W. (2004). RyR2 mutations linked to ventricular tachycardia and sudden death reduce the threshold for store-overload-induced  $\text{Ca}^{2+}$  release (SOICR). *Proceedings of the National Academy of Sciences of the United States of America*, 101(35), 13062–13067. <https://doi.org/10.1073/pnas.0402388101>
- Jones, L. R., Zhang, L., Sanborn, K., Jorgensen, A. O., & Kelley, J. (1995). Purification, primary structure, and immunological characterization of the 26-kDa calsequestrin binding protein (junctin) from cardiac

- junctional sarcoplasmic reticulum. *Journal of Biological Chemistry*, 270(51), 30787–30796.  
<https://doi.org/10.1074/jbc.270.51.30787>
- Jones, P. P., MacQuaide, N., & Louch, W. E. (2018). Dyadic Plasticity in Cardiomyocytes. *Frontiers in Physiology*, 9, 1773. <https://doi.org/10.3389/fphys.2018.01773>
- Kawaguchi, Y., Kovacs, J. J., McLaurin, A., Vance, J. M., Ito, A., & Yao, T. P. (2003a). The deacetylase HDAC6 regulates aggresome formation and cell viability in response to misfolded protein stress. *Cell*, 115(6), 727–738. [https://doi.org/10.1016/S0092-8674\(03\)00939-5](https://doi.org/10.1016/S0092-8674(03)00939-5)
- Kawaguchi, Y., Kovacs, J. J., McLaurin, A., Vance, J. M., Ito, A., & Yao, T. P. (2003b). The deacetylase HDAC6 regulates aggresome formation and cell viability in response to misfolded protein stress. *Cell*, 115(6), 727–738. [https://doi.org/10.1016/S0092-8674\(03\)00939-5](https://doi.org/10.1016/S0092-8674(03)00939-5)
- Khandia, R., Dadar, M., Munjal, A., Dhama, K., Karthik, K., Tiwari, R., Yatoo, M. I., Iqbal, H. M. N., Singh, K. P., Joshi, S. K., & Chaicumpa, W. (2019). A Comprehensive Review of Autophagy and Its Various Roles in Infectious, Non-Infectious, and Lifestyle Diseases: Current Knowledge and Prospects for Disease Prevention, Novel Drug Design, and Therapy. *Cells*, 8(7), 674.  
<https://doi.org/10.3390/cells8070674>
- Kim, E. J., Youn, B., Kemper, L., Campbell, C., Milting, H., Varsanyi, M., & Kang, C. H. (2007). Characterization of Human Cardiac Calsequestrin and its Deleterious Mutants. *Journal of Molecular Biology*, 373(4), 1047–1057. <https://doi.org/10.1016/j.jmb.2007.08.055>
- Kim, K. C., Caswell, A. H., Talvenheimo, J. A., & Brandt, N. R. (1990). Isolation of a Terminal Cisterna Protein Which May Link the Dihydropyridine Receptor to the Junctional Foot Protein in Skeletal Muscle. *Biochemistry*, 29(39), 9281–9289. <https://doi.org/10.1021/bi00491a025>
- Kim, S. T., Tasaki, T., Zakrzewska, A., Yoo, Y. D., Sung, K. S., Kim, S. H., Cha-Molstad, H., Hwang, J., Kim, K. A., Kim, B. Y., & Kwon, Y. T. (2013). The N-end rule proteolytic system in autophagy. *Autophagy*, 9(7), 1100–1103. <https://doi.org/10.4161/auto.24643>
- Klionsky, D. J., Abdelmohsen, K., Abe, A., Abedin, M. J., Abeliovich, H., Acevedo Arozena, A., Adachi, H., Adams, C. M., Adams, P. D., Adeli, K., Adhihetty, P. J., Adler, S. G., Agam, G., Agarwal, R., Aghi, M. K., Agnello, M., Agostinis, P., Aguilar, P. V., Aguirre-Ghiso, J., ... Zughaier, S. M. (2016). Guidelines for the use and interpretation of assays for monitoring autophagy (3rd edition). *Autophagy*, 12(1), 1–222. <https://doi.org/10.1080/15548627.2015.1100356>
- Knollmann, B. C., Chopra, N., Hlaing, T., Akin, B., Yang, T., Etensohn, K., Knollmann, B. E. C., Horton, K. D., Weissman, N. J., Holinstat, I., Zhang, W., Roden, D. M., Jones, L. R., Franzini-Armstrong, C., & Pfeifer, K. (2006). Casq2 deletion causes sarcoplasmic reticulum volume increase, premature Ca<sup>2+</sup> release, and catecholaminergic polymorphic ventricular tachycardia. *Journal of Clinical Investigation*, 116(9), 2510–2520. <https://doi.org/10.1172/JCI29128>
- Kobayashi, Y. M., & Jones, L. R. (1999). Identification of triadin 1 as the predominant triadin isoform

- expressed in mammalian myocardium. *Journal of Biological Chemistry*, 274(40), 28660–28668.  
<https://doi.org/10.1074/jbc.274.40.28660>
- Kohl, T., Westphal, V., Hell, S. W., & Lehnart, S. E. (2013). Superresolution microscopy in heart - Cardiac nanoscopy. In *Journal of Molecular and Cellular Cardiology* (Vol. 58, Issue 1, pp. 13–21). J Mol Cell Cardiol. <https://doi.org/10.1016/j.yjmcc.2012.11.016>
- Kwon, Y. T., & Ciechanover, A. (2017). The Ubiquitin Code in the Ubiquitin-Proteasome System and Autophagy. In *Trends in Biochemical Sciences* (Vol. 42, Issue 11, pp. 873–886). Elsevier Ltd.  
<https://doi.org/10.1016/j.tibs.2017.09.002>
- Landstrom, A. P., Kellen, C. A., Dixit, S. S., Van Oort, R. J., Garbino, A., Weisleder, N., Ma, J., Wehrens, X. H. T., & Ackerman, M. J. (2011). Junctophilin-2 expression silencing causes cardiocyte hypertrophy and abnormal intracellular calcium-handling. *Circulation: Heart Failure*, 4(2), 214–223.  
<https://doi.org/10.1161/CIRCHEARTFAILURE.110.958694>
- Lee, S. H., Hadipour-Lakmehsari, S., Murthy, H. R., Gibb, N., Miyake, T., Teng, A. C. T., Cosme, J., Yu, J. C., Moon, M., Lim, S. H., Wong, V., Liu, P., Billia, F., Fernandez-Gonzalez, R., Stagljar, I., Sharma, P., Kislinger, T., Scott, I. C., & Gramolini, A. O. (2020). REEP5 depletion causes sarco-endoplasmic reticulum vacuolization and cardiac functional defects. *Nature Communications*, 11(1), 1–20.  
<https://doi.org/10.1038/s41467-019-14143-9>
- Leenhardt, A., Lucet, V., Denjoy, I., Grau, F., Dien Do Ngoc, & Coumel, P. (1995a). Catecholaminergic polymorphic ventricular tachycardia in children: A 7- year follow-up of 21 patients. *Circulation*, 91(5), 1512–1519. <https://doi.org/10.1161/01.CIR.91.5.1512>
- Leenhardt, A., Lucet, V., Denjoy, I., Grau, F., Dien Do Ngoc, & Coumel, P. (1995b). Catecholaminergic polymorphic ventricular tachycardia in children: A 7- year follow-up of 21 patients. *Circulation*, 91(5), 1512–1519. <https://doi.org/10.1161/01.CIR.91.5.1512>
- Lehnart, S. E., Wehrens, X. H. T., & Marks, A. R. (2004). Calstabin deficiency, ryanodine receptors, and sudden cardiac death. *Biochemical and Biophysical Research Communications*, 322(4), 1267–1279.  
<https://doi.org/10.1016/j.bbrc.2004.08.032>
- Li, W., & Ye, Y. (2008). Polyubiquitin chains: Functions, structures, and mechanisms. In *Cellular and Molecular Life Sciences* (Vol. 65, Issue 15, pp. 2397–2406). NIH Public Access.  
<https://doi.org/10.1007/s00018-008-8090-6>
- Lipp, P., Hüser, J., Pott, L., & Niggli, E. (1996). Spatially non-uniform Ca<sup>2+</sup> signals induced by the reduction of transverse tubules in citrate-loaded guinea-pig ventricular myocytes in culture. *Journal of Physiology*, 497(3), 589–597. <https://doi.org/10.1113/jphysiol.1996.sp021792>
- Liu, N., & Priori, S. G. (2008). Disruption of calcium homeostasis and arrhythmogenesis induced by mutations in the cardiac ryanodine receptor and calsequestrin. In *Cardiovascular Research* (Vol. 77, Issue 2, pp. 293–301). Cardiovasc Res. <https://doi.org/10.1093/cvr/cvm004>



- Liu, W., Tang, X., Qi, X., Fu, X., Ghimire, S., Ma, R., Li, S., Zhang, N., & Si, H. (2020). The ubiquitin conjugating enzyme: An important ubiquitin transfer platform in ubiquitin-proteasome system. In *International Journal of Molecular Sciences* (Vol. 21, Issue 8). MDPI AG. <https://doi.org/10.3390/ijms21082894>
- Lodola, F., Morone, D., Denegri, M., Bongianino, R., Nakahama, H., Rutigliano, L., Gosetti, R., Rizzo, G., Vollero, A., Buonocore, M., Napolitano, C., Condorelli, G., Priori, S. G., & Di Pasquale, E. (2016). Adeno-associated virus-mediated CASQ2 delivery rescues phenotypic alterations in a patient-specific model of recessive catecholaminergic polymorphic ventricular tachycardia. *Cell Death and Disease*, 7(10). <https://doi.org/10.1038/cddis.2016.304>
- Logan, C. M., & Menko, A. S. (2019). Microtubules: Evolving roles and critical cellular interactions. In *Experimental Biology and Medicine* (Vol. 244, Issue 15, pp. 1240–1254). SAGE Publications Inc. <https://doi.org/10.1177/1535370219867296>
- MacLennan, D. H., & Wong, P. T. (1971). Isolation of a calcium-sequestering protein from sarcoplasmic reticulum. *Proceedings of the National Academy of Sciences of the United States of America*, 68(6), 1231–1235. <https://doi.org/10.1073/pnas.68.6.1231>
- Macquart, C., Jüttner, R., Morales Rodriguez, B., Le Dour, C., Lefebvre, F., Chatzifrangkeskou, M., Schmitt, A., Gotthardt, M., Bonne, G., & Muchir, A. (2019). Microtubule cytoskeleton regulates Connexin 43 localization and cardiac conduction in cardiomyopathy caused by mutation in A-type lamins gene. *Human Molecular Genetics*, 28(24), 4043–4052. <https://doi.org/10.1093/hmg/ddy227>
- Manfredi, J. J., Parness, J., & Horwitz, S. B. (1982). Taxol binds to cellular microtubules. *Journal of Cell Biology*, 94(3), 688–696. <https://doi.org/10.1083/jcb.94.3.688>
- Maragna, R., & Napolitano, C. (2018). Catecholaminergic Polymorphic Ventricular Tachycardia. In *Cardiac and Vascular Biology* (Vol. 6, pp. 231–256). Springer Science and Business Media Deutschland GmbH. [https://doi.org/10.1007/978-3-319-77812-9\\_10](https://doi.org/10.1007/978-3-319-77812-9_10)
- Marban, E., Kusuoka, H., & Yue, D. T. (1986). Maximal Ca<sup>2+</sup>-activated force elicited by tetanization of ferret papillary muscle and whole heart: Mechanism and characteristics of steady contractile activation in intact myocardium. *Circulation Research*, 59(3), 262–269. <https://doi.org/10.1161/01.RES.59.3.262>
- Marshall, R. S., & Vierstra, R. D. (2019). Dynamic regulation of the 26S proteasome: From synthesis to degradation. In *Frontiers in Molecular Biosciences* (Vol. 6, Issue JUN, p. 40). Frontiers Media S.A. <https://doi.org/10.3389/fmolb.2019.00040>
- Martínez-Bartolomé, S., Navarro, P., Martín-Maroto, F., López-Ferrer, D., Ramos-Fernández, A., Villar, M., García-Ruiz, J. P., & Vázquez, J. (2008). Properties of average score distributions of SEQUEST: The probability ratio method. *Molecular and Cellular Proteomics*, 7(6), 1135–1145. <https://doi.org/10.1074/mcp.M700239-MCP200>
- Marty, I. (2015). Triadin regulation of the ryanodine receptor complex. In *Journal of Physiology* (Vol. 593,

- Issue 15, pp. 3261–3266). Blackwell Publishing Ltd. <https://doi.org/10.1113/jphysiol.2014.281147>
- Marty, I., Fauré, J., Fourest-Lieuvin, A., Vassilopoulos, S., Oddoux, S., & Brocard, J. (2009). Triadin: What possible function 20 years later? *Journal of Physiology*, 587(13), 3117–3121. <https://doi.org/10.1113/jphysiol.2009.171892>
- Marty, I., Thevenon, D., Scotto, C., Groh, S., Sainnier, S., Robert, M., Grunwald, D., & Villaz, M. (2000). Cloning and characterization of a new isoform of skeletal muscle triadin. *Journal of Biological Chemistry*, 275(11), 8206–8212. <https://doi.org/10.1074/jbc.275.11.8206>
- Masumiya, H., Wang, R., Zhang, J., Xiao, B., & Chen, S. R. W. (2003). Localization of the 12.6-kDa FK506-binding protein (FKBP12.6) binding site to the NH2-terminal domain of the cardiac Ca<sup>2+</sup> release channel (ryanodine receptor). *Journal of Biological Chemistry*, 278(6), 3786–3792. <https://doi.org/10.1074/jbc.M210962200>
- Matsushita, Y., Furukawa, T., Kasanuki, H., Nishibatake, M., Kurihara, Y., Ikeda, A., Kamatani, N., Takeshima, H., & Matsuoka, R. (2007). Mutation of junctophilin type 2 associated with hypertrophic cardiomyopathy. *Journal of Human Genetics*, 52(6), 543–548. <https://doi.org/10.1007/s10038-007-0149-y>
- McFarland, T. P., Milstein, M. L., & Cala, S. E. (2010). Rough endoplasmic reticulum to junctional sarcoplasmic reticulum trafficking of calsequestrin in adult cardiomyocytes. *Journal of Molecular and Cellular Cardiology*, 49(4), 556–564. <https://doi.org/10.1016/j.yjmcc.2010.05.012>
- McKinsey, T. A. (2012). Therapeutic potential for HDAC inhibitors in the heart. *Annual Review of Pharmacology and Toxicology*, 52, 303–319. <https://doi.org/10.1146/annurev-pharmtox-010611-134712>
- Meissner, G. (2004). Molecular regulation of cardiac ryanodine receptor ion channel. *Cell Calcium*, 35(6), 621–628. <https://doi.org/10.1016/j.ceca.2004.01.015>
- Meunier, B., Quaranta, M., Daviet, L., Hatzoglou, A., & Leprince, C. (2009). The membrane-tubulating potential of amphiphysin 2/BIN1 is dependent on the microtubule-binding cytoplasmic linker protein 170 (CLIP-170). *European Journal of Cell Biology*, 88(2), 91–102. <https://doi.org/10.1016/j.ejcb.2008.08.006>
- Minamisawa, S., Oshikawa, J., Takeshima, H., Hoshijima, M., Wang, Y., Chien, K. R., Ishikawa, Y., & Matsuoka, R. (2004). Junctophilin type 2 is associated with caveolin-3 and is down-regulated in the hypertrophic and dilated cardiomyopathies. *Biochemical and Biophysical Research Communications*, 325(3), 852–856. <https://doi.org/10.1016/j.bbrc.2004.10.107>
- Monroy, B. Y., Sawyer, D. L., Ackermann, B. E., Borden, M. M., Tan, T. C., & Ori-Mckenney, K. M. (2018). Competition between microtubule-associated proteins directs motor transport. *Nature Communications*, 9(1), 1–12. <https://doi.org/10.1038/s41467-018-03909-2>
- Morimoto, D., Walinda, E., Fukada, H., Sou, Y. S., Kageyama, S., Hoshino, M., Fujii, T., Tsuchiya, H.,

- Saeki, Y., Arita, K., Ariyoshi, M., Tochio, H., Iwai, K., Namba, K., Komatsu, M., Tanaka, K., & Shirakawa, M. (2015). The unexpected role of polyubiquitin chains in the formation of fibrillar aggregates. *Nature Communications*, 6. <https://doi.org/10.1038/ncomms7116>
- Murphy, R. M., Mollica, J. P., Beard, N. A., Knollmann, B. C., & Lamb, G. D. (2011). Quantification of calsequestrin 2 (CSQ2) in sheep cardiac muscle and Ca<sup>2+</sup>-binding protein changes in CSQ2 knockout mice. *American Journal of Physiology - Heart and Circulatory Physiology*, 300(2), H595. <https://doi.org/10.1152/ajpheart.00902.2010>
- Navarro, P., Trevisan-Herraz, M., Bonzon-Kulichenko, E., Núñez, E., Martínez-Acedo, P., Pérez-Hernández, D., Jorge, I., Mesa, R., Calvo, E., Carrascal, M., Hernáez, M. L., García, F., Bárcena, J. A., Ashman, K., Abian, J., Gil, C., Redondo, J. M., & Vázquez, J. (2014). General statistical framework for quantitative proteomics by stable isotope labeling. *Journal of Proteome Research*, 13(3), 1234–1247. <https://doi.org/10.1021/pr4006958>
- Navarro, P., & Vazquez, J. (2009). A refined method to calculate false discovery rates for peptide identification using decoy databases. *Journal of Proteome Research*, 8(4), 1792–1796. <https://doi.org/10.1021/pr800362h>
- Osseni, A., Sébastien, M., Sarrault, O., Baudet, M., Couté, Y., Fauré, J., Fourest-Lieuvin, A., & Marty, I. (2016). Triadin and CLIMP-63 form a link between triads and microtubules in muscle cells. *Journal of Cell Science*, 129(20), 3744–3755. <https://doi.org/10.1242/jcs.188862>
- Otsu, K., Willard, H. F., Khanna, V. K., Zorzato, F., Green, N. M., & MacLennan, D. H. (1990). Molecular cloning of cDNA encoding the Ca<sup>2+</sup> release channel (ryanodine receptor) of rabbit cardiac muscle sarcoplasmic reticulum. *Journal of Biological Chemistry*, 265(23), 13472–13483. [https://doi.org/10.1016/s0021-9258\(18\)77371-7](https://doi.org/10.1016/s0021-9258(18)77371-7)
- Pandey, U. B., Nie, Z., Batlevi, Y., McCray, B. A., Ritson, G. P., Nedelsky, N. B., Schwartz, S. L., Diprospero, N. A., Knight, M. A., Schuldiner, O., Padmanabhan, R., Hild, M., Berry, D. L., Garza, D., Hubbert, C. C., Yao, T. P., Baehrecke, E. H., & Taylor, J. P. (2007). HDAC6 rescues neurodegeneration and provides an essential link between autophagy and the UPS. *Nature*, 447(7146), 859–863. <https://doi.org/10.1038/nature05853>
- Park, H. J., Park, Y. Il, Kim, E. J., Youn, B., Fields, K., Dunker, A. K., & Kang, C. H. (2004). Comparing skeletal and cardiac calsequestrin structures and their calcium binding: A proposed mechanism for coupled calcium binding and protein polymerization. *Journal of Biological Chemistry*, 279(17), 18026–18033. <https://doi.org/10.1074/jbc.M311553200>
- Park, H. J., Wu, S., Dunker, A. K., & Kang, C. H. (2003). Polymerization of calsequestrin: Implications for Ca<sup>2+</sup> regulation. *Journal of Biological Chemistry*, 278(18), 16176–16182. <https://doi.org/10.1074/jbc.M300120200>
- Park, Y., Park, J., & Kim, Y. K. (2018). Crosstalk between translation and the aggresome–autophagy

- pathway. In *Autophagy* (Vol. 14, Issue 6, pp. 1079–1081). Taylor and Francis Inc.  
<https://doi.org/10.1080/15548627.2017.1358849>
- Peng, W., Shen, H., Wu, J., Guo, W., Pan, X., Wang, R., Chen, S. R. W., & Yan, N. (2016). Structural basis for the gating mechanism of the type 2 ryanodine receptor RyR2. *Science*, 354(6310).  
<https://doi.org/10.1126/science.aah5324>
- Perriard, J. C., Hirschy, A., & Ehler, E. (2003). Dilated cardiomyopathy: A disease of the intercalated disc? In *Trends in Cardiovascular Medicine* (Vol. 13, Issue 1, pp. 30–38). Trends Cardiovasc Med.  
[https://doi.org/10.1016/S1050-1738\(02\)00209-8](https://doi.org/10.1016/S1050-1738(02)00209-8)
- Portran, D., Gaillard, J., Vantard, M., & Thery, M. (n.d.). *Quantification of MAP and Molecular Motor Activities on Geometrically Controlled Microtubule Networks*. <https://doi.org/10.1002/cm.21081>
- Postma, A. V., Denjoy, I., Hoorntje, T. M., Lupoglazoff, J. M., Da Costa, A., Sebillon, P., Mannens, M. M. A. M., Wilde, A. A. M., & Guicheney, P. (2002). Absence of calsequestrin 2 causes severe forms of catecholaminergic polymorphic ventricular tachycardia. *Circulation Research*, 91(8).  
<https://doi.org/10.1161/01.res.0000038886.18992.6b>
- Priori, S. G., Napolitano, C., Tiso, N., Memmi, M., Vignati, G., Bloise, R., Sorrentino, V., & Danieli, G. a. (2001). Mutations in the cardiac ryanodine receptor gene (hRyR2) underlie catecholaminergic polymorphic ventricular tachycardia. *Circulation*, 103(2), 196–200.  
<https://doi.org/10.1161/01.CIR.103.2.196>
- Priori, Silvia G., Mazzanti, A., Santiago, D. J., Kukavica, D., Trancuccio, A., & Kovacic, J. C. (2021). Precision Medicine in Catecholaminergic Polymorphic Ventricular Tachycardia: JACC Focus Seminar 5/5. In *Journal of the American College of Cardiology* (Vol. 77, Issue 20, pp. 2592–2612). Elsevier Inc.  
<https://doi.org/10.1016/j.jacc.2020.12.073>
- Priori, Silvia G., & Napolitano, C. (2005). Cardiac and skeletal muscle disorders caused by mutations in the intracellular Ca<sup>2+</sup> release channels. In *Journal of Clinical Investigation* (Vol. 115, Issue 8, pp. 2033–2038). American Society for Clinical Investigation. <https://doi.org/10.1172/JCI25664>
- Priori, Silvia G., Napolitano, C., Memmi, M., Colombi, B., Drago, F., Gasparini, M., DeSimone, L., Coltorti, F., Bloise, R., Keegan, R., Cruz Filho, F. E. S., Vignati, G., Benatar, A., & DeLogu, A. (2002). Clinical and molecular characterization of patients with catecholaminergic polymorphic ventricular tachycardia. *Circulation*, 106(1), 69–74. <https://doi.org/10.1161/01.CIR.0000020013.73106.D8>
- Priori, Silvia G., Napolitano, C., Tiso, N., Memmi, M., Vignati, G., Bloise, R., Sorrentino, V., & Danieli, G. A. (2001). Mutations in the cardiac ryanodine receptor gene (hRyR2) underlie catecholaminergic polymorphic ventricular tachycardia. *Circulation*, 103(2), 196–200.  
<https://doi.org/10.1161/01.CIR.103.2.196>
- Prosser, B. L., Ward, C. W., & Lederer, W. J. (2011). X-ROS signaling: Rapid mechano-chemo transduction in heart. *Science*, 333(6048), 1440–1445. <https://doi.org/10.1126/science.1202768>

- Protasi, F. (2002). *Structural interaction between RYRs and DHPRs in calcium release units of cardiac and skeletal muscle cells* - PubMed. <https://pubmed.ncbi.nlm.nih.gov/11861217/>
- Ralston, S. H. (2008). Pathogenesis of Paget's disease of bone. In *Bone* (Vol. 43, Issue 5, pp. 819–825). Bone. <https://doi.org/10.1016/j.bone.2008.06.015>
- Ramkumar, A., Jong, B. Y., & Ori-McKenney, K. M. (2018). ReMAPping the microtubule landscape: How phosphorylation dictates the activities of microtubule-associated proteins. In *Developmental Dynamics* (Vol. 247, Issue 1, pp. 138–155). John Wiley and Sons Inc. <https://doi.org/10.1002/dvdy.24599>
- Rees, C., Yang, J.-H., Santolini, M., Lusi, A., Weiss, J., & Karma, A. (2018). Variability and compensation of cardiomyocyte ionic conductances at the population level. *BioRxiv*, 283275. <https://doi.org/10.1101/283275>
- Reid, D. S., Tynan, M., Braidwood, L., & Fitzgerald, G. R. (1975). Bidirectional tachycardia in a child. A study using His bundle electrography. *British Heart Journal*, 37(3), 339–344. <https://doi.org/10.1136/hrt.37.3.339>
- Ríos, E., Figueroa, L., Manno, C., Kraeva, N., & Riazi, S. (2015). The couplonopathies: A comparative approach to a class of diseases of skeletal and cardiac muscle. *Journal of General Physiology*, 145(6), 459–474. <https://doi.org/10.1085/jgp.201411321>
- Rizzi, N., Liu, N., Napolitano, C., Nori, A., Turcato, F., Colombi, B., Biciato, S., Arcelli, D., Spedito, A., Scelsi, M., Villani, L., Esposito, G., Boncompagni, S., Protasi, F., Volpe, P., & Priori, S. G. (2008). Unexpected Structural and Functional Consequences of the R33Q Homozygous Mutation in Cardiac Calsequestrin: A Complex Arrhythmogenic Cascade in a Knock in Mouse Model. *Circulation Research*, 103(3), 298–306. <https://doi.org/10.1161/CIRCRESAHA.108.171660>
- Robison, P., Caporizzo, M. A., Ahmadzadeh, H., Bogush, A. I., Chen, C. Y., Margulies, K. B., Shenoy, V. B., & Prosser, B. L. (2016). Detyrosinated microtubules buckle and bear load in contracting cardiomyocytes. *Science*, 352(6284). <https://doi.org/10.1126/science.aaf0659>
- Robison, P., & Prosser, B. L. (2017). Microtubule mechanics in the working myocyte. In *Journal of Physiology* (Vol. 595, Issue 12, pp. 3931–3937). Blackwell Publishing Ltd. <https://doi.org/10.1113/JP273046>
- Rosen, M. R., & Danilo, P. (1980). Effects of tetrodotoxin, lidocaine, verapamil, and AHR-2666 on ouabain-induced delayed afterdepolarizations in canine purkinje fibers. *Circulation Research*, 46(1), 117–124. <https://doi.org/10.1161/01.RES.46.1.117>
- Rosso, R., Kalman, J. M., Rogowski, O., Diamant, S., Birger, A., Biner, S., Belhassen, B., & Viskin, S. (2007). Calcium channel blockers and beta-blockers versus beta-blockers alone for preventing exercise-induced arrhythmias in catecholaminergic polymorphic ventricular tachycardia. *Heart Rhythm*, 4(9), 1149–1154. <https://doi.org/10.1016/j.hrthm.2007.05.017>
- Roux-buisson, N., Cacheux, M., Fourest-lieuvain, A., Fauconnier, J., Brocard, J., Denjoy, I., Durand, P.,

- Guicheney, P., Kyndt, F., Leenhardt, A., Le maret, H., Lucet, V., Mabo, P., Probst, V., Monnier, N., Ray, P. F., Santoni, E., Trémeaux, P., Lacampagne, A., ... Marty, I. (2012). Absence of triadin, a protein of the calcium release complex, is responsible for cardiac arrhythmia with sudden death in human. *Human Molecular Genetics*, 21(12), 2759–2767. <https://doi.org/10.1093/hmg/dds104>
- Sadowski, M., Suryadinata, R., Tan, A. R., Roesley, S. N. A., & Sarcevic, B. (2012). Protein monoubiquitination and polyubiquitination generate structural diversity to control distinct biological processes. In *IUBMB Life* (Vol. 64, Issue 2, pp. 136–142). John Wiley & Sons, Ltd. <https://doi.org/10.1002/iub.589>
- Sambrano, G. R., Frasert, I., Han, H., Ni, Y., O’Connell, T., Yan, Z., & Stull, J. T. (2002). Navigating the signalling network in mouse cardiac myocytes. In *Nature* (Vol. 420, Issue 6916, pp. 712–714). Nature. <https://doi.org/10.1038/nature01306>
- Sandoz, P. A., Denhardt-Eriksson, R. A., Abrami, L., Abriata, L., Spreemann, G., MacLachlan, C., Ho, S., Kunz, B., Hess, K., Knott, G., Hatzimanikatis, V., & van der Goot, F. G. (2018). The architecture of the endoplasmic reticulum is regulated by the reversible lipid modification of the shaping protein CLIMP-63. In *bioRxiv* (p. 431106). bioRxiv. <https://doi.org/10.1101/431106>
- Sandri, M., & Robbins, J. (2014). Proteotoxicity: An underappreciated pathology in cardiac disease. In *Journal of Molecular and Cellular Cardiology* (Vol. 71, pp. 3–10). Academic Press. <https://doi.org/10.1016/j.yjmcc.2013.12.015>
- Schweizer, A., Ericsson, M., Bachi, T., Griffiths, G., & Hauri, H. P. (1993). Characterization of a novel 63 kDa membrane protein. Implications for the organization of the ER-to-Golgi pathway. *Journal of Cell Science*, 104(3), 671–683. <https://doi.org/10.1242/jcs.104.3.671>
- Scriven, D. R. L., Asghari, P., & Moore, E. D. W. (2013). Microarchitecture of the dyad. In *Cardiovascular Research* (Vol. 98, Issue 2, pp. 169–176). <https://doi.org/10.1093/cvr/cvt025>
- Scriven, D. R. L., Dan, P., & Moore, E. D. W. (2000). Distribution of proteins implicated in excitation-contraction coupling in rat ventricular myocytes. *Biophysical Journal*, 79(5), 2682–2691. [https://doi.org/10.1016/S0006-3495\(00\)76506-4](https://doi.org/10.1016/S0006-3495(00)76506-4)
- Seigneurin-Berny, D., Verdel, A., Curtet, S., Lemerrier, C., Garin, J., Rousseaux, S., & Khochbin, S. (2001). Identification of Components of the Murine Histone Deacetylase 6 Complex: Link between Acetylation and Ubiquitination Signaling Pathways. *Molecular and Cellular Biology*, 21(23), 8035–8044. <https://doi.org/10.1128/mcb.21.23.8035-8044.2001>
- Shacklock, P. S., Wier, W. G., & Balke, C. W. (1995). Local Ca<sup>2+</sup> transients (Ca<sup>2+</sup> sparks) originate at transverse tubules in rat heart cells. *The Journal of Physiology*, 487(3), 601–608. <https://doi.org/10.1113/jphysiol.1995.sp020903>
- Shen, B., Zheng, P., Qian, N., Chen, Q., Zhou, X., Hu, J., Chen, J., & Teng, J. (2019). Calumenin-1 Interacts with Climp63 to Cooperatively Determine the Luminal Width and Distribution of Endoplasmic

- Reticulum Sheets. *IScience*, 22, 70–80. <https://doi.org/10.1016/j.isci.2019.10.067>
- Shibata, Y., Shemesh, T., Prinz, W. A., Palazzo, A. F., Kozlov, M. M., & Rapoport, T. A. (2010). Mechanisms determining the morphology of the peripheral ER. *Cell*, 143(5), 774–788. <https://doi.org/10.1016/j.cell.2010.11.007>
- Sleiman, N. H., McFarland, T. P., Jones, L. R., & Cala, S. E. (2015). Transitions of protein traffic from cardiac ER to junctional SR. *Journal of Molecular and Cellular Cardiology*, 81, 34–45. <https://doi.org/10.1016/j.yjmcc.2014.12.025>
- Sommer, J. R. (1982). The Anatomy of the Sarcoplasmic Reticulum in Vertebrate Skeletal Muscle: Its Implications for Excitation Contraction Coupling. *Zeitschrift Fur Naturforschung - Section C Journal of Biosciences*, 37(7–8), 665–678. <https://doi.org/10.1515/znc-1982-7-816>
- Song, Y., Kirkpatrick, L. L., Schilling, A. B., Helseth, D. L., Chabot, N., Keillor, J. W., Johnson, G. V. W., & Brady, S. T. (2013). Transglutaminase and Polyamination of Tubulin: Posttranslational Modification for Stabilizing Axonal Microtubules. *Neuron*, 78(1), 109–123. <https://doi.org/10.1016/j.neuron.2013.01.036>
- Soppina, V., Herbstman, J. F., Skiniotis, G., & Verhey, K. J. (2012). Luminal Localization of  $\alpha$ -tubulin K40 Acetylation by Cryo-EM Analysis of Fab-Labeled Microtubules. *PLoS ONE*, 7(10). <https://doi.org/10.1371/journal.pone.0048204>
- Stanhope, K. T., & Ross, J. L. (2015). Microtubules, MAPs, and motor patterns. *Methods in Cell Biology*, 128, 23–38. <https://doi.org/10.1016/bs.mcb.2015.02.003>
- Stewart, R., Zissimopoulos, S., & Lai, F. A. (2003). Oligomerization of the cardiac ryanodine receptor C-terminal tail. *Biochemical Journal*, 376(3), 795–799. <https://doi.org/10.1042/BJ20030597>
- Stürner, E., & Behl, C. (2017). The role of the multifunctional bag3 protein in cellular protein quality control and in disease. In *Frontiers in Molecular Neuroscience* (Vol. 10). Frontiers Media S.A. <https://doi.org/10.3389/fnmol.2017.00177>
- Su, H., & Wang, X. (2011a). Autophagy and p62 in cardiac protein quality control. In *Autophagy* (Vol. 7, Issue 11, pp. 1382–1383). Taylor and Francis Inc. <https://doi.org/10.4161/auto.7.11.17339>
- Su, H., & Wang, X. (2011b). P62 Stages an Interplay Between the Ubiquitin-Proteasome System and Autophagy in the Heart of Defense Against Proteotoxic Stress. In *Trends in Cardiovascular Medicine* (Vol. 21, Issue 8, pp. 224–228). NIH Public Access. <https://doi.org/10.1016/j.tcm.2012.05.015>
- Sudo, H., & Baas, P. W. (2010). Acetylation of microtubules influences their sensitivity to severing by katanin in neurons and fibroblasts. *Journal of Neuroscience*, 30(21), 7215–7226. <https://doi.org/10.1523/JNEUROSCI.0048-10.2010>
- Sumitomo, N., Harada, K., Nagashima, M., Yasuda, T., Nakamura, Y., Aragaki, Y., Saito, A., Kurosaki, K., Jouo, K., Koujiro, M., Konishi, S., Matsuoka, S., Oono, T., Hayakawa, S., Miura, M., Ushinohama, H., Shibata, T., & Niimura, I. (2003). Catecholaminergic polymorphic ventricular tachycardia:

- Electrocardiographic characteristics and optimal therapeutic strategies to prevent sudden death. *Heart*, 89(1), 66–70. <https://doi.org/10.1136/heart.89.1.66>
- Swan, H., Piippo, K., Viitasalo, M., Heikkilä, P., Paavonen, T., Kainulainen, K., Kere, J., Keto, P., Kontula, K., & Toivonen, L. (1999). Arrhythmic disorder mapped to chromosome 1q42-q43 causes malignant polymorphic ventricular tachycardia in structurally normal hearts. *Journal of the American College of Cardiology*, 34(7), 2035–2042. [https://doi.org/10.1016/S0735-1097\(99\)00461-1](https://doi.org/10.1016/S0735-1097(99)00461-1)
- Takahashi, M., Kitaura, H., Kakita, A., Kakihana, T., Katsuragi, Y., Nameta, M., Zhang, L., Iwakura, Y., Nawa, H., Higuchi, M., Komatsu, M., & Fujii, M. (2018). USP10 Is a Driver of Ubiquitinated Protein Aggregation and Aggresome Formation to Inhibit Apoptosis. *IScience*, 9, 433–450. <https://doi.org/10.1016/j.isci.2018.11.006>
- Takeshima, H., Hoshijima, M., & Song, L. S. (2015). Ca<sup>2+</sup> microdomains organized by junctophilins. In *Cell Calcium* (Vol. 58, Issue 4, pp. 349–356). Churchill Livingstone. <https://doi.org/10.1016/j.ceca.2015.01.007>
- Takeshima, H., Nishimura, S., Matsumoto, T., Ishida, H., Kangawa, K., Minamino, N., Matsuo, H., Ueda, M., Hanaoka, M., Hirose, T., & Numa, S. (1989). Primary structure and expression from complementary DNA of skeletal muscle ryanodine receptor. *Nature*, 339(6224), 439–445. <https://doi.org/10.1038/339439a0>
- Tanaka, K. (2009). The proteasome: Overview of structure and functions. In *Proceedings of the Japan Academy Series B: Physical and Biological Sciences* (Vol. 85, Issue 1, pp. 12–36). The Japan Academy. <https://doi.org/10.2183/pjab.85.12>
- Tannous, P., Zhu, H., Johnstone, J. L., Shelton, J. M., Rajasekaran, N. S., Benjamin, I. J., Nguyen, L., Gerard, R. D., Levine, B., Rothermel, B. A., & Hill, J. A. (2008). Autophagy is an adaptive response in desmin-related cardiomyopathy. *Proceedings of the National Academy of Sciences of the United States of America*, 105(28), 9745–9750. <https://doi.org/10.1073/pnas.0706802105>
- Tannous, P., Zhu, H., Nemchenko, A., Berry, J. M., Johnstone, J. L., Shelton, J. M., Miller, F. J., Rothermel, B. A., & Hill, J. A. (2008). Intracellular protein aggregation is a proximal trigger of cardiomyocyte autophagy. *Circulation*, 117(24), 3070–3078. <https://doi.org/10.1161/CIRCULATIONAHA.107.763870>
- te Rijdt, W. P., van Tintelen, J. P., Vink, A., van der Wal, A. C., de Boer, R. A., van den Berg, M. P., & Suurmeijer, A. J. H. (2016). Phospholamban p.Arg14del cardiomyopathy is characterized by phospholamban aggregates, aggresomes, and autophagic degradation. *Histopathology*, 69(4), 542–550. <https://doi.org/10.1111/his.12963>
- Teng, A. C. T., Miyake, T., Yokoe, S., Zhang, L., Rezende, L. M., Sharma, P., MacLennan, D. H., Liu, P. P., & Gramolini, A. O. (2015). Metformin increases degradation of phospholamban via autophagy in cardiomyocytes. *Proceedings of the National Academy of Sciences of the United States of America*,



112(23), 7165–7170. <https://doi.org/10.1073/pnas.1508815112>

- Tenno, T., Fujiwara, K., Tochio, H., Iwai, K., Morita, E. H., Hayashi, H., Murata, S., Hiroaki, H., Sato, M., Tanaka, K., & Shirakawa, M. (2004). Structural basis for distinct roles of Lys63- and Lys48-linked polyubiquitin chains. *Genes to Cells*, 9(10), 865–875. <https://doi.org/10.1111/j.1365-2443.2004.00780.x>
- Terasaki, M., Chen, L. B., & Fujiwara, K. (1986). Microtubules and the endoplasmic reticulum are highly interdependent structures. *Journal of Cell Biology*, 103(4), 1557–1568. <https://doi.org/10.1083/jcb.103.4.1557>
- Terentyev, D., Cala, S. E., Houle, T. D., Viatchenko-Karpinski, S., Gyorke, I., Terentyeva, R., Williams, S. C., & Gyorke, S. (2005a). Triadin overexpression stimulates excitation-contraction coupling and increases predisposition to cellular arrhythmia in cardiac myocytes. *Circulation Research*, 96(6), 651–658. <https://doi.org/10.1161/01.RES.0000160609.98948.25>
- Terentyev, D., Cala, S. E., Houle, T. D., Viatchenko-Karpinski, S., Gyorke, I., Terentyeva, R., Williams, S. C., & Gyorke, S. (2005b). Triadin overexpression stimulates excitation-contraction coupling and increases predisposition to cellular arrhythmia in cardiac myocytes. *Circulation Research*, 96(6), 651–658. <https://doi.org/10.1161/01.RES.0000160609.98948.25>
- Terentyev, D., Nori, A., Santoro, M., Viatchenko-Karpinski, S., Kubalova, Z., Gyorke, I., Terentyeva, R., Vedamoorthyrao, S., Blom, N. A., Valle, G., Napolitano, C., Williams, S. C., Volpe, P., Priori, S. G., & Gyorke, S. (2006). Abnormal interactions of calsequestrin with the ryanodine receptor calcium release channel complex linked to exercise-induced sudden cardiac death. *Circulation Research*, 98(9), 1151–1158. <https://doi.org/10.1161/01.RES.0000220647.93982.08>
- Terentyev, D., Viatchenko-Karpinski, S., Vedamoorthyrao, S., Oduru, S., Györke, I., Williams, S. C., & Györke, S. (2007). Protein-protein interactions between triadin and calsequestrin are involved in modulation of sarcoplasmic reticulum calcium release in cardiac myocytes. *Journal of Physiology*, 583(1), 71–80. <https://doi.org/10.1113/jphysiol.2007.136879>
- Thevenon, D., Smida-Rezgui, S., Chevessier, F., Groh, S., Henry-Berger, J., Romero, N. B., Villaz, M., DeWaard, M., & Marty, I. (2003). Human skeletal muscle triadin: Gene organization and cloning of the major isoform, Trisk 51. *Biochemical and Biophysical Research Communications*, 303(2), 669–675. [https://doi.org/10.1016/S0006-291X\(03\)00406-6](https://doi.org/10.1016/S0006-291X(03)00406-6)
- Treves, S., Feriotto, G., Moccagatta, L., Gambari, R., & Zorzato, F. (2000). Molecular cloning, expression, functional characterization, chromosomal localization, and gene structure of junctate, a novel integral calcium binding protein of sarco(endo)plasmic reticulum membrane. *Journal of Biological Chemistry*, 275(50), 39555–39568. <https://doi.org/10.1074/jbc.M005473200>
- Trevisan-Herraz, M., Bagwan, N., García-Marqués, F., Rodríguez, J. M., Jorge, I., Ezkurdia, I., Bonzon-Kulichenko, E., & Vázquez, J. (2019). SanXoT: A modular and versatile package for the quantitative

- analysis of high-throughput proteomics experiments. *Bioinformatics*, 35(9), 1594–1596.  
<https://doi.org/10.1093/bioinformatics/bty815>
- Tsutsui, H., Ishihara, K., & Cooper IV, G. (1993). Cytoskeletal role in the contractile dysfunction of hypertrophied myocardium. *Science*, 260(5108), 682–687. <https://doi.org/10.1126/science.8097594>
- Valente, A. J., Maddalena, L. A., Robb, E. L., Moradi, F., & Stuart, J. A. (2017). A simple ImageJ macro tool for analyzing mitochondrial network morphology in mammalian cell culture. *Acta Histochemica*, 119(3), 315–326. <https://doi.org/10.1016/j.acthis.2017.03.001>
- Valle, G., Galla, D., Nori, A., Priori, S. G., Gyorke, S., De Filippis, V., & Volpe, P. (2008). Catecholaminergic polymorphic ventricular tachycardia-related mutations R33Q and L167H alter calcium sensitivity of human cardiac calsequestrin. *Biochemical Journal*, 413(2), 291–303.  
<https://doi.org/10.1042/BJ20080163>
- Vandecandelaere, A., Martin, S. R., & Engelborghs, Y. (1997). Response of microtubules to the addition of colchicine and tubulin-colchicine: Evaluation of models for the interaction of drugs with microtubules. In *Biochemical Journal* (Vol. 323, Issue 1, pp. 189–196). Portland Press Ltd.  
<https://doi.org/10.1042/bj3230189>
- Vassilopoulos, S., Thevenont, D., Rezguit, S. S., Brocard, J., Chapel, A., Lacampagne, A., Lunardi, J., Dewaard, M., & Marty, I. (2005). Triadins are not triad-specific proteins: Two new skeletal muscle triadins possibly involved in the architecture of sarcoplasmic reticulum. *Journal of Biological Chemistry*, 280(31), 28601–28609. <https://doi.org/10.1074/jbc.M501484200>
- Vedrenne, C., & Hauri, H. P. (2006). Morphogenesis of the endoplasmic reticulum: Beyond active membrane expansion. In *Traffic* (Vol. 7, Issue 6, pp. 639–646). Traffic. <https://doi.org/10.1111/j.1600-0854.2006.00419.x>
- Vedrenne, C., Klopfenstein, D. R., & Hauri, H. P. (2005). Phosphorylation controls CLIMP-63-mediated anchoring of the endoplasmic reticulum to microtubules. *Molecular Biology of the Cell*, 16(4), 1928–1937. <https://doi.org/10.1091/mbc.E04-07-0554>
- Vega, A. L., Yuan, C., Votaw, V. S., & Santana, L. F. (2011). Dynamic changes in sarcoplasmic reticulum structure in ventricular myocytes. *Journal of Biomedicine and Biotechnology*, 2011, 14.  
<https://doi.org/10.1155/2011/382586>
- Vishwakarma, S., Iyer, L. R., Muley, M., Singh, P. K., Shastry, A., Saxena, A., Kulathingal, J., Vijaykanth, G., Raghul, J., Rajesh, N., Rathinasamy, S., Kachhadia, V., Kilambi, N., Rajgopal, S., Balasubramanian, G., & Narayanan, S. (2013). Tubastatin, a selective histone deacetylase 6 inhibitor shows anti-inflammatory and anti-rheumatic effects. *International Immunopharmacology*, 16(1), 72–78. <https://doi.org/10.1016/j.intimp.2013.03.016>
- Wandosell, F., Serrano, L., & Avila, J. (1987). Phosphorylation of alpha-tubulin carboxyl-terminal tyrosine prevents its incorporation into microtubules. *Journal of Biological Chemistry*, 262(17), 8268–8273.

[https://doi.org/10.1016/s0021-9258\(18\)47559-x](https://doi.org/10.1016/s0021-9258(18)47559-x)

- Wang, F., Zheng, L., Yi, Y., Yang, Z., Qiu, Q., Wang, X., Yan, W., Bai, P., Yang, J., Li, D., Pei, H., Niu, T., Ye, H., Nie, C., Hu, Y., Yang, S., Wei, Y., & Chen, L. (2018). SKLB-23bb, A HDAC6-Selective inhibitor, exhibits superior and broad-spectrum antitumor activity via additionally targeting microtubules. *Molecular Cancer Therapeutics*, 17(4), 763–775. <https://doi.org/10.1158/1535-7163.MCT-17-0332>
- Wang, Q., VanDusen, W. J., Petroski, C. J., Garsky, V. M., Stern, A. M., & Friedman, P. A. (1991). Bovine liver aspartyl  $\beta$ -hydroxylase: Purification and characterization. *Journal of Biological Chemistry*, 266(21), 14004–14010. [https://doi.org/10.1016/s0021-9258\(18\)92802-4](https://doi.org/10.1016/s0021-9258(18)92802-4)
- Wang, S., Trumble, W. R., Liao, H., Wesson, C. R., Dunker, A. K., & Kang, C. H. (1998). Crystal structure of calsequestrin from rabbit skeletal muscle sarcoplasmic reticulum. *Nature Structural Biology*, 5(6), 476–483. <https://doi.org/10.1038/nsb0698-476>
- Wang, Z., Leng, Y., Wang, J., Liao, H. M., Bergman, J., Leeds, P., Kozikowski, A., & Chuang, D. M. (2016). Tubastatin A, an HDAC6 inhibitor, alleviates stroke-induced brain infarction and functional deficits: Potential roles of  $\alpha$ -tubulin acetylation and FGF-21 up-regulation. *Scientific Reports*, 6. <https://doi.org/10.1038/srep19626>
- Watanabe, H., Chopra, N., Laver, D., Hwang, H. S., Davies, S. S., Roach, D. E., Duff, H. J., Roden, D. M., Wilde, A. A. M., & Knollmann, B. C. (2009). Flecainide prevents catecholaminergic polymorphic ventricular tachycardia in mice and humans. *Nature Medicine*, 15(4), 380–383. <https://doi.org/10.1038/nm.1942>
- Waterman-Storer, C. M., & Salmon, E. D. (1998). Endoplasmic reticulum membrane tubules are distributed by microtubules in living cells using three distinct mechanisms. *Current Biology*, 8(14), 798–807. [https://doi.org/10.1016/s0960-9822\(98\)70321-5](https://doi.org/10.1016/s0960-9822(98)70321-5)
- Wehrens, X. H. T., Lehnart, S. E., Huang, F., Vest, J. A., Reiken, S. R., Mohler, P. J., Sun, J., Guatimosim, S., Song, L. S., Rosemblyt, N., D'Armiento, J. M., Napolitano, C., Memmi, M., Priori, S. G., Lederer, W. J., & Marks, A. R. (2003). FKBP12.6 deficiency and defective calcium release channel (ryanodine receptor) function linked to exercise-induced sudden cardiac death. *Cell*, 113(7), 829–840. [https://doi.org/10.1016/S0092-8674\(03\)00434-3](https://doi.org/10.1016/S0092-8674(03)00434-3)
- Xiao, H., Wang, H., Zhang, X., Tu, Z., Bulinski, C., Khrapunovich-Baine, M., Hogue Angeletti, R., & Horwitz, S. B. (2012). Structural evidence for cooperative microtubule stabilization by taxol and the endogenous dynamics regulator MAP4. *ACS Chemical Biology*, 7(4), 744–752. <https://doi.org/10.1021/cb200403x>
- Xu, L., & Meissner, G. (2004). Mechanism of Calmodulin Inhibition of Cardiac Sarcoplasmic Reticulum Ca<sup>2+</sup> Release Channel (Ryanodine Receptor). *Biophysical Journal*, 86(2), 797–804. [https://doi.org/10.1016/S0006-3495\(04\)74155-7](https://doi.org/10.1016/S0006-3495(04)74155-7)

- Xu, Z., Schaedel, L., Portran, D., Aguilar, A., Gaillard, J., Peter Marinkovich, M., Théry, M., & Nachury, M. V. (2017). Microtubules acquire resistance from mechanical breakage through intralumenal acetylation. *Science*, 356(6335), 328–332. <https://doi.org/10.1126/science.aai8764>
- Yao, L., Xie, D., Geng, L., Shi, D., Huang, J., Wu, Y., Lv, F., Liang, D., Li, L., Liu, Y., Li, J., & Chen, Y. H. (2018). REEP5 (Receptor Accessory Protein 5) acts as a sarcoplasmic reticulum membrane sculptor to modulate cardiac function. *Journal of the American Heart Association*, 7(3). <https://doi.org/10.1161/JAHA.117.007205>
- Zhang, C., Chen, B., Guo, A., Zhu, Y., Miller, J. D., Gao, S., Yuan, C., Kutschke, W., Zimmerman, K., Weiss, R. M., Wehrens, X. H. T., Hong, J., Johnson, F. L., Santana, L. F., Anderson, M. E., & Song, L. S. (2014). Microtubule-mediated defects in junctophilin-2 trafficking contribute to myocyte transverse-tubule remodeling and Ca<sup>2+</sup> handling dysfunction in heart failure. *Circulation*, 129(17), 1742–1750. <https://doi.org/10.1161/CIRCULATIONAHA.113.008452>
- Zhang, D., Hu, X., Henning, R. H., & Brundel, B. J. J. M. (2016). Keeping up the balance: Role of HDACs in cardiac proteostasis and therapeutic implications for atrial fibrillation. In *Cardiovascular Research* (Vol. 109, Issue 4, pp. 519–526). Oxford University Press. <https://doi.org/10.1093/cvr/cvv265>
- Zhang, D., Wu, C. T., Qi, X. Y., Meijering, R. A. M., Hoogstra-Berends, F., Tadevosyan, A., Deniz, G. C., Durdu, S., Akar, A. R., Sibon, O. C. M., Nattel, S., Henning, R. H., & Brundel, B. J. J. M. (2014). Activation of histone deacetylase-6 induces contractile dysfunction through derailment of  $\alpha$ -tubulin proteostasis in experimental and human atrial fibrillation. *Circulation*, 129(3), 346–358. <https://doi.org/10.1161/CIRCULATIONAHA.113.005300>
- Zhang, L., Kelley, J., Schmeisser, G., Kobayashi, Y. M., & Jones, L. R. (1997). Complex formation between junctin, triadin, calsequestrin, and the ryanodine receptor: Proteins of the cardiac junctional sarcoplasmic reticulum membrane. *Journal of Biological Chemistry*, 272(37), 23389–23397. <https://doi.org/10.1074/jbc.272.37.23389>
- Zhang, S. S., & Shaw, R. M. (2014). Trafficking highways to the intercalated disc: New insights unlocking the specificity of connexin 43 localization. In *Cell Communication and Adhesion* (Vol. 21, Issue 1, pp. 43–54). Informa Healthcare. <https://doi.org/10.3109/15419061.2013.876014>
- Zheng, Q., & Wang, X. (2010). Autophagy and the ubiquitin-proteasome system in cardiac dysfunction. In *Panminerva Medica* (Vol. 52, Issue 1, pp. 9–25). NIH Public Access. [/pmc/articles/PMC2840262/](https://pubmed.ncbi.nlm.nih.gov/2840262/)
- Zorzato, F., Fujii, J., Otsu, K., Phillips, M., Green, N. M., Lai, F. A., Meissner, G., & MacLennan, D. H. (1990). Molecular cloning of cDNA encoding human and rabbit forms of the Ca<sup>2+</sup> release channel (ryanodine receptor) of skeletal muscle sarcoplasmic reticulum. *Journal of Biological Chemistry*, 265(4), 2244–2256. [https://doi.org/10.1016/s0021-9258\(19\)39968-5](https://doi.org/10.1016/s0021-9258(19)39968-5)